

UNIVERSITY OF TRENTO - Italy

Department of Civil, Environmental  
and Mechanical Engineering



Doctoral School in Civil, Environmental and Mechanical  
Engineering  
Doctoral Thesis - April 6, 2020

MICHELE BOTTAZZI

# **Transpiration theory and the Prospero component of GEOframe**

## **Supervisors:**

Riccardo RIGON (University of Trento, Italy)  
Giacomo BERTOLDI (Eurac research, Italy))



# TABLE OF CONTENTS

	<b>Page</b>
<b>List of Tables</b>	<b>v</b>
<b>List of Figures</b>	<b>vii</b>
<b>1 Introduction</b>	<b>1</b>
<b>2 Transpiration theory</b>	<b>7</b>
2.1 According to Budyko . . . . .	8
2.2 Momentum and water vapor transport in turbulent atmosphere . . . . .	9
2.2.1 Dalton's law of evaporation . . . . .	14
2.2.2 Convective transport of thermal energy (sensible heat) . . . . .	17
2.3 Derivation of the energy balance . . . . .	18
2.3.1 The energy budget . . . . .	18
2.3.2 The Clausius-Clapeyron equation . . . . .	19
2.3.3 The Penman linearization . . . . .	20
2.3.4 Solving the Penman-Monteith System step by step . . . . .	21
2.3.5 Different transpiring surfaces: the case of leaves and soils . . . . .	24
2.3.6 The radiatively coupled system . . . . .	25
2.3.7 Including the Monin-Obukhov Similarity Theory (MOST) . . . . .	26

## TABLE OF CONTENTS

---

2.4	Introducing the water budget . . . . .	29
2.4.1	The case of soils . . . . .	31
2.4.2	Stage I evaporation from soil . . . . .	32
2.4.3	Stage II evaporation from soil . . . . .	34
2.4.4	A new set of equations for the evaporation processes in soil . . . . .	35
2.4.5	Some simplification to show that the system above is actually solvable . . . . .	36
2.4.6	Vapor, momentum and energy budget in the turbulent layer . . . . .	38
<b>3</b>	<b>Upscale the transpiration theory</b>	<b>41</b>
3.1	Where does the water go? . . . . .	42
3.1.1	Leaves . . . . .	44
3.1.2	Water vapor diffusion . . . . .	47
3.1.3	Stomatal conductance in the absence of stress . . . . .	50
3.2	The families of conductance models with stress .	51
3.2.1	Models based on climatic control only .	52
3.2.2	Models based on the conductance-photosynthesis relationship . . . . .	54
3.3	Transpiration from the canopy . . . . .	55
3.4	Upscaling from the leaf to canopies . . . . .	55
3.4.1	Big-Leaf Approach . . . . .	56
3.4.2	Two-Leaf Approach . . . . .	57
3.4.3	Clumping Simulations . . . . .	58
3.5	Upscaling at the canopy scale . . . . .	59
3.5.1	Upscaling strategy . . . . .	59
<b>4</b>	<b>Prospero</b>	<b>61</b>
4.1	Sun/Shade model . . . . .	63
4.2	Water stress & conductance model . . . . .	67
4.2.1	Stress factors . . . . .	68

4.2.2	Maximum stomatal conductance . . . . .	71
4.3	Prospero's ET . . . . .	73
<b>5</b>	<b>Pointwise estimates</b>	<b>75</b>
5.1	Torgnon . . . . .	76
5.2	Viote . . . . .	77
5.3	Data . . . . .	78
5.4	Model parametrization and results . . . . .	85
<b>6</b>	<b>Catchment-based estimates</b>	<b>97</b>
6.1	Rio Ressi . . . . .	97
6.2	Data . . . . .	99
6.3	Model calibration . . . . .	100
6.4	Results . . . . .	101
<b>7</b>	<b>Conclusion</b>	<b>109</b>
<b>A</b>	<b>Appendix A: GEOframe</b>	<b>113</b>
A.1	Replicability . . . . .	114
A.2	GEOframe structure . . . . .	118
A.3	Embedded reservoir model . . . . .	120
A.4	Evapotranspiration . . . . .	121
A.4.1	Priestley-Taylor . . . . .	122
A.4.2	Penman-Monteith FAO . . . . .	123
<b>B</b>	<b>Appendix B: The design, deployment, and testing of kriging models in GEOframe with SIK-0.9.8</b>	<b>125</b>
<b>C</b>	<b>Appendix C: More green and less blue water in the Alps during warmer summers</b>	<b>131</b>
<b>D</b>	<b>Acknowledgements</b>	<b>139</b>
	<b>Bibliography</b>	<b>141</b>



## LIST OF TABLES

TABLE	Page
3.1 Representative values of conductances . . . . .	49
5.1 Soil composition in Viote and Torgnon site. . . . .	84
5.2 Values of field capacity and wilting point obtained for the two sites based on the soil composition . . . . .	84
5.3 Values for PM-FAO component for the two sites. . . . .	87
5.4 Parameters used for Prospero simulations in Viote and Torgnon. . . . .	88
5.5 <i>Root mean square error and mean absolute error ob-</i> <i>tained on Viote and Torgnon simulations . . . . .</i>	<i>88</i>
6.1 FAO's vegetation parameters used for the Rio Ressi simulation . . . . .	100
6.2 Parameters range of the Embedded Reservoir Model .	101
6.3 Performance of the ERM using different components for the evapotranspiration . . . . .	104
A.1 List of the current components of GEOframe . . . . .	120



## LIST OF FIGURES

<b>FIGURE</b>	<b>Page</b>
2.1 Critical Zone surfaces and components . . . . .	10
3.1 Pressure in the xylem . . . . .	43
3.2 Cross section of typical angiosperm leaf . . . . .	45
4.1 Conceptual scheme of Prospero . . . . .	62
4.2 LAI and absorbed shortwave radiation with the Sun/Shade model . . . . .	65
4.3 Shortwave penetration inside the canopy . . . . .	68
4.4 Typical values of the stress factor functions at the variation of the forcing. . . . .	72
5.1 Map of the case studies:Torgnon and Viote . . . . .	76
5.2 Monthly distribution of latent heat in Viote . . . . .	79
5.3 Monthly distribution of latent heat in Torgnon . . . . .	80
5.4 Energy balance residual on Viote. . . . .	81
5.5 Energy balance residual on Torgnon. . . . .	82
5.6 Total annual evapotranspiration simulated and observed on Viote. . . . .	85
5.7 Total annual evapotranspiration simulated and observed on Torgnon. . . . .	86
5.8 Ratio between the total annual evapotranspiration, both simulated and observed, and precipitation on Viote. . . . .	89

## LIST OF FIGURES

---

5.9	Ratio between the total annual evapotranspiration, both simulated and observed, and precipitation on Torgnon. . . . .	90
5.10	Boxplot of the difference between simulated and ob- served grouped at monthly timescale for Viote site. .	91
5.11	Boxplot of the difference between simulated and ob- served grouped at monthly timescale for Torgnon site.	91
5.12	Boxplot of the difference between simulated and ob- served grouped at daily timescale. . . . .	92
5.13	Scatter plot simulated vs observed. . . . .	93
5.14	Scatter plot simulated vs observed. . . . .	94
6.1	Experimental basin of Rio Ressi. . . . .	98
6.2	Total annual precipitation and evapotranspiration .	102
6.3	Total monthly evapotranspiration and runoff, simu- lated and observed. . . . .	106
6.4	Observed and simulated hydrogramm and cumulated runoff, compared with precipitation, obtained with the ERM model and the Prospero component. . . . .	107
A.1	The GEOframe universe and its component. . . . .	115
A.2	Example of modelling solution for ET in GEOframe .	115
B.1	Geo-location of study area and position of meteoro- logical stations. . . . .	127
B.2	Maps of spatialized temperature for 15 February 2008 and 15 June 2008. . . . .	128
C.1	Spatial heterogeneity in latent heat on the Alps . . . .	133
C.2	Analysis of anomalies in blue-and green-water fluxes during the 2003 drought . . . . .	137

C H A P T E R



## INTRODUCTION

Evapotranspiration (ET) plays a key role in the hydrological cycle and land-atmosphere interaction, thus, a correct evaluation of this variable is fundamental in several fields of application, such as sustainable water management at the basin scale and irrigation planning, at the field scale.

In fact, the estimation of atmospheric turbulent fluxes (sensible and latent heat) at the land surface has long been recognized as the most important process in the determination of the exchanges of energy and mass among hydrosphere, atmosphere and biosphere (e.g. Bowen, 1926; Penman, 1948; Monteith, 1965; Priestley and Taylor, 1972; Brutsaert, 2013; Morton, 1983; Famiglietti and Wood, 1994; Su et al., 1999; Su and Jacobs, 2001).

At global scale latent heat represents the 38% of the net radiation absorbed and the corresponding evaporated water amounts to the 40% of total precipitation. Transpiration impacts on the evapotranspiration up to 60%. However there is a large uncertainty associated with the vegetation response to water stress (Mastrotheodoros et al., 2020).

There is an urgent need to move towards a more sustainable approach to manage water resources and mitigate and prevent natural hazards. Water-related aspects of climate change (CC) and extremes, such as droughts, put pressure on alpine ecosystems, but their response to hydrological variability is not yet fully understood (Beniston, 2012; Pepin et al., 2015) as the "drought paradox" (Mastrotheodoros et al., 2020, see appendix C).

In recent years, the development of world-wide networks such as the Long-Term Socio-Ecological Research (LTSER) or FLUXNET has led to a deeper experimental knowledge on plant-water interactions.

At the same time, new and improved techniques for area-wide observation (proximal sensing through Unmanned Aerial Vehicle (UAV) devices, RS platforms as European Space Agency (ESA) satellite Sentinel mission, Berger et al., 2012) have provided new options for upscaling to landscape-scale.

Despite the increasing experimental knowledge of plant's hydrology and the availability of high-resolution observations, there is still a lack of appropriate modelling methods able to incorporate this information in a physically consistent way (Demirel et al., 2018).

To analyze the effects of short-term climatic and small-scale spatial variability on mountain biophysical cycles (Foley) the development of Reliable, Robust and Realistic (R3) predicting tools are required (Prentice et al., 2015).

However, in order to build R3 predicting modelling tools, there is the need to translate this observational knowledge in mathematical and numerical form, which balances functional complexity to practical needs (Prentice et al., 2015).

Plants water-use strategies are driven by plant functional traits (PFT) (examples are leaf size, toughness and longevity, seed size and dispersal mode, canopy height and structure, capacity for

---

nitrogen fixation, Mitchell et al., 2008) and in recent years, plant-physiology studies provided an increasingly detailed knowledge of plants behaviour, but only some of them started to be implemented in ecohydrological models (Fatichi et al., 2016).

Models simulating plant-hydraulic processes are still rare and confined to specific studies (Hölttä et al., 2009; Mackay et al., 2015; Nikinmaa et al., 2014). Other studies account explicitly for topographic attributes and lateral water and mass exchanges (Ivanov et al., 2008; Shen et al., 2013; Tague et al., 2013), but their treatment of plant processes is often oversimplified (Zhou et al., 2013). In mountain terrain, even the effect of plot-scale ( $0.01 - 0.1 \text{ km}^2$ ) spatial variability of the energy fluxes is still largely not understood (Rollinson and Kaye, 2015) notwithstanding pioneering studies which account for various feedbacks are available, which show that vegetation productivity and water use do not change linearly through spatial gradients (Niedrist et al., 2016).

Most advanced plot-to-catchment scale models include a three-dimensional treatment of the water fluxes in soil (e.g. Pütz et al., 2013), explicit spatial variability of atmospheric forcing and turbulence (e.g. Katul et al., 2013) and a well-balanced complexity in the formulation of the water and energy budgets. However, vegetation dynamics modelling (VDMs) and water flow in plants should be included. Among the VDMs are GEOTop-dv (Rigon et al., 2006a; Della Chiesa et al., 2014; Endrizzi et al., 2014) and T&C (Fatichi et al., 2012). Vegetation hydraulic was recently reviewed by Stroock et al. (2014), providing the idea that a new synthesis is necessary between the modelling of water and carbon fluxes, and that an upscaling from cells through plants to landscape is required. In recent years, plant-physiology studies provided an increasingly detailed knowledge of the plants behaviour (Brodribb et al., 2005), but only some aspects of it

started to be implemented in ecohydrological models (Fatichi et al., 2015). Two main categories of models can be roughly identify: those who approach the problem mechanistically (Fatichi et al., 2012), by adding detailed processes parameterizations, and those who make reference to optimality principles, claiming that feedback mechanisms were discovered during plants evolution to maintain good performances under sub-optimal conditions (Prentice et al., 2015).

To further develop these models, a new infrastructure is necessary in order to enable comparisons of the alternatives that are emerging from last years of research. In fact, the monolithic informatics of traditional design (Rizzoli et al., 2004) hinder any change of the code and slow-down progresses of research. Fortunately, recently "component-oriented" modelling approaches (David et al., 2013; Formetta et al., 2014a; Bancheri, 2017) were deployed. Such approaches make it easier to change modules simulating specific processes, while maintaining unchanged the others.

Modellers had to face different challenges, such as joining the plant physiology with the biosphere and considering the interactions with pedo and atmosphere (including spatial and temporal patterns). This task involves an appropriate modelling of the environmental conditions (Bertoldi et al., 2007; Siqueira et al., 2009); the mathematical description of the water flow in the soil interaction with roots and the reciprocal influence of plants for accessing nutrient resources (Manoli et al., 2014); a more accurate separation of soil evaporation from transpiration (Jung et al., 2010); the need to upscale the mathematics of plants behaviour at the landscape scale, with the appropriate degree of complexity (Pappas et al., 2016).

In a recent study we published on Nature Climate Change (Mastrotheodoros et al., 2020), we find that with climate change, the

---

partition between evaporative fluxes and runoff is changing, enhancing the ET during the drought period ('drought paradox', see appendix C). This further highlights the need to have precise models for ET, which calculate separately evaporation and transpiration, in order to better understand the response to climate change of the individual processes (soil and vegetation) but also of model that can be easily implemented in distributed models. In chapter 2 we present an extensive literature review of the transpiration theory starting from the milestones until the newest works. In particular, the physics of transpiration is analyzed, defining the energy balance and its components. In particular, some omissions rising from recent studies are highlighted.

In chapter 3 we face the physiological component of transpiration and how it manages the exchange of fluxes between the vegetation and the atmosphere. We also analyze some strategies commonly used to adapt the transpiration's equations at the canopy scale.

In chapter 4 is presented a newly developed model, called "Prospero" used to estimate the evapotranspiration, that can be used as a component in the GEOframe hydrological modelling system. Finally, in chapter 5 and 6, Prospero is applied to two different types of case studies, both at point-wise scale and catchment scale. Performances are compared with other GEOframe's tools for evapotranspiration and with observed measurements.

Furthermore, in the appendix, two papers I worked on are presented, since they are not closely related to the development of Prospero, as well as the informatics structure of GEOframe.



C H A P T E R



## TRANSPiration THEORY

We are interested in the compound of all generation and transport at various scales, which makes the analysis of the problem of evapotranspiration complicate and not completely well resolved due to heterogeneity of the control volumes and entangled processes. As a matter of facts, the description of vapor transport has dominated the way we treat evapotranspiration in hydrology and we start from there.

In this literature review, we inherit a lot from papers and conferences by G.K Katul (even if we are not able to indicate specific papers) and D. Or in his work with Haghghi (on soil) and with S. Schymanski, besides, obviously the various classics of the subject, which are more properly cited in the manuscript. Our effort is to give an updated overview of the transpiration theory, underlining the still open research questions and the more promising approaches for evapotranspiration modelling.

## 2.1 According to Budyko

Mass conservation in hydrological cycle can be written as:

$$\Delta S = (ET - P - Q)\Delta t \quad (2.1)$$

where  $\Delta S$  is the soil moisture storage, ET is the evapotranspiration, P the precipitation, Q the runoff and  $\Delta t$  is the temporal time step.

Considering the runoff as the sum:

$$Q = Q_{sup} + Q_s + Q_G \quad (2.2)$$

Where  $Q_{sup}$  is the surface runoff,  $Q_s$  is the subsurface runoff and  $Q_G$  is the recharge term. Budyko considers that an area is large enough ( $\approx 1000 \text{ km}^2$ ), the effect of groundwater is minimized. Furthermore if the time step is quite long ( $\Delta t > 1 \text{ year}$ ), we can assume the storage variation is more or less zero.

Inverting the water balance we can express the evapotranspiration as:

$$ET = (P - Q) - A \frac{\Delta S}{\Delta t} \quad (2.3)$$

According to Budyko, it can be deduced that the maximum of evapotranspiration is obtained, besides neglecting the water storage variation, when  $Q = 0$ . If this happens, the maximum evapotranspiration is equal to the rainfall.

$$ET_{max} = P \quad (2.4)$$

Assuming the soil heat flux G equal to zero and the sensible heat H is positive, the energy balance  $\Delta E$  can be expressed as:

$$\Delta E = R_n - \lambda ET - H \quad (2.5)$$

where  $R_n$  is the net radiation, H is the sensible heat and  $\lambda$  the latent heat of evaporation.

When energy is a limiting factor, the maximum possible ET is when  $H = 0$  and the first member of the equation ( $\Delta E$ ) is negligible. Then, when energy is the limiting factor, it is:

$$R_n > \lambda ET_{max} = \lambda P \quad (2.6)$$

where  $ET_{max}$  indicates the maximum possible evaporation, which therefore is equal to  $P$  (from mass conservation equation).

Finally we can say that:

$$ET_{max} = \min\left(P, \frac{R_n}{\lambda}\right) \quad (2.7)$$

This equation makes evident that both the water and the energy budgets rule evapotranspiration and limit it. When there is not enough water,  $ET$  is said water-limited; when there is not enough energy,  $ET$  is said energy limited. We use these concepts later on in the thesis.

## 2.2 Momentum and water vapor transport in turbulent atmosphere

The control volume we are considering is the Earth surface and a portion of atmosphere above it (i.e. the critical zone). In its minimalist conceptualization, a semi-indefinite volume below, the ground, and a semi-indefinite volume above it, the atmosphere, Dalton's studies were mostly experimental (Brutsaert, 1986), and the current transport theory used to in the area, is the semi-empiric mixing length theory (Prandtl, 1925, 1926). It finds that any quantity of concentration  $x$  is transported in atmosphere by the vertical fluctuation of velocity,  $w'$ , positive upward. So, for instance, it is:

$$\text{Transport of } x = \overline{(\rho_x x) w'} \quad (2.8)$$

where:

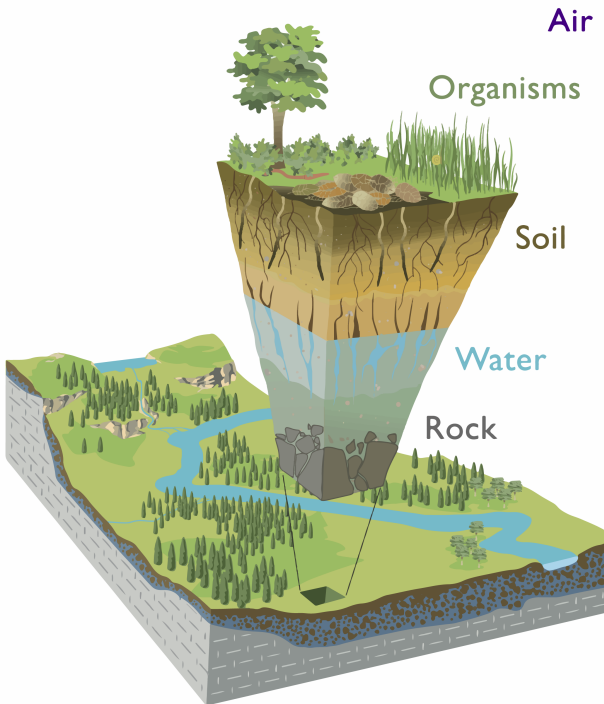


Figure 2.1: Critical Zone surfaces and components (Chorover et al., 2007). Image from [Critical Zone Observatories](#)

- $x$  is a generic quantity
- $\rho_x$  is its density
- $w'$  is the fluctuation of air velocity

The rational of the above formula is simply understood, since  $\rho_x x$  is the mass of the quantity  $x$  present in the control volume, and  $w'$  is the upward net velocity excess.

The relevant quantities transported in our cases are:

- $-\rho_a u'$  is the momentum [ $\text{Kg m}^{-2} \text{ s}^{-1}$ ],  $u'$  is the fluctuation of horizontal velocity of air [ $\text{m s}^{-1}$ ] and  $\rho_a$  is the air density [ $\text{kg m}^{-3}$ ].

- specific thermal energy or sensible heat:  $\rho_a c_p T'$  [ $\text{W m}^{-2}$ ], where  $c_p$  [ $\text{J kg}^{-1} \text{K}^{-1}$ ] is the thermal capacity of air and  $T$  its temperature [ $^\circ\text{K}$ ].
- vapor,  $-\rho_a q'$  [ $\text{Kg m}^{-3}$ ], where  $q$  is the specific humidity of air (mass concentration of water vapor in air)

Momentum has a negative sign because it is transported downward. Thus we have, accordingly to the above consideration, the momentum flux,  $\tau$  [ $\text{N m}^{-2}$ ]:

$$\tau = -\overline{\rho_a w' u'} \quad (2.9)$$

Thermal energy flux,  $H$ , [ $\text{W m}^{-2}$ ]:

$$H = \overline{\rho_a c_p w' T'} \quad (2.10)$$

Vapor flux, a.k.a as evapotranspiration,  $ET$  [ $\text{m s}^{-1}$ ]:

$$ET = \overline{\rho_a w' q'} \quad (2.11)$$

The momentum transfer is regulated by Navier-Stokes equations (NSE):

$$\rho_a \left( \frac{\partial \vec{v}}{\partial t} + \vec{v} \nabla \cdot \vec{v} \right) = -\vec{\nabla} p + \nabla \cdot \mathbf{T} + \vec{f} \quad (2.12)$$

i.e. (Batchelor, 1967), where:

- $\vec{v}$  is the velocity of the air (fluid)
- $\nabla \cdot$  is the divergence operator
- $\vec{\nabla}$  is the gradient operator
- $p$  is the normal stresses (pressure)
- $\mathbf{T}$  is the stresses tensor
- $\vec{f}$  are the external forces acting

NSe can be, in fact, the starting point for a simplifications journey which arrives to results similar to the mixing layer theory based on the assumptions that:

- we can separate the average flow velocity from fluctuations:  
 $\vec{v} = (\bar{u} + u', \bar{v} + v', \bar{w} + w')$
- the flow is over a plane (it throws away the vertical axes dependencies on the left hand side of the equation)
- it is stationary (it eliminates the time derivative)
- homogeneous
- without subsidence
- the molecular viscosity can be neglected

The simplification path takes away almost everything for NSe and leaves only:

$$\frac{\partial}{\partial z} \overline{u'w'} = 0 \rightarrow \overline{u'w'} = \text{constant} \quad (2.13)$$

or  $\overline{u'w'} = \text{constant}$  which gives an important information about the momentum transport in equation (2.9). It can be considered also an empirical results, coming from one hundred year and more of experiments on turbulent flows.

A further leap in Prandtl theory is that:

- fluctuations in equation 2.9, 2.10, 2.11 can be substituted by spatial finite gradients of the same quantities
- the vertical fluctuation of velocity is proportional to the mean horizontal velocity such that:

$$\overline{w'T'} = C_H \Delta \bar{u} \cdot \Delta \bar{T} \quad (2.14)$$

where  $C_H$  is called Stanton Number;

$$\overline{w' u'} = C(\Delta \bar{u})^2 \quad (2.15)$$

where  $C$  is called drag number;

$$\overline{w' q'} = C_E \Delta u \Delta q \quad (2.16)$$

where  $C_E$  is called Dalton Number.

These assumptions make the Prandtl expressions in 2.9, 2.10, 2.11 evaluable once the coefficients  $C, C_H, C_E$  are determined. Concentrating our attention to the momentum transfer, the horizontal flow velocity at the surface is zero and, therefore,  $\Delta \bar{u} = u$ . Besides, because  $\overline{u' w'} = constant$ , we can define:

$$\overline{u' w'} := u_x^2 \quad (2.17)$$

where  $u_*^2$  is called friction velocity. By comparison of (2.17) with (2.15), it results then:

$$C \equiv \frac{u_x^2}{\bar{u}^2} \quad (2.18)$$

which does not help yet, but will be useful soon. Finally, experiments (McDonough, 2007) and recent mathematical treatments of the NSe (She et al., 2017), confirm that, closely to the boundary, in the conditions above specified, the velocity in a turbulent field grows with a logarithmic profile. This translates, in our notation into:

$$\bar{u} = \frac{u_x}{k} \ln \left( \frac{z - z_d}{z_0} \right) \quad (2.19)$$

where

- $k \sim 0.41$  is the von Karman constant
- $z$  is the height above the plane,
- $z_d$  is the zero displacement level and
- $z_0$  is the surface roughness.

Consequently, it is:

$$C = \frac{u_x^2}{\bar{u}^2} = \frac{k^2}{\ln^2 \frac{z-z_d}{z_0}} \quad (2.20)$$

which is the well known formula for *aerodynamic conductance* or its inverse, the *aerodynamics resistance*:

$$r_a := \frac{1}{C} \quad (2.21)$$

We do not enter for now in the estimation of  $C_E$  and  $C_H$  which, however, should be related to  $C$  and, in some peculiar cases, should be set equal to it.

### 2.2.1 Dalton's law of evaporation

Therefore our starting point is the acceptance of the Dalton equation:

$$ET = C_E \bar{u} (q_{z_0} - q_z) \quad (2.22)$$

which derives directly from (2.16) where:

- $ET$  is evapotranspiration,  $[\text{m s}^{-1}]$
- $C_E$  is a dimensionless evaporation “conductance”
- $\bar{u}$  is the mean horizontal velocity (of a turbulent air field),  $[\text{m s}^{-1}]$
- $q_{z_0}$  is specific humidity at the evaporation source position ( $z_0$ ,  $[\text{m}]$ ) [adimensional]
- $q_z$  is the specific humidity of air at quote  $z$  [adimensional]

Dalton's law expresses that a certain quantity of water vapor is taken from a region where its concentration is  $q_{z_0}$  to a region where it is  $q_z$ , if  $q_{z_0} > q_z$ . Also viceversa can happen if  $q_{z_0} < q_z$ .

Nothing moves in case of equality of  $q_{z_0}$  and  $q_z$ . It does not express anything on the physical reasons that cause concentration having those values at the bottom and top boundaries of the control volume.

All the expression and, in particular,  $C_E$  is a suitable simplification of the turbulence that moves it all. In principle, it can be substituted by the direct resolution (by numerical integration) of the NSe or one of its simplification, like large eddy simulations (LES), (e.g. McDonough (2002)) and the appropriate transport equation. If the water mass flux of water is desired, the Dalton equation must be multiplied by the density of air  $\rho_a$  so that the formula, in that case is:

$$ET^{[m]} = \rho_a C_E \bar{u} (q_{z_0} - q_z) \quad (2.23)$$

[Kg m<sup>-2</sup>] If the equivalent (latent) energy transported is desired, the mass formula must be further multiplied by the latent heat of (water) vaporization, usually denoted as  $\lambda$ . Its value is  $\lambda = 2264.705$  [at 100°, KJ Kg<sup>-1</sup>]. We will denote the latent heat flux as  $\lambda ET$  ( $\lambda$  multiplied by  $ET$ ). Specific humidity is the mass of water divided by the mass of air (air gas plus water vapor). Therefore:

$$q := \frac{M_w}{M_a} = \frac{\rho_a}{\rho_a} \quad (2.24)$$

where

- $\rho_a$  is the vapor density and
- $\rho_a$  is the air density.

the expression containing the densities allows for using the ideal gas law and relating the previous expression with those containing the partial pressures of water vapor.

Traditionally for water vapor, pressure is denoted as  $e$  and therefore the ideal gas law reads:

$$e = \rho_a R_v T \quad (2.25)$$

where:

- $\rho_a$  is the density of water vapor,
- $R_v = 461 \text{ [J } ^\circ \text{K}^{-1} \text{ kg}^{-1}]$  and

For dry air we can write, equally likely:

$$p_d = \rho_d R_v T \quad (2.26)$$

where:

- $\rho_d$  is the density of dry air,  $R_v = 287 \text{ [J } ^\circ \text{K}^{-1} \text{ kg}^{-1}]$ .

Therefore, it is

$$q \sim \epsilon \frac{e}{p_d} \quad (2.27)$$

where:

- $\epsilon := R_d/R_v \sim 0.622$ .

This allows for writing the Dalton evaporation law in term of mass flow as:

$$ET^{[m]} = \rho_a C_E \bar{u} \frac{\epsilon}{p_d} (e^*(z_0) - e(z)) \quad (2.28)$$

Evapotranspiration, is also expressed in terms of moles:

$$ET^{[mol]} = E_{l,mol} M_w \lambda_E \quad (2.29)$$

Where:

- $M_w$  is the molar mass of water  $[\text{kg mol}^{-1}]$
- $\lambda_E$  is the latent heat of vaporisation  $[\text{J kg}^{-1}]$
- $E_{l,mol}$  was computed in molar units  $[(\text{mol m}^{-2} \text{ s}^{-1})]$  as a function of the concentration of water vapour at the emitting surface ( $C_{wl}$ ,  $[\text{mol m}^{-3}]$ ) and in the free air ( $C_{wa}$ ,  $[\text{mol m}^{-3}]$ ) (Frank P. Incropera, David P. DeWitt, Theodore L. Bergman, 2002).

In this case the Dalton laws takes the form:

$$E_{l,mol} = g_{tw}(C_{wl} - C_{wa}) \quad (2.30)$$

$g_{tw}$  is the total conductance for water vapor [ $m s^{-1}$ ].

### 2.2.2 Convective transport of thermal energy (sensible heat)

As we can derive from section 2, transport of thermal energy (or sensible heat, as it is known), follows a law similar to Dalton law:

$$H = \rho_a C c_p \bar{u} (T_{z_0} - T_z) \quad (2.31)$$

where:

- $H$  is the latent heat flux per unit area [ $\text{W m}^{-2}$ ]
- $\rho_a$  is the air density [ $\text{kg m}^{-3}$ ]
- $C$  is the Stanton number [-]
- $c_p$  is the specific thermal capacity or air, [ $\text{J Kg}^{-1} \text{ }^{\circ}\text{K}^{-1}$ ]
- $\bar{u}$  is the mean horizontal velocity [ $\text{m s}^{-1}$ ]
- $T$  is temperature [ ${}^{\circ}\text{K}$ ]

Inspection of the formula makes clear that it is homogeneous dimensions with  $\lambda ET$ .

## 2.3 Derivation of the energy balance

### 2.3.1 The energy budget

A third equation that contains evapotranspiration is the energy budget. It can be written, for a unit area, as:

$$\frac{dU}{dt} = \underbrace{P + E_A}_{advection} + \underbrace{R_s + R_l}_{radiation} - \underbrace{aH - b\lambda ET^{(m)}}_{convection} - \underbrace{G}_{conduction} - \underbrace{E_V}_{chemical energy} \quad (2.32)$$

where:

- $U$  is the internal energy of the element considered [ $\text{J m}^{-2}$ ]
- $R_s$  is the net shortwave radiation [ $\text{W m}^{-2}$ ]
- $R_l$  is the net longwave radiation [ $\text{W m}^{-2}$ ]
- $a$  is the ratio between the heating/cooling surface and its projection (usually equal to 1 or 2)
- $H$  is the thermal energy transport
- $b$  is the ratio between the evaporating surface and its projection on a horizontal plane (usually equal to 1 or 2)
- $ET$  is evapotranspiration
- $G$  is the outgoing thermal flux due to conduction [ $\text{W m}^{-2}$ ]
- $P$  is the incoming energy due to precipitation [ $\text{W m}^{-2}$ ]
- $E_A$  is the advected energy into the control volume [ $\text{W m}^{-2}$ ]
- $E_V$  is the energy stored in chemical bounds (due, for instance, to photosynthesis that produces carbohydrates) inside the control volume [ $\text{W m}^{-2}$ ]
- $S_{rc}$  are positive if source of energy

- $S_{nk}$  are positive if sink of energy

We neglect in the budget the action of external forces fields, like gravity, which can be added when required. As written, the equation is of general validity, but usually  $P$ ,  $E_A$  and  $E_V$  are neglected. In the simplest approaches also  $dU/dt$  is neglected, assuming either that the system is stationary or that its dynamics can be considered as a sequence of stationary states, in equilibrium with the energy forcings. Therefore, the form of the equation we deal with here is:

$$R_s + R_{ll} = aH + b\lambda ET + S_{nk} \quad (2.33)$$

where we have taken away the sources of energy and left all the sinks in aggregate form.

### 2.3.2 The Clausius-Clapeyron equation

As product of the previous analysis, we have then three equations that needs to be solved simultaneously:

$$ET^{(m)} = \rho_a C_E \bar{u}(q^\#(z_0) - q_z) = \frac{\epsilon}{p_d} \rho_a C_E \bar{u}(e^\#(z_0) - e(z)) \quad (2.28)$$

$$H = \rho_a C c_p \bar{u}(T_{z_0} - T_z) \quad (2.31)$$

$$R_s + R_{ll} = aH + b\lambda ET^{(m)} + S_{nk} \quad (2.33)$$

The unknown of these equation are, however, four: (1)  $ET$ , (2)  $q_\Delta := (q^\#(z_0) - q_z)$ , (3)  $H$  and (4)  $T_\Delta := (T_{z_0} - T_z)$ , if  $R_{ll}$  is assumed measured (in this case we are dealing with the so called radiatively uncoupled-energy budget). With three equations and four unknowns, we cannot get the solutions, and, therefore, we need to find out another equation. Under the hypothesis that the specific humidity at the evaporating surface is the equilibrium one,

this equation, can be provided by the Clausius-Clapeyron equation (CCe). This is, often forgotten, a strong assumption, that requires, in particular that the system is not water limited.

It relates saturation vapor pressure to temperature and reads, for the case of ideal gases:

$$e^*(T) = e^*(T_{ref}) \exp^{-\frac{\lambda}{R} \left( \frac{1}{T} - \frac{1}{T_{ref}} \right)} \quad (2.34)$$

where  $e^*(T_{ref})$  and  $T_{ref}$  are respectively the saturation water pressure at  $T_{ref}$  and  $T_{ref}$  is a reference temperature (in Kelvin).

As we said, the form of Dalton equation that derives from the use of saturated specific humidity in it is an educated guess which could not work in all occasions. Certainly it works for a water surface (with corrections for salinity, if the case applies) but could not work for vegetation or soil under scarce water supply. At the moment, however, we apply it.

The set of equations (2.28),(2.31),(2.33) and(2.34) is now well formed. However, it is a non linear system (because CCe is a non-linear relation) and a closed solution cannot be found for it.

### 2.3.3 The Penman linearization

To get a linear system instead of the previous non linear one, Penman (1948) had the idea to eliminate the specific equilibrium humidity as a function of surface temperature by using its Taylor's expansion, around air temperature (which is actually the same that linearizing the CCe):

$$q^*(z_0) \approx q^*(T_{z_0}) \quad (2.35)$$

$$q^*(T_{z_0}) = q(T_z) + \frac{dq^*}{dT}|_{T=T_z} (T_{z_0} - T_z) + O((T_{z_0} - T_z)^2) \quad (2.36)$$

where:

$$\frac{dq^*}{dT} = \frac{\epsilon}{p_d} \Delta_{eT} \quad (2.37)$$

and  $\Delta_{eT}$  is the derivative of the Clausius-Clapeyron equation with respect to temperature.

$$\Delta_{eT} = \frac{de^*}{dT} = \frac{25083}{(T + 273.3)^2} e^{\frac{17.3T}{T+273.3}} \quad (2.38)$$

where:

- $T$  is the temperature [ $^{\circ}\text{C}$ ],
- $e$  is the pressure [mb].

Accordingly to previous equations we also define:

$$e^*(z_0) = e^*(z) + \Delta_{eT}(T_{z_0} - T_z) \quad (2.39)$$

and

$$e^*(z_0) - e(z) = \underbrace{e^*(z) - e(z)}_{\delta e(z)} + \Delta_{eT}(T_{z_0} - T_z) \quad (2.40)$$

where:

- $\delta e(z)$  is called evaporation demand.

Finally (2.39) can be rewritten as:

$$e_{\Delta} = \delta e(z) + \Delta_{eT} T_{\Delta} \quad (2.41)$$

Other authors, used quadratic approximation of the CCe (still obtaining a closed form solution).

### 2.3.4 Solving the Penman-Monteith System step by step

We call Penman-Monteith system (PMs), the system of equations (2.28), (2.31), (2.33) and (2.41). Monteith (1985) in fact, is the one who assumed first that drag and Dalton coefficients could be

different. PMS is linear and can be solved by substitution.

First insert (2.28) into (2.33), obtaining:

$$R_s = a_{sH}H + a_{sE}\lambda\rho_a C_{Da} \frac{\epsilon}{p} \bar{u} e_\Delta + R_{ll} + S_{nk} \quad (2.42)$$

Equation (2.31) can be then inserted into (2.42), obtaining:

$$R_s = a_{sH}\rho_a C_{Dr} c_p \bar{u} T_\Delta + a_{sE}\lambda\rho_a C_{Da} \frac{\epsilon}{p} \bar{u} e_\Delta + R_{ll} + S_{nk} \quad (2.43)$$

Substituting (2.41) into the previous equation, we then obtain an expression where the only variable is  $T_\Delta$ :

$$R_s = a_{sH}\rho_a C_{Dr} c_p \bar{u} T_\Delta + a_{sE}\lambda\rho_a C_{Da} \frac{\epsilon}{p} \bar{u} (\delta e(z) + \Delta_{eT} T_\Delta) + R_{ll} + S_{nk} \quad (2.44)$$

Collecting  $T_\Delta$ , we obtain:

$$R_s - R_{ll} - S_{nk} - a_{sH}\lambda\rho_a C_{Da} \frac{\epsilon}{p} \bar{u} \delta e(z) = T_\Delta (a_{sH}\rho_a C_{Dr} c_p \bar{u} + a_{sH}\lambda\rho_a C_{Da} \frac{\epsilon}{p} \bar{u} \Delta_{eT}) \quad (2.45)$$

or:

$$T_\Delta = \frac{R_s - R_{ll} - S_{nk} - a_{sE}\lambda\rho_a C_{Da} \frac{\epsilon}{p} \bar{u} \delta e(z)}{a_{sH}\rho_a C_{Dr} c_p \bar{u} + a_{sE}\lambda\rho_a C_{Da} \frac{\epsilon}{p} \bar{u} \Delta_{eT}} \quad (2.46)$$

Collecting  $\rho_a \bar{u}$  at the denominator results:

$$T_\Delta = \frac{R_s - R_{ll} - S_{nk}}{\rho_a \bar{u} (a_{sH}C_{Dr} c_p + a_{sE}\lambda C_{Da} \frac{\epsilon}{p} \Delta_{eT})} - \frac{a_{sH}\lambda C_{Da} \frac{\epsilon}{p} \delta e(z)}{a C c_p + b \lambda C_{Da} \frac{\epsilon}{p} \Delta_{eT}} \quad (2.47)$$

Once defined the psychrometric "constant" as:

$$\gamma := \frac{c_p p}{\epsilon \lambda} \quad (2.48)$$

equation (2.47) becomes:

$$T_\Delta = \frac{\gamma}{a_{sH}C_{Dr}\gamma + a_{sE}C_{Da}\Delta} \frac{R_s - R_{ll} - S_{nk}}{\rho_a \bar{u} c_p} - \frac{C_{Da}}{a_{sH}C_{Dr}\gamma + a_{sE}C_{Da}\Delta_{eT}} \delta e(z) \quad (2.49)$$

At this point the value of  $T_\Delta$  can be substituted back into the other equations. Using (2.41) first, we obtain:

$$e_\Delta = \delta e(z) + \Delta_{eT} \left[ \frac{\gamma}{a_{sH}C_{Dr}\gamma + a_{sE}C_{Da}\Delta_{eT}} \frac{R_s - R_{ll} - S_{nk}}{\rho_a \bar{u} c_p} - \frac{C_{Da}}{a_{sH}C_{Dr}\gamma + a_{sE}C_{Da}\Delta_{eT}} \right] \quad (2.50)$$

which results in:

$$e_\Delta = \frac{\gamma \Delta_{eT}}{a_{sH}C_{Dr}\gamma + a_{sH}C_{Da}\Delta_{eT}} \frac{R_s - R_{ll} - S_{nk}}{\rho_a \bar{u} c_p} + \frac{a_{sH}C_{Dr}\gamma + (a_{sE} - 1)C_{Da}\Delta_{eT}}{a_{sH}C_{Dr}\gamma + a_{sH}C_{Da}\Delta_{eT}} \delta e(z) \quad (2.51)$$

For what regards the enthalpy transport in (2.31):

$$H = \frac{C_{Dr}\gamma}{a_{sH}C_{Dr}\gamma + a_{sE}C_{Da}\Delta_{eT}} (R_s - R_{ll} - S_{nk}) - \frac{\rho_a c_p \bar{u} C_{Dr} C_{Da}}{a_{sH}C_{Dr}\gamma + a_{sE}C_{Da}\Delta_{eT}} \delta e(z) \quad (2.52)$$

Finally for  $ET$  substitution results in:

$$ET = \rho_a C_{Da} \frac{\epsilon}{p} \bar{u} \left[ \frac{\gamma \Delta_{eT}}{a_{sE}C_{Dr}\gamma + a_{sE}C_{Da}\Delta_{eT}} \frac{R_s - R_{ll} - S_{nk}}{\rho_a \bar{u} c_p} + \frac{a_{sH}C_{Dr}\gamma + (a_{sE} - 1)C_{Da}\Delta_{eT}}{a_{sH}C_{Dr}\gamma + a_{sE}C_{Da}\Delta_{eT}} \delta e(z) \right] \quad (2.53)$$

from which, by multiplying for  $\lambda$  and using the definition of the psychometric constant, it is obtained:

$$\lambda ET = \frac{C_{Da}\Delta_{eT}}{C_{Dr}\gamma + a_{sE}C_{Da}\Delta_{eT}} (R_s - R_{ll} - S_{nk}) + \frac{\rho_a \bar{u} c_p a_{sE}C_{Dr} C_{Da} + (a_{sE} - 1)C_L^2}{a_{sH}C_{Dr}\gamma + a_{sE}C_{Da}\Delta_{eT}} \quad (2.54)$$

Equations (2.49), (2.51), 2.52 and (2.54) are explicit solutions of the Penman-Monteith system, as obtained by Schymanski and Or (2017), and we call them PMSO solutions.

There are a few remarks to be done on PMSO (excluding those implied by the approximations they contain).

- The first is that those equations are valid for any time interval (not specifically for hourly, daily or monthly intervals), as soon as the forcings are given with the appropriate time step.

- The second is that, and the merit of this has to be given to Schymanski and Or (2017), that is a system resolution, which gives, not only  $ET$ , but also  $H$ ,  $e_\Delta$ , and  $T_\Delta$ .

If, for a given problem, we have  $e(z)$  and  $T_z$  as Dirichlet type of boundary conditions, then we immediately have  $e^*(z)$  (which is not a surprise when understood that CCe was used) and  $T_{z_0}$  as a consequence. The solutions obtained are the so called radiatively uncoupled solutions. In fact it was assumed  $R_{ll}$  to be independent from the evaporating surface temperature, which is not actually the case. The coupled system implies further linearizations to obtain closed form solutions of the PMs, which we will describe in next sections.

### 2.3.5 Different transpiring surfaces: the case of leaves and soils

We now specialise the budget for a single leaf. The problem with leaves, as brought to evidence by Schymanski and Or (2017), is that leaves have 2 faces and, therefore they exchange heat from the two sides, i.e., in the previous formulas,  $a_{sH} = 2$ . Stomata are instead can be either on the bottom side of the leaves ( $a_{sE} = 1$ ), which is the most diffuse case and it is called hypostomatous case, and on both the sides of a leave (amphistomatous,  $a_{sE} = 2$ ). Besides, for leaves, conduction of heat can be neglected and  $S_{nk} = 0$ . So, for the hypostomatous case, the PM solutions read:

$$T_\Delta = \frac{\gamma}{2C_{Dr}\gamma + C_{Da}\Delta_{eT}} \frac{R_s - R_{ll}}{\rho_a \bar{u} c_p} - \frac{C_{Da}}{2C_{Dr}\gamma + C_{Da}\Delta_{eT}} \delta e(z) \quad (2.55)$$

$$e_\Delta = \frac{\gamma \Delta_{eT}}{2C_{Dr}\gamma + C_{Da}\Delta_{eT}} \frac{R_s - R_{ll}}{\rho_a \bar{u} c_p} + \frac{2C_{Dr}\gamma}{2C_{Dr}\gamma + C_{Da}\Delta_{eT}} \delta e(z) \quad (2.56)$$

$$H = \frac{C_{Dr}\gamma}{2\Delta_{eT}\gamma + C_{Da}\Delta_{eT}} (R_s - R_{ll}) - \frac{\rho_a c_p \bar{u} C_{Dr} C_{Da}}{2C_{Dr}\gamma + C_{Da}\Delta_{eT}} \delta e(z) \quad (2.57)$$

$$\lambda ET = \frac{C_{Da}\Delta_{eT}}{2C_{Dr}\gamma + C_{Da}\Delta_{eT}}(R_s - R_{ll}) + \frac{2\rho_a \bar{u} c_p C_{Dr} C_{Da}}{2C\gamma + C_{Da}\Delta_{eT}} \delta e(z) \quad (2.58)$$

The case of amphistomatous leaves has instead both  $a_{sH} = 2$  and  $a_{sE} = 2$  and the related formulas are easily obtainable. In the case of soil, a trivial application of the Schymanski and Or equations is obtained with both  $a_{sH} = 1$  and  $a_{sE} = 1$ . This is actually used in literature but it is known not to work well, unless corrections, in form of limitation of fluxes in dependence on water soil content, is used. We do not start this debate here but we will try to dig into the topic later on.

### 2.3.6 The radiatively coupled system

Unfortunately, even if the previous equations (in some wrong form) were applied for more than fifty years, the longwave radiation,  $R_{ll}$  is coupled to the evaporating surface temperature. In fact, it can be usually decomposed into two main contribution:

$$R_{ll} = R_{ll} \uparrow - R_{ll} \downarrow \quad (2.59)$$

where:

- $R_{ll} \uparrow$  is the upwelling longwave radiation outgoing from the surface and
- $R_{ll} \downarrow$  is the downwelling longwave radiation, coming mainly from the sky and clouds

For the parameterization of the latter, please see for instance Formetta et al. (2016). The first simply depends on the evaporating surface temperature according to the Stefan-Boltzmann law:

$$R_{ll} \uparrow = \epsilon \sigma T_{z_0}^4 \quad (2.60)$$

where:

- $\epsilon \approx 1$  is the surface emissivity (for the most of surfaces),
- $\sigma$  is the Stefan-Boltzman constant [ $\sigma = 5.670374419 \times 10^{-8} \text{ W m}^{-2}\text{K}^{-4}$ ]

We can then assume that  $R_l \downarrow$  is given, while  $R_l \uparrow$  must be obtained by the resolution of the system. Unfortunately, the energy budget becomes a non linear equation in  $T_{z_0}$ . In fact, it is:

$$R_s = a_{sH}\rho_a C_{Dr} c_p \bar{u}(T_{z_0} - T_z) + a_{sE}\lambda\rho_a C_{Da} \frac{\epsilon}{p} \bar{u}(\delta e(z) + \Delta(T_{z_0} - T_z)) + \epsilon\sigma T_{z_0}^4 + S_{nk} \quad (2.61)$$

This is a polynomial system of the type:

$$aT_{z_0}^4 + bT_{z_0} + c = 0 \quad (2.62)$$

and the four exact solutions can be found (with only one of physical significance).

Alternatively it can be implemented an iterative solution of the system, assuming for instance  $T^4(z_0) = T_0^3 T_{z_0}$  where:

- $T_0$  is some approximate value of T (for instance the one given by the solution at the last past time interval).

Notably, because here, we have to possibly resort to iterative numerics, the CCe can be used directly in the system, instead of using one of its approximations.

### 2.3.7 Including the Monin-Obukhov Similarity Theory (MOST)

All the previous derivation is affected by the treatment of turbulence according to the mixing length theory especially for the Dalton's law and the thermal energy flux. The obvious extension of Prandtl's theory is the application of the MOST (Foken, 2006),

which brings the following corrections to the drag coefficient (e.g. Yang et al. 2001, Banerjee et al. 2017):

$$C = k^2 \bar{u}(z) \left[ \ln \left( \frac{z - z_d}{z_{0m}} \right) - \psi_m(\zeta_d, \zeta_{0m}) \right]^{-1} \left[ \left( \frac{z - z_d}{z_{0*}} \right) - \psi_*(\zeta_d, \zeta_{0*}) \right]^{-1} \quad (2.63)$$

where:

- $z_{0m}$  is the roughness length for momentum transfer
- $z_{0*}$  is the roughness length for the specific transport (i.e. thermal energy or enthalpy)
- $\psi_m$  is an integral stability correction function for momentum
- $\psi_*$  is an integral stability correction function for the specific transport \*
- $\zeta_d := (z - z_d)/L$
- $\zeta_{0m} := z_{0m}/L$  is the roughness length for momentum
- $\zeta_{0*} := z_{0*}/L$  is the roughness length for the specific transport
- $L = -u_*^3 * / (kg \overline{w'^*})$  is the Obukhov length for the specific transport
- $g = 9.81 \text{ [m s}^{-2}\text{]}$  is the gravitational acceleration
- \* Is the transported quantity

Banerjee et al. (2017) suggests also that a correction must be given for obtaining the conductance for thermal energy transfer and latent heat transfer such that:

$$C_E = \frac{C_{Dr}}{P_E} \quad (2.64)$$

and

$$C_H = \frac{C_{Dr}}{P_H} \quad (2.65)$$

where  $P_E$  is the turbulent Prandtl number for latent heat transport and  $P_H$  is the Prandtl number for sensible heat:

- $P_E := \frac{K_m}{K_E}$
- $P_H := \frac{K_m}{K_H}$
- $K_m$  is the momentum eddy diffusivity
- $K_E$  is the latent heat eddy diffusivity
- $K_H$  is the sensible heat eddy diffusivity

The so called stability parameters  $\zeta_{0*}$  can be obtained as follows:

- $\zeta_{0m} = \frac{z_{0m}}{L}$
- $\zeta_{0H} = \frac{z_{0H}}{L}$
- $\zeta_{0E} = \frac{z_{0E}}{L}$

Negative  $\zeta$  indicates unstable stratification; positive values indicate stable stratification.

Finally, the integral stability correction functions  $\psi$  can be obtained as in Liu et al. (2007) such that:

$$\psi_m(\zeta, \zeta_{0m}) = 2 \ln \left( \frac{1+x}{1+x_0} \right) + \ln \left( \frac{1+x^2}{1+x_0^2} \right) - 2 \tan^{-1} z + 2 \tan^{-1} x_0 \quad (2.66)$$

where:

- $x := (1 - \gamma_m \zeta)^{1/4}$
- $x_0 := (1 - \gamma_m \zeta_{0m})^{1/4}$

$$\psi_H(\zeta, \zeta_{0h}) = 2 \ln \left( \frac{1+y}{1+y_0} \right) \quad (2.67)$$

where:

- $y = (1 - \gamma_H \zeta)^{1/2}$
- $y_0 = (1 - \gamma_H \zeta_{0H})^{1/2}$

The  $\gamma$ s are parameters whose values differ in literature. Paulson (1970) suggests  $\gamma_H = \gamma_m = 16$ . For more details, please refer to Banerjee et al. (2017).

## 2.4 Introducing the water budget

The water budget is missing in the previous sections after the introduction of the Clausius-Clapeyron equation as key for getting solutions. It reads, for a generic control volume:

$$\frac{dS}{dt} = P - ET - R \quad (2.68)$$

where:

- $S$  [kg] or [m] is the water content
- $P$  [kg] or [m] is (any type of) precipitation
- $ET$  is evapotranspiration [kg] or [m]
- $R$  represents all the runoffs [kg] or [m]

Either the mass or the length or the mass units must be used consistently. Given for granted that this equation has to be satisfied simultaneously with the other four that we dealt with in the previous sections, it remains unclear how it interacts with the others. The hypothesis to use the saturated water vapor and the Clausius-Clapeyron formula, in fact, decouples the mass budget from the other equations.

It is evident that mass budget poses a limiting behavior, i.e.  $ET$  cannot be greater than  $P - \frac{dS}{dt}$  and in literature, this limitation

is accomplished by introducing a stress factor,  $f$  such that:

$$AET = f ET \quad (2.69)$$

where:

- $f$  is a dimensionless stress factor
- $AET$  is the actual evapotranspiration

The stress factor is usually function of the relative water content, the fraction of the existing water content over the maximum water content possible in the control volume. Another approach, popularized by Monteith (1985) is that missing water acts like an additional resistance, to add to the aerodynamic ones, given by  $1/C_{Dr}$ ,  $1/C_E$  and  $1/C_H$ . In this case the derivation made in the previous section remains valid after the appropriate substitution of  $C_E$  with the appropriate conductances.

For example, assuming soil produces a resistance, it will be:

$$\hat{C} = \frac{1}{1/C_E + 1/C_s} \quad (2.70)$$

where

- $\hat{C}$  is the new total conductance
- $C_s$  is the soil conductance

The analogy with the electric circuitry is evident. In the case of vegetation, the stomatal ( $g_{sw}$ ) and the boundary layer conductance ( $g_{bw}$ ) are those that enters in a similar formula:

$$g_{tw} = \frac{1}{\frac{1}{g_{sw}} + \frac{1}{g_{bw}}} \quad (2.71)$$

As the analysis performed in this manuscript supports, we suggest that a more proper way to cope with the phenomenon of water stress is to give a proper expression of  $e^{\#}(z_0)$  in Eq. 2.28,

substituting an appropriate value for it which differ from the CCe derived  $e^*(z_0)$ .

Another, more subtle maybe, aspect is that, when we deal with evaporating surfaces like the leaf or soil, because evaporation ultimately is emitted from stomata or pores, the effective evaporating surface can be less than the total surface, a fact enlightened by Shahraeeni et al. (2012). We propose therefore below a more detailed analysis of these aspects, starting from soils in the next section and for vegetation in the next chapter.

### 2.4.1 The case of soils

Lehmann et al. (2008) provides a comprehensive analysis of the dynamics of evaporation from soil. At the small scales, soil is a fractal random medium: a set of voids of different diameter, that, as a first approximation, can be considered, as a 3D bundle of tubes of varying radius with a certain distribution which varies with soils texture and structure. When we have stratified soil where the mean properties and the statistics can vary abruptly from one horizon to the other, still each horizon is described as a random porous medium.

As all know, water is retained with different energies inside these pores, according to the radius and the Young-Laplace law (e.g., Lu and Godt, chapter 3)

$$\psi = -\frac{2\gamma}{\rho_w gr} \quad (2.72)$$

where  $\psi$  [m] is the pressure head in the vadose soil,  $\gamma = 0.0728$  [ $J/m^2$  at  $20^\circ C$ ] is the surface tension and  $r$  [m] the pore radius.

Thus, when soil is filled with water and water starts to evaporate, large pores are emptied first because their suction is smaller than that of smaller pores. The evaporating demand is uniform and withdraw water from any place, but, at the same time, water is

supplied from the largest pores to the smaller ones when they are emptied. Experiments and measures (e.g. Or et al., 2013) show that evaporation is working as  $e^\# = e^*$  even in non saturated conditions (stage I evaporation) up to a threshold condition when it starts to decrease fast to zero. The latter is called stage II, evaporation.

### 2.4.2 Stage I evaporation from soil

According to Lehmann et al. (2008), stage I evaporation continues until water capillary flow can arrive at the soil surface and falls when the water supply to the surface breaks. During stage I evaporation, the liquid phase is connected, in stage II it is disconnected, at least at the surface, and evaporation is supported by water flow (as opposed to water flow). We are concerned here with the duration of stage I, under which we can think that the vapor phase at the surface is closely at the saturation content.

According to Lehmann et al. (2008), we can recognize a bulk water phase, below a certain level from the surface, i.e. a water table, which feeds an upward water flow until this depth arrives to a critical value,  $L_C$ . Below this level, continuity of the water phase cannot be sustained anymore. To estimate this  $L_C$  capillary forces, gravity and viscous losses must be in equilibrium as Lehmann et al. (2008) accurately derives.  $L_C$  depends on soil characteristics and it is:

$$L_C = \frac{L_G}{1 + \frac{ET(z_0)}{k(\theta)}} \quad (2.73)$$

where  $L_G$  can be expressed as a function of soil parameters. i.e., choosing for the soil characteristics the van Genuchten-Mualem curves:

$$L_G = \frac{1}{\alpha(n-1)} \left( \frac{2n-1}{n} \right)^{(2n-1)/n} \left( \frac{n-1}{n} \right)^{(1-n)/n} \quad (2.74)$$

The variables present above are:

- $\alpha$  [ $m^{-1}$ ] is the van Genuchten (vG)  $\alpha$  parameter, usually associated with the air entry point
- $n$  [-] is another vG parameter
- $ET(z_0)$  is the evaporation demand at the surface
- $K(\theta)$  [ $m s^{-1}$ ] is the vG-Mualem hydraulic conductivity
- $\theta$  [-] is the dimensionless volumetric water conductivity

To put forward some numbers, in sandy soil, this length results of the order of 5 to 10 cm.

Assuming to have a completely saturated soil at the beginning, thus evaporation works as we have vapor saturation at soil surface until the water table depth arrive to  $L_C$ .

To control how this happens, we can use Richards equation or, if we adopt a simpler reservoir model, we can follow the water budget:

$$\frac{d\xi}{dt} = +ET + R - P \quad (2.75)$$

where:

- $\xi$  [m] is the water deficit  $\xi = S_{max-S}$  where  $S_{max}$  is the maximum storage available in the control volume
- $ET$  [ $m s^{-1}$ ] is evaporation
- $R$  [ $m s^{-1}$ ] contains all the types of runoff and
- $P$  [ $m s^{-1}$ ] is liquid precipitation

when  $\xi > L_C$  stage I evaporation ends. The resilience of the stage I evaporation reminds that water is a cohesive medium, which can resist to large tensions, as shown in plants hydromechanics (e.g. Choat et al., 2005). Soils do not have the mechanism that vegetation has to prevent embolism.

### 2.4.3 Stage II evaporation from soil

Stage II  $E_t$  is controlled by the fractal nature of the evaporating medium. As anticipated above, according to Lehmann et al. (2008), a dynamic capillary fringe whose extension to the soil surface is responsible for the evaporation rates. When the capillary fringe lowers and detaches from the surface, evaporation stage II starts. This situation is well represented in Figure 1 of Shokri and Or (2011) and seems to be appropriately described by the percolation theory developed by Wilkinson (1986) and Sapoval et al. (1985).

Equation (3) from Shokri and Or (2011) can be used to establish the evaporative flux. It reads:

$$ET_0 = D \frac{dq}{dz} \sim \frac{\theta_a^{2.5}}{\theta_s} D_{atm} \frac{q^* - q(z_0)}{\xi} \quad (2.76)$$

with  $\xi > L_C$  defined above and:

- $ET_0$  [ $\text{m s}^{-1}$ ] evaporation at the soil surface (technically at the end of the viscous layer)
- $D$  is the water vapor diffusion in porous media
- $\theta_a$  is the vapour dimensionless (volumetric) content
- $D_{atm} \sim 2.5 \cdot 10^{-5}$  [ $\text{m}^2 \text{s}^{-1}$ ] is the water vapor diffusion coefficient in free air
- $q^*$  [-] is the specific humidity at saturation ( $27 \cdot 10^{-3}$  [ $\text{kg m}^{-3}$ ])
- $q$  [-] is the actual specific humidity at the soil surface

In the following, we will use the finite difference form of the above equation, but approximate solution for the diffusion process at constant coefficient are also available and worth to be explored (e.g. ? Nobel, 2013).

#### 2.4.4 A new set of equations for the evaporation processes in soil

The above indications refers to lab experiments in controlled situations and we try now to give indication of how to use them in daily modelling of soil evaporation.

The first suggestion is that we can continue to use the PMSO solutions until the critical depth is obtained. This critical depth can be computed from (2.74) and its overcoming monitored by solving the deficit budget (2.75).

After the stage II evaporation starts, we can possibly subdivide the evaporation domain into two. One going from the depth  $\xi$  to the end of the viscous atmospheric layer. And a second one form the top of the viscous layer to the open atmosphere.

Dalton equation should remain valid (as soon as we consider the Prandtl mixing layer theory valid) but the lower level of specific humidity,  $q^\#$  should be the one made available by the molecular diffusion at the domain from the dry domain.

In this domain, we can consider, as suggested by the PMSO treatment in the previous section and having made the appropriate changes, the energy budget, the water mass budget, the molecular diffusion of vapor, the Fourier law for heat transfer, and, if reasonably, the sensible heat molecular transport:

$$\frac{c_p dT}{dt} = R_n - \lambda ET_0 - G - H + \rho_w \lambda P \quad (2.77)$$

where:

- $c_p$  is the soil bulk specific thermal capacity (depending on water content, i.e. on  $\xi$ );
- $T$  is temperature in Kelvin
- $R_n$  is the net radiation

- $G$  the heat transfer by conduction
- $H$  the heat transfer by molecular diffusion
- $\rho_w \lambda P$  the energy content of precipitations

$$\frac{d\xi}{dt} = +ET_0 + R - P \quad (2.75)$$

$$ET_0 = D \frac{dq}{dz} \sim \frac{\theta_a^{2.5}}{\theta_s} D_{atm} \frac{q^* - q(z_0)}{\xi} \quad (2.76)$$

where we can use CCe:

$$q^*(T) = \frac{\epsilon}{p} e^*(T) = \frac{\epsilon}{p} e^*(T_{ref}) \exp^{-\frac{\lambda}{R} \left( \frac{1}{T} - \frac{1}{T_{ref}} \right)} \quad (2.34)$$

for determining the value of  $q^*$ . We can decide, at present to neglect  $H$  and, finally,

$$G = -\lambda_T (T(z_0) - T(\xi)) \quad (2.78)$$

The unknowns of this systems are  $\xi$ ,  $q(z_0)$ ,  $T(z_0) - T(\xi)$ ,  $ET_0$ ,  $G$  and their number is matched by the number of equations available which now however, contain the water budget.

## 2.4.5 Some simplification to show that the system above is actually solvable

In this section, we simplify the non linear problem posed by the above equation to actually show that we can arrive to a solution, a fact that could not be so evident to the reader. To sketch this, we do some simplifications and assume that:

- $c_p$  and  $\lambda_T$  are independent from  $\xi$
- $\rho_w \lambda P$  can be neglected
- the Penman approximation of  $q^*$  can be used
- the system is radiatively decoupled

The Penman ansatz (2.36) can then be used inside the energy budget, discretized at this point, as a finite difference:

$$c_p \frac{T_{z_0}^n - T_{z_0}^{n-1}}{(\delta t)} = R_n - \frac{\lambda D}{\xi^n} \Delta(T_{z_0} - T(\xi)) - \lambda_T (T_{z_0} - T(\xi)) \quad (2.79)$$

where:

- $D$  is the water vapor diffusion in porous media
- $\xi^n$  is the deficit at time interval  $t = n$
- $\delta t$  is the discretized time interval

The above equation (2.79) would be an equation containing the only independent variable ( $T_{z_0} - T(\xi)$ ) if  $\xi$  was not there.  $\xi$ , in turn, is a product of the water budget (2.75), which can be rewritten also as a finite difference:

$$\frac{\xi^n - \xi^{n-1}}{\delta t} = ET_0 + R_n - P \quad (2.80)$$

or:

$$\xi^n = \xi^{n-1} + (\delta t) \left( \frac{\lambda D \Delta}{\xi^n} (T_{z_0} - T(\xi)) + R_n - P \right) \quad (2.81)$$

where the expression for  $ET_0$  has been already substituted in producing a quadratic equation in  $\xi$ . We can now observe that (2.79) and (2.81) are a non linear system in  $\xi$  and  $(T_{z_0} - T(\xi))$  which can be solved iteratively. Once (2.81) is solved for  $\xi$  as a function of  $(T_{z_0} - T(\xi))$ , the result can be introduced in (2.79) to obtain  $T_{z_0}$ , substitutions then give the solution for  $\xi$ ,  $ET_0$ ,  $G$  and  $q^\#$ .

These solutions provide what happens in the viscous transport zone, inside the soil and up to the viscous layer). What happens instead in the overlying turbulent layer ?

## 2.4.6 Vapor, momentum and energy budget in the turbulent layer

Obviously in the turbulent layer are still valid Dalton law and the turbulent exchange equation:

$$ET^{(m)} = \rho_a C_E \bar{u} (q^\#(z_0) - q_z) \quad (2.28)$$

$$H = \rho_a C c_p \bar{u} (T_{z_0} - T_z) \quad (2.31)$$

Now, however, temperature at soil level,  $T_{z_0}$  can be given by the results of the previous section and, upon measuring  $T_z$ ,  $H$  is determined. The same argument apply to the Dalton law:  $q^\#$  is given as well as  $q_z$  could be measured. Otherwise, we can assume that one of  $q_z$  and  $T_z$  are unknown, and therefore use the energy budget to determine it. Following the classic use of the stationary energy budget, it reads, for the turbulent control volume:

$$0 = R_l \uparrow - ET - H = \epsilon \sigma T_{z_0}^4 - \lambda C_E (q^\#(z_0) - q_z) - C_H (T_{z_0} - T_z) \quad (2.82)$$

assuming that:

- shortwave radiation does not interacts with air
- the air thermal capacity is negligible

Using (2.82), as promised, either  $q_z$  or  $T_z$  can be estimated instead than measured. However, if we measure both, we can consider to solve (2.82) simultaneously together with the soil vapor budget equations to obtain  $T(\xi)$ , the temperature at a certain depth. Realistically, we can also think to introduce a calibration parameter where appropriate in the soil budget to cope with simplifications made and use both measurements for calibration of such a parameter, when both  $q_z$  and  $T_z$  are available.

In any case, the previous estimations show that there is a flux out of the viscous layer  $ET_0$  and a different flux out of the turbulent layer,  $ET$  whose difference gives the water vapor budget in the turbulent layer as:

$$\frac{dV}{dt} = ET_0 - ET + v_{adv} \quad (2.83)$$

where:

- $v_{adv}$  [ $\text{m s}^{-1}$ ] is the net advected vapor



C H A P T E R



## UPSCALE THE TRANSPiration THEORY

The case of the evaporation from the vegetation, i.e. transpiration, is different from the ground/soil evaporation. The soil is a porous medium from which evaporation is essentially governed by the energy balance and water balance. The case of vegetation involves also plants physiology and the energy budget and the water budget are more tightly entangled in the process of photosynthesis.

Transpiration is not simply a loss of water but a necessary functional activity of plants. With stomata closed (no transpiration), the plants carbohydrate building engine does not work, photosynthesis does not happen since it is the water flow that makes it possible. Water transpiration is not just a byproduct of photosynthesis, but full part of it.

The core of the theory developed in previous chapters is obviously still valid and the main task to perform is to go and determine  $e^*$  above the leaves surface.

There is another apparent difference between vegetation and soil which is that in vegetation we need to use the cohesion tension

theory to drive water, while in soil such a theory is overlooked.

### 3.1 Where does the water go?

The answer to the question is simple: the water from soil goes into the roots, then to the stems and then evaporates or goes back with solute through the phloem. In fact, the right question is: how the water goes where it goes ?

The current understanding is that the water is pulled along the plants by differences in pressures between the atmosphere and the soil. These differences are very high and often around 30 MPa. In doing this, plants resolve various problems like the one of avoiding cavitation. A couple of papers, in particular, Manzoni et al. (2013) and Bonan et al. (2014a) offer two remarkable points of view of the matter. Manzoni et al. is more interested to processes, equations and general issues with plants hydraulics. Bonan et al. goal is the implementation of a model of the soil-plant-atmosphere continuum and therefore its appendixes can be useful to understand some of the details that can be perceived as ambiguous by the beginners in the field. Bonan et al.'s treatment is "traditional" being based on the set of assumptions all literature use which give you back an already well packaged simplification of the physics involved. Manzoni et al. put more emphasis on the biophysical aspects and their connections with plants physiology and use partial differential equations to illustrate the concepts. Both of them have a large list of references and, together with the recent work of Verhoef and Egea (2014) and the work of Dewar (2002), can be a solid start for any study of the subject. Verhoef and Egea in particular, compares various approaches to modelling the water stress and discuss their ability to reproduce experimental data. One of its main interest is to clarify if either water content or the water pressure explains better

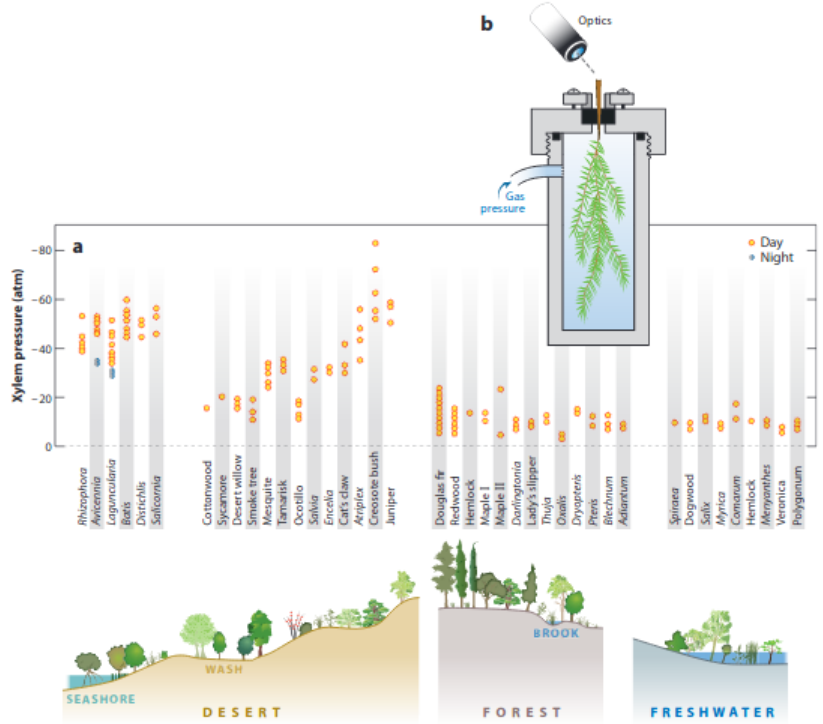


Figure 3.1: Pressure in the xylem. (a) The pressure relative to atmospheric pressure in leaves and needles ( $P_{X,l} - P_0$ ) is reported in atmospheres ( $\approx 0.1 \text{ MPa}$ ) for a variety of species in a variety of climates. The values are negative. (b) Schematic depiction of the Scholander leaf pressure chamber. A cut leaf or terminal shoot is placed in the chamber with its stem exposed through a seal. The air pressure is raised within the chamber until a droplet of liquid is observed optically at the cut surface of the stem. This positive balance pressure is taken as an estimate of the negative pressure in the xylem before excision. This method has been shown to agree with more direct, mechanical measurements (Holbrook et al., 1995; Melcher et al., 1998). Figure taken from Stroock et al. (2014) and readapted from Scholander et al. (1965).

plant's transpiration behavior. The problem of plants hydraulics in connection with transpiration is overwhelming interesting but in these thesis we focus just in finding a reasonable way to parametrize water movement in a model and we will keep the the description as simple as possible.

### 3.1.1 Leaves

If all the machine starts from atmosphere demanding, the very next thing to consider in plants is the leaves functioning.

In order to obtain this result it is useful to understand the structure of a typical angiosperm leaf. Looking at the cross section of a leaf (Fig. 3.2), an epidermis cover both the upper and lower surface and the thick of a leaf is generally few hundred micrometers. Epidermis (epidermal cells) is a relatively thick waterproof cuticle placed on the upper and lower side. Between the two epidermal layers there is the mesophyll tissue, which is usually differentiated into chloroplast ("palisade" and "spongy" cells, Fig. 3.2).

The palisade cells are often elongated perpendicular to the upper epidermis and are found immediately beneath it. The spongy mesophyll cells are located between the palisade mesophyll cells and the lower epidermis, are loosely packed, and intercellular air spaces are conspicuous. In fact, most of the surface area of both spongy and palisade mesophyll cells is exposed to air in the intercellular spaces, facilitating diffusion of gases into or out of the cells.

The pathway of least resistance for gases to cross the epidermis and enter or to exit into the leaf is through the adjustable space between a pair of guard cells.

The pore and the surrounding guard cells are called stoma (or stomata if more than one).

When guard cells are open, the stomatal pores allow exchange

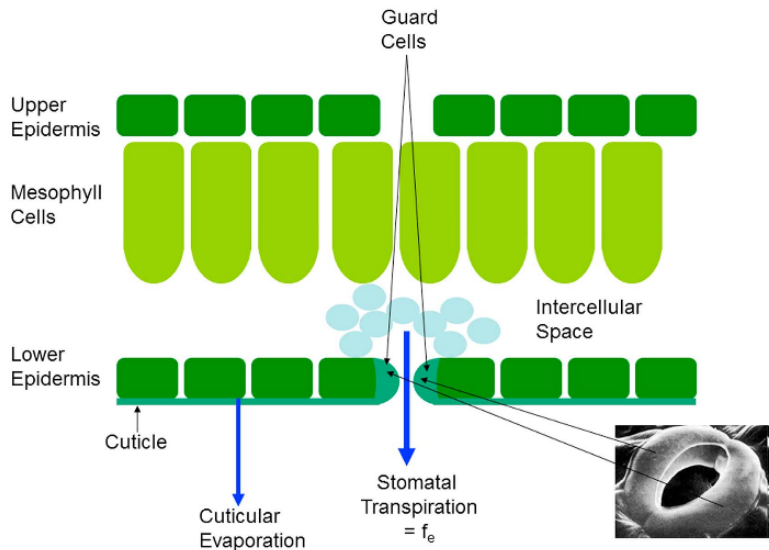


Figure 3.2: Cross section of typical angiosperm leaf. Image taken from Katul et al. (2012)

of incoming  $\text{CO}_2$  into the leaf and the emission dioxygen, produced by photosynthesis. However this implies the loss of water vapor (i.e. transpiration) also occurs mainly through the stomatal pores.

The degree of stomata opening depends also by the  $\text{CO}_2$  concentration near to the guard cells. When a leaf is illuminated, the  $\text{CO}_2$  concentration start to decrease, due to the fixation inside the leaf for photosynthesis activity, this decrease triggers the stoma opening in order to get more water from roots to supply oxygen and nutrients necessary and assimilate more  $\text{CO}_2$  to build carbohydrates.

It is known that in leaves, and especially for those in shade, the degree of stomata opening increases proportionally with the photosynthetic photon flux (PPF) until they reach the saturation point (around  $45 \text{ W/m}^2$  and generally expressed as micromol of photons,  $\mu\text{mol m}^{-2}\text{s}^{-1}$ ) beyond this value the opening degree

does not change even if the PPF value keeps increasing. On the other hand, others leaves show an increment of the opening degree up to a PPF of approximately  $2000 \mu\text{mol } m^{-2}s^{-1}$ . This is because the leaves in shadow seem to be more efficient in the absorption of  $\text{CO}_2$  than those placed in sunlight. The lack of water in a leaf can be intuitively dangerous for the survival of the leaf itself. To avoid losing too much water in fact stomata tend to close when there is a decrease in the leaf water potential, that varies between 1MPa for garden vegetables up to 6MPa for some desert shrubs. For the same reason, even a decrease in the humidity of the air leads to a partial or complete closure of the stomata. If there is no closure of the stomata for these reasons, if a leaf is exposed it will tend to open the stomata with the increase in temperature: in fact the optimal photophosphorylation temperature is around  $35^\circ\text{C}$ , a value that is generally higher in leaves in shadow (Nobel et al., 1999).

Stomata provide a control on this trade off, between the freely assimilation of  $\text{CO}_2$ , supply of water oxygen, needed for photosynthesis and at the same time preventing excessive loss of water vapor from the plant, which would cause the stop of the photosynthesis engine caused by cavitation. The loss of water at the same time helps to lower the temperature of the leaf avoiding that it overheats and keeps, as much as possible, the optimal temperature for photophosphorilation to happen.

Finally the transpiration is performed only when stomata are open and this opening is given by the presence of light. When there is enough photosynthetically active radiation (PAR) stoma start to opening to assimilate  $\text{CO}_2$ . Since  $\text{CO}_2$  diffuses across the same pathway used by vapour, when the carbon dioxide fixation starts, water vapour movement takes place. The PAR threshold for photosynthesis activation is different for each species and also for sunlit and shaded leaves.

To sum up a few major factors were identified to control transpiration from stomata: water content, light availability, radiation input and temperature.

### 3.1.2 Water vapor diffusion

Whatever the controls on water and vapor movements, the key passage in modelling is to understand how to model them in equation and understand if the tool set developed for the turbulent transport can be re-arranged for the vapor movements inside the cells and the plants tissues. On this topic we follow the treatment by Nobel et al. (1999).

Fick's first law is usually used to represent concentration-driven gas diffusion of a generic gas  $j$ :

$$J_j = D_j \frac{\partial c_j}{\partial x} \quad (3.1)$$

Fortunately, it can be recasted in a form that is similar to Dalton's law:

$$J_j = D_j \frac{\partial c_j}{\partial x} = D_j \frac{\Delta c_j}{\Delta x} = D_j \frac{\Delta c_j^{bl}}{\delta x^{bl}} = g_j^{bl} \Delta c_j^{bl} = \frac{\Delta c_j^{bl}}{r_j^{bl}} \quad (3.2)$$

$$g_j^{bl} = \frac{J_j}{\Delta c_j^{bl}} = \frac{D_j}{\delta x^{bl}} = \frac{1}{r_j^{bl}} \quad (3.3)$$

Where:

- $J_j$  is the net flux density in  $[mol m^{-2} s^{-1}]$ ,
- $c_j$  is the concentration coefficient in  $[mol m^{-3}]$ ,
- $D_j$  is the diffusion coefficient in  $[m^2 s^{-1}]$ ,
- $\delta^{bl}$  is the boundary layer thickness in [mm],
- $g_j^{bl}$  is the boundary layer conductance in  $[ms^{-1}]$ ,

- $r_j^{bl}$  is the boundary layer resistance in  $[sm^{-1}]$ ,

Therefore, arguments similar to those already expressed in Chapter 2 can be used for transpiration and vapor movements insides cells but using Fick's law coefficients instead of those derived by turbulent analysis, i.e. Dalton law, to which equation (3.3). Thus, once the stomatal conductances are appropriately estimated, PMSO solutions remain valid, changed what has to be changed, also in this case. To obtain the final result of transpiration, (besides the determination of roots and stem resistances), there is the further problem of the coupling of stoma with the Vegetation Boundary Layer (VBL). The tradition assumes quasi-stationarity of the fluxes and uses the resistance metaphor, assigning to the VBL a resistance according to an integrated Fick's law. Also in this case, resistances are summed to obtain the comprehensive flux law that regulates the water ascending.

New questions arise: which is the dominant between the two resistances ? Is the resistance metaphor really applicable ?

Nobel et al. (1999) essentially identifies 3 different conductance to water vapor diffusion in leaves:

- stomatal conductance: linked to the size of the stoma,
- boundary layer conductance: that is the resistance that meets the water vapor spreading in the turbulent atmosphere
- intercellular air space conductance: due to the irregular shape of the air space inside the leaves.

To complete what said above, from the hydrological point of view, the most important cause to resistance is given by the water availability. If there are no water available to be transpired no transpiration is possible.

There are several factor influencing water vapor availability in

Components	Conductance		Resistance	
	$\frac{mm}{s}$	$\frac{mmol}{m^2 s}$	$\frac{s}{m}$	$\frac{m^2 s}{mol}$
<b>Boundary layer</b>				
Thin	80	3200	13	0.3
Thick		320	130	3
<b>Stomata</b>				
Large stoma/open	20	800	50	1.3
Small stoma/open	1.8	72	560	14
Closed	0	0	$\infty$	$\infty$
<b>Cuticle</b>				
Crops	0.1- 0.4	4-16	2500- 10000	60- 250
Trees	0.05- 0.2	2-8	5000- 20000	125- 500
<b>Intercellular air space</b>				
Typical	40- 100	1600- 4000	10-25	0.2- 0.6
<b>Leaf</b>				
Crops/open stomata	2-10	80- 400	100- 500	2.5-13
Trees/open stomata	0.5-3	20- 120	300- 2000	8-50

Table 3.1: Representative values of conductances and resistances for water vapor diffusing out of leaves (Nobel et al., 1999).

the leaves, starting from the water availability in soil.

Experimental studies about soil tend to say that flux (to the atmosphere) is sustained at the maximum rate to a critical point of soil suction (which actually can be seen as similar to what happens in soils).

There is a variety of ways plants actually regulate the stomatal resistance but they can be summarised in the isohydric and

anisohydric behavior (Martínez-Vilalta and Garcia-Forner, 2017) types.

In the first case, the plant progressively closes the stoma as reaction to water stress to maintain as much as possible a balanced water content. In the other case the plant delays stoma closure in the measure it can resist to manifestation of cavitation and produces in its interior a very uneven water distribution.

Actually the stomatal opening is not the only one affecting plants. Plants have roots and a stem that convey water fluxes. Usually this flux there is treated as a viscous flow with some resistance and they have to be accounted for.

### 3.1.3 Stomatal conductance in the absence of stress

We use the derivation of stomatal conductance proposed by Lehmann and Or (2015) in absen. The stomatal resistance is computed as the sum of two terms:

- the throat resistance ( $r_{sp}$ ), dependent on the area and the thickness of the pores (respectively  $A_p$  and  $d_p$ ),
- the vapour shell resistance ( $r_{vs}$ ), related to the distribution of the water vapor sources over the layer, i.e. to the size and the spacing of the stomata .

The throat resistance is computed as (Lehmann and Or, 2015):

$$r_{sp} = \frac{d_p}{A_p k_{dv} n_p} \quad (3.4)$$

where  $k_{dv}$  is the ratio of the vapour diffusion coefficient and the molar volume of air ( $D_{va}/V_m$ ), and  $A_p = \pi r_p^2$ .

The vapour shell resistance was proposed by Bange (1953):

$$r_{vs} = \left( \frac{1}{4r_p} - \frac{1}{\pi s_p} \right) \frac{1}{k_{dv} n_p} \quad (3.5)$$

Where  $s_p$  is the spacing between stomata expressed in meters, and  $n_p = 1/s_p^2$ .

The stomatal conductance to water vapour  $g_{tw,mol}$ , expressed in  $mol m^{-2} s^{-1}$ , can be computed as:

$$g_{sw,mol} = \frac{1}{(r_{sp} + r_{vs})} \quad (3.6)$$

In order to obtain  $g_{tw}$  in  $m s^{-1}$ :

$$g_{sw} = \frac{g_{sw,mol} R_{mol} T_a}{P_a} \quad (3.7)$$

Typically we can assume  $g_{tw,mol} \approx 40 \text{ mol m}^{-3} \cdot g_{tw}$

Even if this method gives a very good representation of the physical resistance (or conductance) of the pores it does not consider physiological response. In this way there is no closure of the stoma, especially during the night.

## 3.2 The families of conductance models with stress

There are two main families of stomatal conductance models in literature: those based on the work of Jarvis (1976) and those based on the work of Ball et al. (1987). Both of these model families parametrize the conductance of the stomata which in turn, controls water flow.

In the Jarvis model the stomatal response is related to environmental forcing while the Ball-Berry-Leuning model stomatal response is related to the photosynthesis process.

Although the response of stomata to environmental variables has been extensively discussed in literature, for a long time several models have ignored the dependence of stomata on water stress, impairing the model's capacity to forecast the plant functioning in conditions of limiting water supply.

An extensive review of stomal conductance models was presented by Damour et al. (2010) and Dewar (2002) discussed their validity. A valid reference for practical modelling purposes would be also Bonan et al. (2014a).

### 3.2.1 Models based on climatic control only

The hypothesis on which these models are based is that the stoma responds independently to the variation of each environmental forcing such as radiation and temperature. When these quantities vary, the stoma will open or close to increase or decrease the conductance, therefore to favor or limit the assimilation of CO<sub>2</sub>. In particular, the stomata tend to close in the presence of those conditions that lead to a high vapor loss as in the case of high pressure deficits or that the external temperature is too high or low compared to the optimal photosynthesis temperature (generally between 15-25°C). Obviously it will also depend on the amount of PAR incident (Nobel et al., 1999; Schymanski and Or, 2017).

$$g_s = f(R_{PAR}) \cdot f(T_l) \cdot f(VPD) \cdot f(C_a) \cdot f(\Psi_l) \quad (3.8)$$

Where:

- R<sub>PAR</sub> is the PAR,
- T<sub>l</sub> is the leaf temperature ( $\approx T_a$ ),
- VPD is vapour pressure deficit,
- C<sub>a</sub> is the Co<sub>2</sub> concentration,
- Ψ is the leaf water potential.

Jarvis (1976) was the first to propose this type of approach, currently very widespread. Despite its simplicity, a validation labora-

tory concluded that this model explains 95% of the observed variation of  $g_s$  (Jarvis and Mcnaughton, 1986, Damour et al., 2010). In some variants of this model the function of the leaf water potential  $f(\Psi)$  is replaced with a function of the soil water content (Dewar, 2002).

There are different versions of this model in which only part of the stress is considered. A partial list can be found in Damour et al. (2010).

White et al. (1999) proposes a variant of this model in which the factors are normalized and multiplied by a value of maximum conductance, i.e. the conductance value obtained in well-watered condition ( $g_{smax}$ ) and without any stress. A further variation was proposed by Noe and Giersch (2004), in which the factors are not multiplied, but the minimum among the factors is considered. This last approach is used to obviate the reduction in conductance due to the multiplication of individual stress factors. In fact, if two stress factors cause a reduction of the 80%, the total reduction is equal to 64%. This effect is the greater the number of stress factors considered, so it needs an accurate parametrization or a parameters calibration.

The main criticism of this approach is that the interaction between these factors cannot be ignored, such as that between the vapor pressure deficit and the leaf water potential (Tardieu et al., 1996). Furthermore, even if successfully tested in numerous circumstances, multiplicative or limiting factor-based models are essentially empirical and require new parameterization for each new environmental condition. This is their main drawback, likely resulting from the assumption that environmental factors have independent effects.

### 3.2.2 Models based on the conductance-photosynthesis relationship

Another type of models are those based on the relationship between  $g_s$  and the photosynthesis rate  $A_{net}$  [mol CO<sub>2</sub>m<sup>-2</sup>s<sup>-1</sup>]. The ratio  $g_s/A_{net}$  remains constant if other environmental and soil variables remain constant as the radiation changes (Wong et al., 1979; Mott, 1988; Aphalo and Jarvis, 1991; Buckley et al., 2003).

These models are designed to maximize water use efficiency (WUE): the basic idea is that the plant regulates the opening of the stomata in order to maximize the assimilation of CO<sub>2</sub> and minimize the loss of H<sub>2</sub>O.

One of the most common models is the Ball-Berry-Leuning model (Ball et al., 1987):

$$g = g_0 + \frac{a_1 A_n}{(c_s - \Gamma)(1 + \frac{D_s}{D_0})} \quad (3.9)$$

where:

- $A_n$  is the net leaf CO<sub>2</sub> assimilation rate,
- $D_s$  is the vapour pressure deficit (VPD) and
- $c_s$  is the CO<sub>2</sub> concentration at leaf surface,
- $\Gamma$  is the CO<sub>2</sub> compensation point,
- $g_0$  is the value of  $g$  at the light compensation point,
- $a_1$  and  $D_0$  are empirical coefficient.

Ball et al. (see also Collatz et al. (1992)) has been built out of empirical bases and it was subsequently modified (e.g Verhoef and Egea (2014)) to include physiological reactions and the production of abscisic acid, ABA (Buckley, 2016).

These kind of models (Ball et al., 1987; Leuning, 1995) can be used successfully both at leaf or canopy scale (Misson et al., 2002; Alton et al., 2007). They are easy to use and to parametrize but generally they do not include the soil water stress even if they can be modified in order to model it using an empirical function (Ball et al., 1987; Leuning, 1990; Aphalo and Jarvis, 1993; Leuning, 1995; Damour et al., 2010).

### **3.3 Transpiration from the canopy**

### **3.4 Upscaling from the leaf to canopies**

All the considerations made so far are valid at leaf scale. What happens when they are applied to a canopy scale?

For what we saw before we can therefore argue that transpiration is strictly dependent on photosynthetic activity and therefore on radiation.

If in first approximation we can consider the environmental variables as air temperature and relative humidity constant along the vertical axis of the canopy, this is not true for shortwave radiation, which presents strong heterogeneity.

In fact, we have part of leaves in shadow and part in sunlight.

In literature there is a family of methods used for upscaling the photosynthetic activity on a canopy scale, i.e. the multi-layer canopy model.

Traditionally, many models of ecosystems have used a simple efficiency approach in the use of light (Monteith, 1972,1973) to estimate the assimilation of photosynthetic activity. But starting from the work of Farquhar et al. (1980), the leaf-level model has been adopted more and more often as the basis for canopy scale upscaling, using common parameters throughout the canopy or dividing it into different layers with distinct light response

characteristics. The simplest of these upscaling methodologies is the big leaf approach, which assumes that the canopy have the same responses to the environment as each individual leaf not shaded in the canopy (Sellers et al., 1992, Dai et al., 2004).

Despite its widespread use for the modeling of evapotranspiration at different spatial scales (Raupach and Finnigan, 1988; Moran et al., 1996; Samson and Lemeur, 2001; Weiß and Menzel, 2008), subsequent theoretical and experimental developments (De Pury and Farquhar, 1997; Carswell et al., 2000; Lai et al., 2000; Meir et al., 2002) questioned the assumptions underlying the big-leaf approach in modeling vegetation productivity. Recently it has been discovered that most of the leaves are not saturated with light. These results dispute the assumption that the photosynthetic capacity is exclusively proportional to the absorbed radiation (Friend, 2001; Sprintsin et al., 2012).

### 3.4.1 Big-Leaf Approach

On the leaf scale, Farquhar describes the photosynthetic capacity as the sum of the chloroplastic capacities per surface unit (Farquhar and Von Caemmerer, 1982). It has therefore been hypothesized that the distribution of chloroplasts within the canopy was proportional to the average absorbed radiation, so as to optimize photosynthetic production. This implies that there will be a greater concentration of chloroplasts will result to be in the upper part of the canopy and will decrease towards the base of the canopy. If we assume that the distribution of photosynthetic capacity between the leaves in a canopy is proportional to the irradiance profile absorbed by the Lambert-Beer law, the canopy can be treated as a single homogeneous entity, ie a large leaf. The equations normally applied to the individual leaves can be extended to the entire canopy (De Pury and Farquhar, 1997;

Farquhar, 1989).

### 3.4.2 Two-Leaf Approach

A simpler approach of separating the leaves from the sun-lit shadow, in which the vegetation is treated as two big leaves in different lighting conditions (Sinclair et al., 1976) and since then it has been continuously investigated (De Pury and Farquhar, 1997; Wang and Leuning, 1998; Chen et al., 1999; Mercado et al., 2006). Two-leaf models have been successfully tested for local and regional scale applications and have been found to sufficiently capture much of the variation present in complex multi-level approaches to separating sun-shaded leaves (Kotchenova et al., 2004) that broad-leaf upscaling cannot reach (De Pury and Farquhar, 1997; Chen et al., 1999; Dai et al., 2004; Mercado et al., 2006; Mercado et al., 2007).

We decide to use a two-leaf model and in particular the Sun/Shade model proposed by De Pury and Farquhar (1997). In the two-leaf models, the photosynthetic activity is computed separately for sunlit ( $LAI_{sun}$ ) and shaded ( $LAI_{sh}$ ) parts of the canopy NORMAN and M. (1979). Given the close link that exists between photosynthesis and transpiration, we decide to extend this result to compute the transpiration both from sunlit and shaded canopy. So the total leaf area index ( $L_c$ ) is separated into sunlit and shaded LAI:

$$L_c = L_{sun} + L_{sh} \quad (3.10)$$

$$A_c = A_{sun} \cdot LAI_{sun} + A_{sh} \cdot LAI_{sh} \quad E_c = E_{sun} \cdot LAI_{sun} + E_{sh} \cdot LAI_{sh} \quad (3.11)$$

where  $A_c$  and  $E_c$  are respectively the total canopy photosynthesis and transpiration.

$$L_{sun} = 2 \cdot \cos \theta \left( 1 - \exp - G(\theta) \Omega LAI / \cos \theta \right) \quad (3.12)$$

where

- $\theta$  is the solar zenith angle;
- $G(\theta)$  is the foliage projection coefficient taken as 0.5 assuming a spherical leaf angle distribution;
- $\Omega$  is the leaf spatial distribution pattern.

$\Omega$  is expressed in terms of the degree of its deviation from the random case (assume equal to 1 for randomly distributed leaves and less than one for clumped canopies) and it influences radiation interception by the canopy at a given  $\theta$  as described by Beer's law.

### 3.4.3 Clumping Simulations

Foliage clumping increases the probability of leaf overlapping and decreases the probability of a leaf exposure to the direct radiation. A decrease in  $\Omega$  (increasing clumping) results in a decrease of  $LAI_{sun}$  and a consequent increase in the fraction of the shaded leaves. Since shaded leaves typically have higher light-use efficiency (photosynthetic performance per unit incident photon flux density), then for extremely clumped canopies such as coniferous forests ( $0.5 < \Omega < 0.7$ ) (Chen and Leblanc, 1997),  $LAI_{sh}$  should contribute significantly to total canopy productivity. Furthermore, since  $\Omega$  influences the ratio between sunlit and shaded leaves (as in the two-leaf case) or changes in PAR-intercepted area (as in the big-leaf case), it should have a considerable effect on canopy-level GPP (Baldocchi and Harley, 1995; Chen et al., 2003; Chen et al., 2012). Typical values of  $\Omega$  are 0.5-0.7 for conifer forests, 0.7-0.9 for broadleaf forests, and 0.9-1.0 for grass and crops (Chen and Cihlar, 1996; Chen et al. (1997)).

## 3.5 Upscaling at the canopy scale

The Schymanski and Or method is validated for a single leaf, with the surface perpendicular to the shortwave radiation and in well-watered condition. In order to extend this approach to be used in the hydrological models, we need to introduce an upscale of this method at the canopy level and to include the water stress factors.

### 3.5.1 Upscaling strategy

The upscaling problem rises since we are not able to compute the energy balance on each leaf: we need to consider the inclination of sun rays with respect to the leaf surface, if the leaf is exposed to the direct solar radiation or not (or even partially) and so on. Since our goal is to upscale this method while preserving its simplicity, some assumptions have been necessary: The first assumption is to consider air temperature, relative humidity, wind and longwave radiation more or less constant inside the canopy. This implies also to assume the longwave radiation is isotropic inside the canopy. If the other environmental forcing are constant inside the canopy, the energy balance and the consequently the equilibrium temperature for a leaf depends only by the shortwave radiation, both for sunlit and shaded leaves. The second assumption made is to consider the canopy divided in two parts: the one in sunlight and the one in shadow.

Each of these fractions can be considered as a single big leaf that emits latent heat proportionally to the corresponding area and to the shortwave radiation received.

It is fundamental compute the fraction of canopy area in sunlight and in shadow and the radiation intercepted by these parts of

canopy and the one that reach the soil

$$R_s = R_s^{c,Sun} + R_s^{c,Sh} + R_s^{soil} \quad (3.13)$$

$$A_c = A_c^{Sun} + A_c^{Sh} \quad (3.14)$$

This allow us also to separate transpiration and evaporation because we can write three different energy balance:

$$ET = E_{c,sun} + E_{c,sh} + E_{soil} \quad (3.15)$$

$$= E_{c,sun}(R_{c,sun}) + E_{c,sh}(R_{c,sh}) + E_{soil}(R_{soil}) \quad (3.16)$$

$$E_l^{Sun}(T_l^{Sun}) = R_{sw}^{Sun} - R_{ll}^{Sun}(T_l^{Sun}) - H_l^{Sun}(T_l^{Sun}) \quad (3.17)$$

$$E_l^{Sh}(T_l^{Sh}) = R_{sw}^{Sh} - R_{ll}^{Sh}(T_l^{Sh}) - H_l^{Sh}(T_l^{Sh}) \quad (3.18)$$

$$E_{soil}(T_{soil}) = R_s^{Soil} - G - R_{ll}^{Soil}(T_{soil}) - H_{soil}(T_{soil}) \quad (3.19)$$

The fraction of lit and shaded canopy, as the radiation intercepted by those, is achieved using the Sun/Shade model (De Pury and Farquhar, 1997).

C H A P T E R



## PROSPERO

During my PhD I worked on the development of an upscaled version of the Schymanski and Or formula, making it compatible with the GEOframe modeling system (Appendix A) and we decided to call this module Prospero.

Prospero borns with the purpose to be an ecohydrological and physical based model, even if currently is mainly thought to estimate evapotranspiration, it could be easily extended to the computation of photosynthesis or as the core for a lysimeter model, able to compute the water exchange between soil and atmosphere.

The idea at the base of Propsero is that the evapotranspiration is given by the sum of two different processes: evaporation from the soil and transpiration from the canopy, both the shaded and sunlit ones.

This implies we must compute the those processed separately: the evaporation from soil is computed with a Penman-Monteith FAO process (Eq. A.4.2, Appendix A), with specific coefficients for soil evaporation depending on the case study.

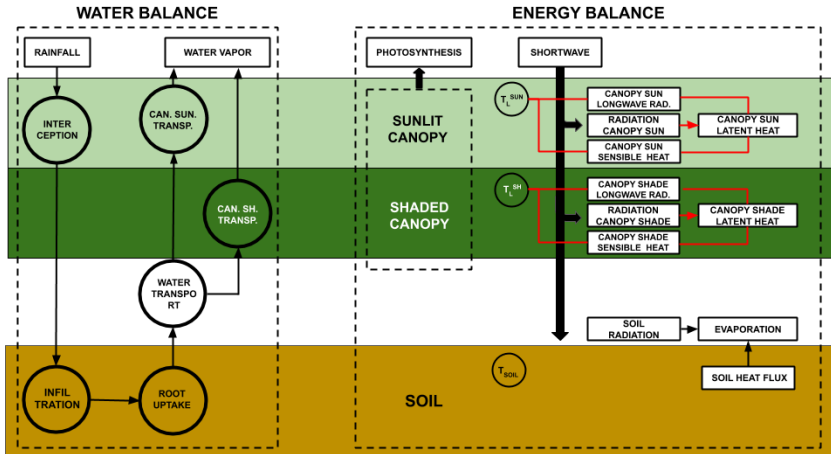


Figure 4.1: Conceptual scheme of Prospero

Transpiration is computed starting from the Schymanski and Or method, since it has demonstrated to ensure the best estimation of latent heat from a leaf. However, the Schymanski-Or equation has been upscaled in order to face the canopy transpiration and the mass conservation (Fig. 4.1). We adopt a multi-layer model in order to compute the incoming shortwave radiation in each layers, and so to uncouple the evaporation-transpiration problem, as shown in Eq. 3.5.1.

$$ET_{Prospero} = EV_{soil} + E_c^{Sun} + E_c^{Sh} \quad (4.1)$$

Where:

- $ET_{Prospero}$  is the evapotranspiration computed with Prospero [ $Wm^{-2}$ ];
- $EV_{soil}$  is the evaporation from the soil [ $Wm^{-2}$ ];
- $E_c^{Sun}$  and  $E_c^{Sh}$  are respectively the transpiration from sun-light and shaded canopy [ $Wm^{-2}$ ].

This is achieved using a multi-layer canopy model: the sun/shade model.

## 4.1 Sun/Shade model

In the Sun/Shade model (De Pury and Farquhar, 1997), as in the multi-layer canopy model, the canopy is represented as an absorbing medium for the shortwave radiation. The penetration of PAR inside the canopy is given by the sunfleck penetration factor,  $f_{Sun}$ , is given by:

$$f_{Sun}(L) = \exp(-k_b L) \quad (4.2)$$

where:

- $k_b$  is the extinction coefficient [-];
- $L$  is the leaf area index [ $m^2 m^{-2}$ ].

$k_b$  depends on several factors like the solar elevation angle, the canopy albedo, the leaves orientation distribution angle and the canopy clustering (Ryu et al., 2011)

$$L_{Sun} = \int_0^{L_c} f_{Sun}(L) dL \quad (4.3)$$

$$L_{Sh} = L_c - L_{Sun} \quad (4.4)$$

where

- $L_{Sh}$  and  $L_{Sun}$  are the fraction of leaf area index in shade and in sunlight
- $L_c$  is the cumulated leaf area index.

$$R_{sw}^{Sun} = \int_0^{L_c} R_{sw}^{Sun} f_{Sun}(L) dL \quad (4.5)$$

$$= \int_0^{L_c} [R_{sw}^{dir}(L) + R_{sw}^{dif}(L) + R_{sw}^{sca}(L)] f_{Sun}(L) dL \quad (4.6)$$

Where:

- $R_{sw}^{Sun}$  is the shortwave radiation intercepted by the sunlit canopy [ $Wm^{-2}$ ];
- $R_{sw}^{dir}$  is the direct component of the shortwave radiation per ground area [ $Wm^{-2}$ ];
- $R_{sw}^{dif}$  is the diffuse component of the shortwave radiation per ground area [ $Wm^{-2}$ ];
- $R_{sw}^{sca}$  is the scattered component of the shortwave radiation per ground area [ $Wm^{-2}$ ].

$$R_{sw}^{Sh} = \int_0^{L_c} R_{sw}^{Sh}[1 - f_{Sun}(L)] dL \quad (4.7)$$

$$= \int_0^{L_c} [R_{sw}^{dif}(L) + R_{sw}^{sca}(L)][1 - f_{Sun}(L)] dL \quad (4.8)$$

The multi layer models are quite useful because they allow to calculate the radiation absorbed by the various vegetation layers and the one that is not intercepted, thus allowing to describe separately the transpiration and evaporation processes. In fact, with these models is possible to compute the radiation absorbed from canopy using the previous equations.

Knowing the radiation absorbed from the canopy it is possible to compute the radiation reaching the soil:

$$R_{soil} = R_s - R_{c,sun} + R_{c,sh} \quad (4.9)$$

Where:

- $R_{soil}$  is the shortwave radiation reaching the soil [ $Wm^{-2}$ ];
- $R_s$  is the incoming shortwave radiation [ $Wm^{-2}$ ];
- $R_{c,sun}$  is the shortwave radiation intercepted by sunlit canopy [ $Wm^{-2}$ ];

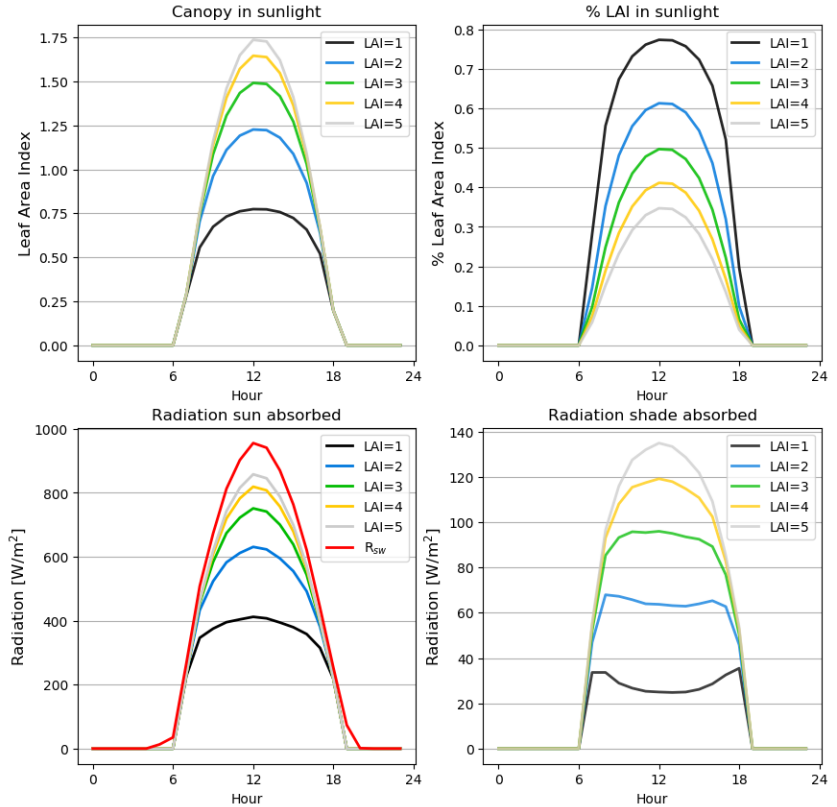


Figure 4.2: LAI and absorbed shortwave radiation with the Sun/Shade model: a) Canopy area in sunlight at the variation of the LAI; b) Fraction of canopy in sunlight with the variation of the LAI; c) Total radiation absorbed by sunlit canopy based on the LAI; d) Total radiation absorbed by shaded canopy based on the LAI.

- $R_{c,sh}$  is the shortwave radiation intercepted by shaded canopy [ $Wm^{-2}$ ].

Consequently, using the different shortwave radiation input it is possible to compute the transpiration and the evaporation for each layers:

$$\begin{aligned} ET &= E_{c,sun} + E_{c,sh} + EV_{soil} \\ &= E_{c,sun}(R_{c,sun}) + E_{c,sh}(R_{c,sh}) + EV_{soil}(R_{soil}) \end{aligned} \quad (4.10)$$

The Schymanski and Or (2017) equation is referred to a single leaf and the latent and sensible heat obtained is computed per area unit. To obtain the total latent heat emitted by a leaf we have to multiply the latent heat for the leaf area  $A_l$ . For sensible heat and longwave radiation is the same but we must include the coefficient  $a_{sH}$ :

$$\begin{cases} E_l = E \cdot A_l \cdot a_{sE} \\ H_l = H \cdot A_l \cdot a_{sH} \\ R_{l,ll} = R_{ll} \cdot A_l \cdot a_{sH} \end{cases}$$

Where:

- $E_l$ ,  $H_l$  and  $R_{l,ll}$  are respectively the latent heat, the sensible heat and the net longwave radiation emitted by the leaf [ $W$ ];
- $E$ ,  $H$  and  $R_{ll}$  are respectively the latent heat, the sensible heat and the net longwave radiation per unit of surface [ $Wm^{-2}$ ];
- $A_l$  is the total area of the leaf [ $m^2$ ].
- $a_{sE}$  are the sides of surface exchanging latent heat, equal to 1 for hypostomatous, 2 for amphistomatous [-];
- $a_{sH}$  are the sides of surface exchanging sensible heat or longwave radiation, equal to 1 for soil, 2 for leaves [-].

We assume the same is still valid also for the canopy, using instead  $A_l$  the canopy area  $A_c$ :

$$\begin{cases} E_c = E \cdot A_c \cdot a_{sE} \\ H_c = H \cdot A_c \cdot a_{sH} \\ R_{c,ll} = R_{ll} \cdot A_c \cdot a_{sH} \end{cases}$$

Where:

- $E_c$ ,  $H_c$  and  $R_{c,ll}$  are respectively the latent heat, the sensible heat and the net longwave radiation emitted by the canopy [ $W$ ];
- $A_c$  is the total area of the canopy [ $m^2$ ].

Furthermore some flux exchanges between the layer could happen and should be considered in order to assess the closure of the energy balance.

For example, in case of longwave radiation, the net balance for a generic layer is given by:

$$R_{ll}^n = R_{l\uparrow}^{n-1}(T_l^{n-1}) + R_{l\downarrow}^{n+1}(T_l^{n+1}) - R_{l\uparrow}^n(T_l^n) + R_{l\downarrow}^n(T_l^n) \quad (4.11)$$

Currently, this kind of feedback is not considered and we approximate all these exchanges as based on the air temperature  $T_a$ . This is an approximation similar to the one made when  $T_w$  is assumed  $\approx T_a$ .

In this version of the model the flux exchange between the layers is not considered. In fact, if fluxes exchange is allowed between layers, both if they are only two (sun/shade) or more, in the energy balance equation will compare terms depending on the leaf temperature of the other layers. In this way the system can be solved only numerically or making some assumptions.

## 4.2 Water stress & conductance model

Even if the stomata conductance values used in Schymanski and Or (2017) gives good results in laboratory, it only represent the conductance of the stoma based on the physical property of the pore, do not considering the stress factors or any closure of the stoma. To improve the representation of Schymanski and

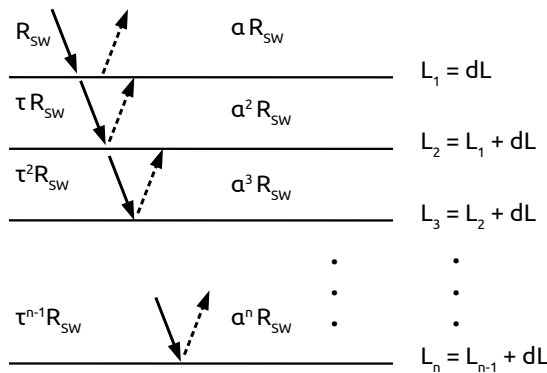


Figure 4.3: Shortwave penetration inside the canopy, assumed divided in  $n$  layers, with transmissivity  $\tau$  and absorbitivity  $\alpha$ .  $R_{SW}$  is the incoming shortwave radiation.

Or formula in real case we must used one of the conductance models discussed in section 3.2.

#### 4.2.1 Stress factors

Even if both type of conductance models (illustrated in 3.2) can be used inside Prospero we decide to conduce all the simulation using a Jarvis-like model and in particular the one proposed by White et al. (1999).

The reason why we choose a model similar to Jarvis is given by the need to apply it on a large basin scale for hydrological applications. In fact, even if Ball-Berry still has good performance, it needs measurement of  $CO_2$ , which are not so common to find. On the contrary, models based on climatic variables use measurements easy to find in most hydro-meteorological stations. Other variables that are not available at stations can be

retrieved using hydrological tools or the other GEOframe (Appendix A) components, like for example the Richards integrator for infiltration.

We use a similar version of the model proposed by White et al. (1999) and by Macfarlane et al. (2004), where the conductance is respectively equal to:

$$g_s = g_{s,max} \cdot f(R_{PAR}) \cdot f(T_a) \cdot f(VPD) \quad (4.12)$$

$$g_s = g_{s,max} \cdot f(R_{PAR}) \cdot f(T_a) \cdot f(VPD) \cdot f(\Psi) \quad (4.13)$$

Where:

- $g_{s,max}$  is the conductance without any kind of stress and in well-watered conditions [ $ms^{-1}$ ];
- $f(R_{PAR})$ ,  $f(T_a)$ ,  $f(VPD)$  and  $f(\Psi)$  are respectively the normalised stress factors induced by the PAR, the air temperature, the water pressure deficit and the leaf water potential.

The difference between the two methods is represented by the dependence of the stress factor by the water content (i.e. the leaf water potential).

We used the model proposed by Macfarlane et al. (2004), but instead of using the stress factor given by the leaf water potential, we used the one based on the soil moisture proposed by FAO approach (Allen, 1986)

$$g_s = g_{s,max} \cdot f(R_{PAR}) \cdot f(\theta) \cdot f(VPD) \cdot K_s \quad (4.14)$$

Where  $K_s$  is the normalised stress factor depending on available soil water.

$$K_s = \frac{TAW - D_r}{TAW - RAW} = \frac{TAW - D_r}{(1 - p) TAW} \quad (4.15)$$

$$RAW = p \cdot TAW \quad (4.16)$$

$$TAW = 1000(\theta_{FC} - \theta_{WP}) \cdot Z_r \quad (4.17)$$

- $K_s$  is a dimensionless transpiration reduction factor dependent on available soil water [0 - 1],
- $D_r$  root zone depletion [mm],
- TAW total available soil water in the root zone [mm],
- p fraction of TAW that a crop can extract from the root zone without suffering water stress [-].
- $\theta_{FC}$  the water content at field capacity [ $m^3 m^{-3}$ ],
- $\theta_{WP}$  the water content at wilting point [ $m^3 m^{-3}$ ],
- Zr the rooting depth [m].

### Air temperature stress

$$f(T) = b(T_a - T_{low})(T_{up} - T_a)^c \quad (4.18)$$

Where b and c are defined as:

$$c = \frac{T_{up} - T_{opt}}{T_{opt} - T_{low}} \quad (4.19)$$

$$b = \frac{1}{(T_{opt} - T_{low})(T_{up} - T_{opt})^c} \quad (4.20)$$

Where:

- $T_{opt}$  is the temperature at maximum conductance [ $^\circ C$ ];
- $T_{low}$  and  $T_{up}$  the lower and upper temperature of the range for which a positive stomatal conductance is predicted [ $^\circ C$ ].

If  $T_{low} \leq T_{air} \leq T_{up}$ ,  $f(T) = 0$ . White et al. (1999) assigned the values for  $T_{low}$ ,  $T_{opt}$  and  $T_{up}$  equal to  $0^\circ C$ ,  $17^\circ C$  and  $38^\circ C$ . These parameters can be set a priori or calibrated.

### Total solar radiation stress

$$f(R_{sw}) = \frac{1}{2\theta} \left( \alpha R_s + 1 - \sqrt{(\alpha R_s + 1)^2 - 4\theta\alpha R_s} \right) \quad (4.21)$$

Where:

- $\alpha$  and  $\theta$  are the slope and shape parameters of the stress function  $f(R_{sw})$  and are set equal to 0.005 and 0.85 [-].

$R_{sw}$  is the total solar radiation expressed in  $\mu\text{mol m}^{-2}\text{s}^{-1}$ . If we want to express it in  $\text{W m}^{-2}$  we must include a conversion factor equal to  $\approx 1/4.6$ .

### Vapour pressure deficit stress

$$f(VPD) = 1.1 \exp[-0.63 \cdot VPD] \quad (4.22)$$

Where b and c are defined as:

$$c = \frac{T_{up} - T_{opt}}{T_{opt} - T_{low}} \quad (4.23)$$

$$b = \frac{1}{(T_{opt} - T_{low})(T_{up} - T_{opt})^c} \quad (4.24)$$

#### 4.2.2 Maximum stomatal conductance

In White et al. (1999) and Noe and Giersch (2004),  $g_{s,max}$  (the maximum stomatal conductance) is parametrized or derived from laboratory measurements.

Since  $g_{s,max}$  is the conductance of the stoma when there are no stress factors (i.e. the  $f(x_n)$  are equal to 1), we assume it is equal to the total leaf conductance for water vapor ( $g_{tw}$ , Eq. 3.7) derived by Lehmann and Or (2015) and used by Schymanski and Or (2017), instead to parametrize it.

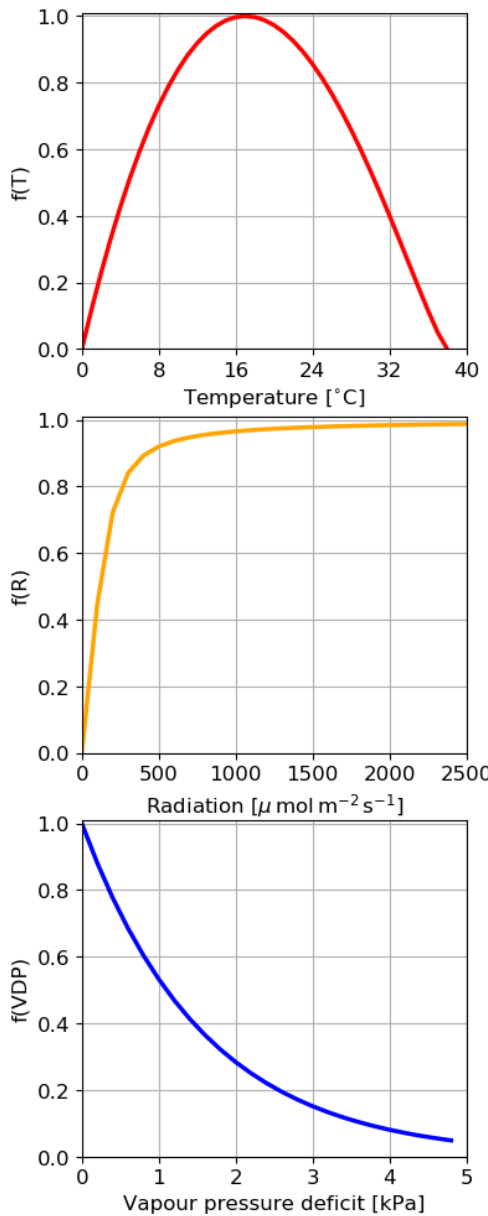


Figure 4.4: Typical values of the stress factor functions at the variation of the forcing.

## 4.3 Prospero's ET

All the previous corrections, due to the multi-layer model and to the conductance model, are used to improve the original Schymanski-Or equation. We need to point out that, for that concerning the conductance model, is not used to obtained the real transpiration by multiplying the potential transpiration, as commonly do in PM-FAO for example. In fact, the application of a stress factor implies a variation on the energy balance and so a different equilibrium leaf temperature.

$$ET = ETP \cdot g_s \quad (4.25)$$

$$ET = ETP(g_s) \quad (4.26)$$

Finally the transpiration is computed starting from the Schymanski and Or method and modified in order to include the dependence from transpiring surface, the conductance model of the stomata, other than the mass conservation. The major improvements of the Schymanski-Or model we did on Prospero are therefore the following:

- modified to use the leaf area index to obtained the **transpiring surface** ( $A_{tr}$ )
- stomata opening based on a **photosynthesis model** (Noe and Giersch, 2004).
- mass conservation asses thank to the **water stress** ((Allen et al., 1998))

We list here again the major of the equations of Prospero approach:

### Energy budget

$$R_s = \textcolor{red}{a_{sE} \cdot A_{tr} \cdot E_l(T_l)} + \textcolor{red}{a_{sH} \cdot A_{tr} \cdot R_{ll}(T_l)} + \textcolor{red}{a_{sH} \cdot A_{tr} \cdot H_l(T_l)} \quad (4.27)$$

**Leaf temperature**

$$\begin{aligned} T_l = & [R_s + \textcolor{red}{a_{sH} \cdot A_{tr}} \cdot \epsilon_l \sigma 4 T_a^4 + c_H(\textcolor{red}{a_{sH}, A_{tr}}) \cdot T_a + \\ & + c_E(\textcolor{red}{a_{sE}, A_{tr}, g_s}) \cdot (\Delta_e T_a + P_w - P_{ws})] \cdot \\ & \cdot \frac{1}{(c_H(\textcolor{red}{a_{sH}, A_{tr}}) + c_E(\textcolor{red}{a_{sE}, A_{tr}, g_s}) \Delta_e) + \textcolor{red}{a_{sH} \cdot A_{tr}} \cdot \epsilon_l \sigma T_a^3} \end{aligned} \quad (4.28)$$

**Longwave radiation**

$$R_{ll} = \textcolor{red}{a_{sH} \cdot A_{tr}} \cdot \epsilon_l \sigma (T_l^4 - T_a^4) \quad (4.29)$$

**Transpiration**

$$E_l = c_E(\textcolor{red}{a_{sE}, A_{tr}}) \cdot [\Delta_e (T_l - T_a) + P_{ws} - P_w] \quad (4.30)$$

**Sensible heat**

$$H_l = c_H(\textcolor{red}{a_{sE}, A_{tr}}) \cdot (T_l - T_a) \quad (4.31)$$

the total evapotranspiration is given by:

$$ET = E_{c,sun}(R_{c,sun}) + E_{c,sh}(R_{c,sh}) + E_{soil}(R_{soil}) \quad (4.32)$$

C H A P T E R



## POINTWISE ESTIMATES

In this section we compare the results obtained with the Prospero component with those obtained with the other components present in the GEOframe system, that is PM FAO and PT.

These methods are applied to two case studies. The performances are compared at plot scale, using direct latent heat measurements provided by eddy covariance stations and at different timescale, both hourly, monthly and annual timescale. The two case studies are represented by two alpine pastures: the Torgnon site, in the Val d'Aosta, and the Viole del Monte Bondone site, in Trentino (Italy). Pastures were chosen as they present a simpler canopy structure and therefore considered more suitable for validating the method. Both are FLUXNET sites and therefore equipped with eddy covariance stations, which provide a direct measure of latent heat.

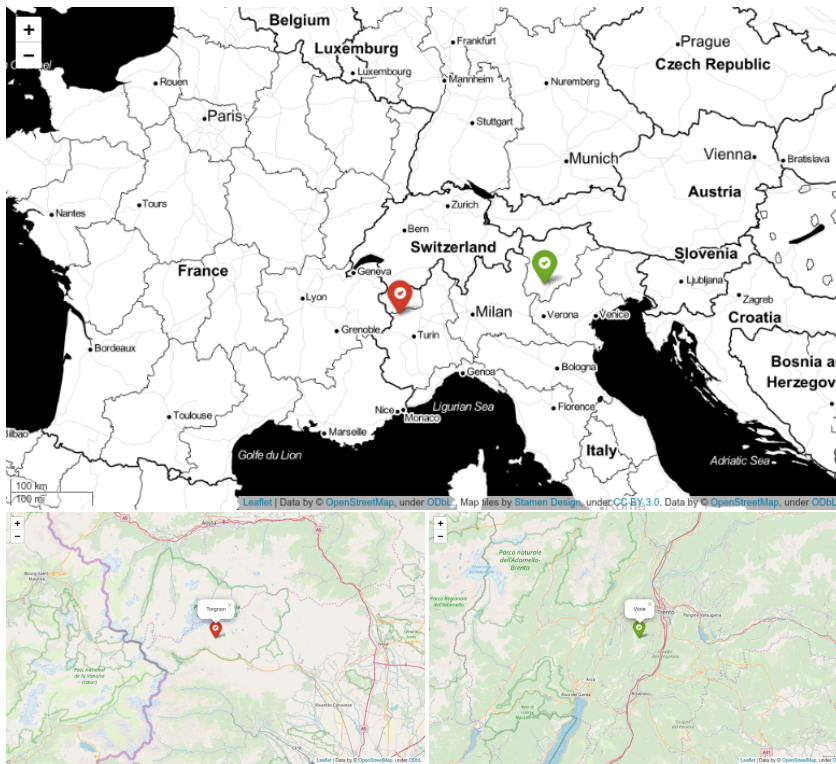


Figure 5.1: Map of the case studies, Torgnon (red marker) and Viole (green marker).

## 5.1 Torgnon

The Torgnon site, active since June 2008, is an unmanaged sub-alpine grassland located a few kilometers from the village of Torgnon in the northwestern Italian Alps (Aosta Valley,  $45^{\circ} 48'25.6''$  N  $07^{\circ}34'15.''2$  E) at an elevation of 2160 m asl. In the past the site was used for domestic livestock grazing and was abandoned in late 1990s (Cremonese et al., 2010). Vegetation is mainly composed by matgrass with other graminoids and forbs as co-dominant species. The site is characterized by an alpine climate with strong seasonality. The mean annual temperature is  $3.1^{\circ}\text{C}$  and mean annual precipitation is about 880 mm, however growing season cumulative precipitation can show huge variations (from 160 to

630 mm). On average, the site is covered by a thick snow mantle (90-120 cm) from the end of October to late May, which limits the growing season length to four-five months. The peak value of leaf area index (LAI) is on average  $2.2 \text{ m}^2/\text{m}^2$  and maximum canopy height is 0.2 m. Continuous eddy covariance (EC) measurements of  $\text{CO}_2$  and  $\text{H}_2\text{O}$  fluxes are carried out since June 2008, additionally, a weather station provided 30-min averaged records of different meteorological parameters, including air and soil temperature, soil water content, soil heat flux, net radiation, photosynthetically active radiation, snow height, precipitation, wind speed. Radiometric indexes like NDVI and PRI and greenness timeseries are collected by different unattended sensors. Soil is mainly composed by silt and sand (40-50% silt, 50-60% sand, 4-6% clay, Galvagno et al., 2013).

This site is managed by the Arpa Valle d'Aosta.

## 5.2 Viote

The Viote site is located at 1550 m asl on a mountain plateau in the Italian Alps (Viote del Monte Bondone,  $46^\circ 01' 46.8''$  N;  $11^\circ 04' 58.3''$  E). The mean annual air temperature is  $5.5^\circ\text{C}$  with monthly averages ranging from  $-2.7^\circ\text{C}$  in January to  $14.4^\circ\text{C}$  in July. The mean annual precipitation is about 1189 mm, with peaks in June (132 mm) and October (142 mm); snow cover occurs between November and April.

The area is managed as an extensive meadow. The maximum canopy height at the peak of the growing season (mid June to early July) can reach up to 30 cm. Meadows represent the main land use on this plateau ( $2\text{ km}^2$ ) and are traditionally managed for hay production with low mineral fertilization and one cut per year in mid-July. (Papale et al., 2015).

Also in this site a continuous eddy covariance (EC) measures  $\text{CO}_2$

and  $H_2O$  fluxes, and a weather station provided 30-min averaged records of different meteorological parameters, including air and soil temperature, soil water content, soil heat flux, net radiation, photosynthetically active radiation, snow height, precipitation, wind speed.

The soil is mainly composed of silt, sand and clay (Papale et al., 2015).

This site is managed by the Edmund Mach foundation of San Michele all'adige.

### 5.3 Data

FLUXNET sites are considered as case studies because they provide complete data sets of meteorological measurements and heat fluxes. Furthermore, the need to compare simulations with eddy covariance measures arises from the fact that these measures are the only ones that allow a direct measurement of the evapotranspiration fluxes. The fluxes measured by eddy covariance stations are often underestimated (Castelli et al., 2018). Since our model is based on the closure of the energy balance, in order to validate our results it is necessary that the measured data also guarantee the closure of the energy balance.

To guarantee this, the energy balance at the station is calculated as the sum of the fluxes (Eq. 5.1) and it is verified that the energy balance is closed. When this does not happen, the energy balance is closed (Wohlfahrt et al., 2009).

$$R_s - R_{ll} - G - E_l - H_l = 0 \quad (5.1)$$

Since the radiation measurements are carried out by common meteorological stations and, therefore generally not affected by bias but only by instrumental errors, it can be assumed that they are accurate and precise and it is therefore reasonable to assume

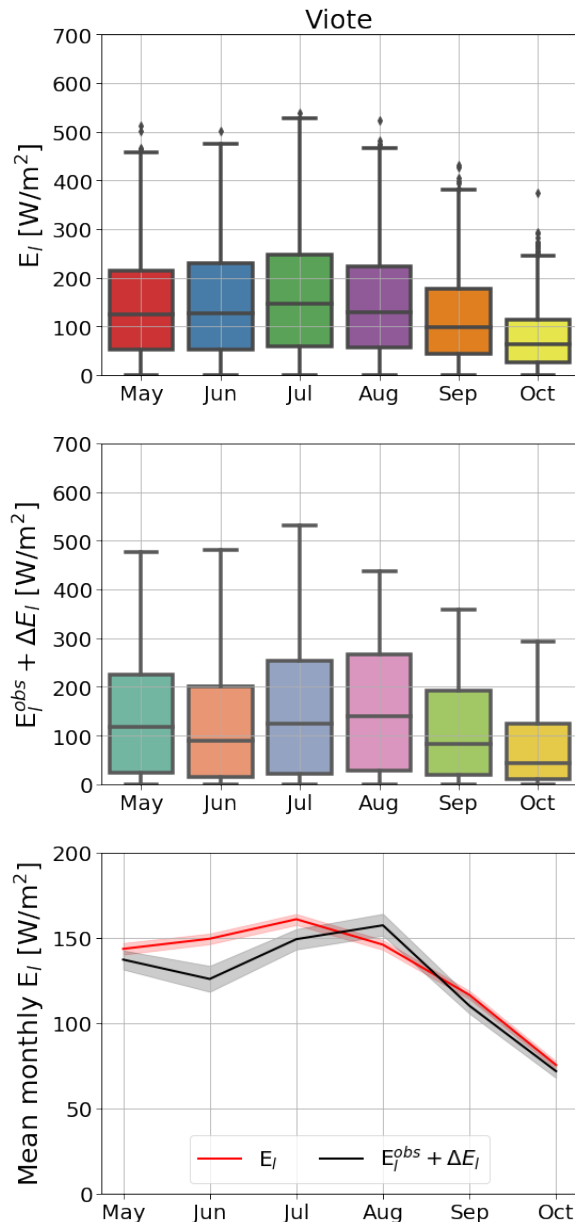


Figure 5.2: Monthly distribution of latent heat in Viote site before and after the correction of the energy balance (boxplot) and the mean monthly value (band represent the 95% of the confidence interval)

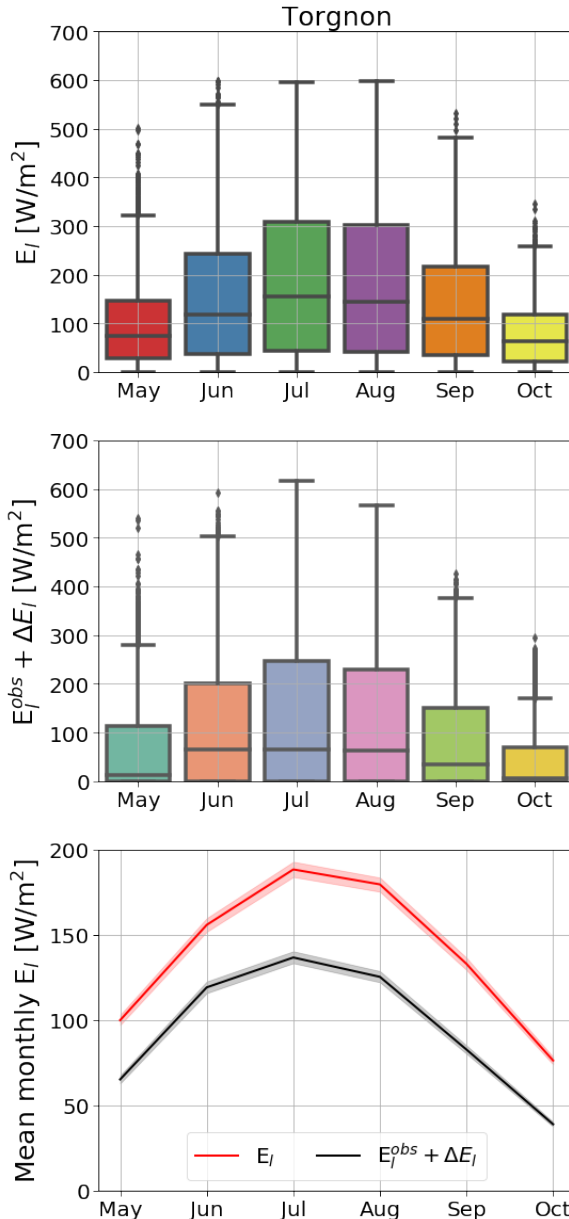


Figure 5.3: Monthly distribution of latent heat in Torgnon site before and after the correction of the energy balance (boxplot) and the mean monthly value (band represent the 95% of the confidence interval)

that the error falls on the measurement of heat flows .

If there is no underestimation, the result of the energy balance should be zero or close to zero. However, this does not occur in most cases and the energy balance returns a non-zero residual. Furthermore, often the residue thus obtained results to be of the same order of magnitude as the observed value. As we can see in the Fig. 5.4 and 5.5 the energy balance is almost never closed.

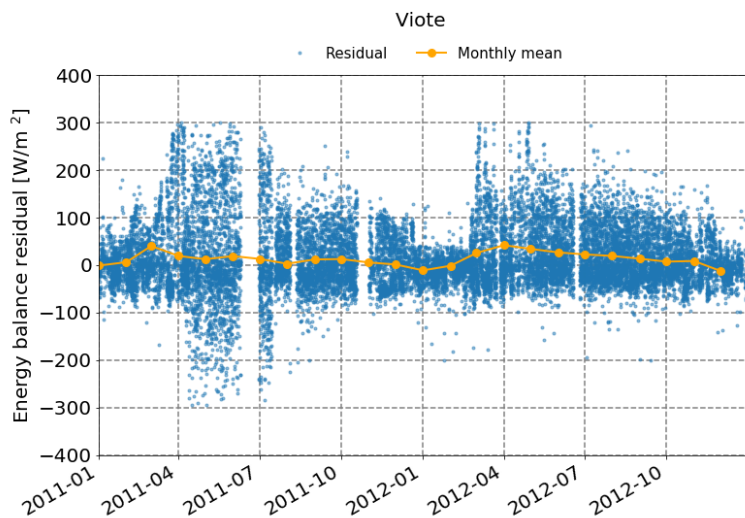


Figure 5.4: Energy balance residual on Viote.

This is generally due to the combination of eddy covariance measurements of latent heat and sensible heat with independent measurements of radiation and soil heat flux, generating a lack of closure of the energy balance for several reasons discussed in (Twine et al., 2000) and in Wohlfahrt and Widmoser (2013).

This problem is well known in the scientific community and widely treated and a detailed analysis is presented by Foken (2008).

Although it is clear that the hypotheses behind the eddy covariance method (Aubinet et al., 1999) are more likely to be violated

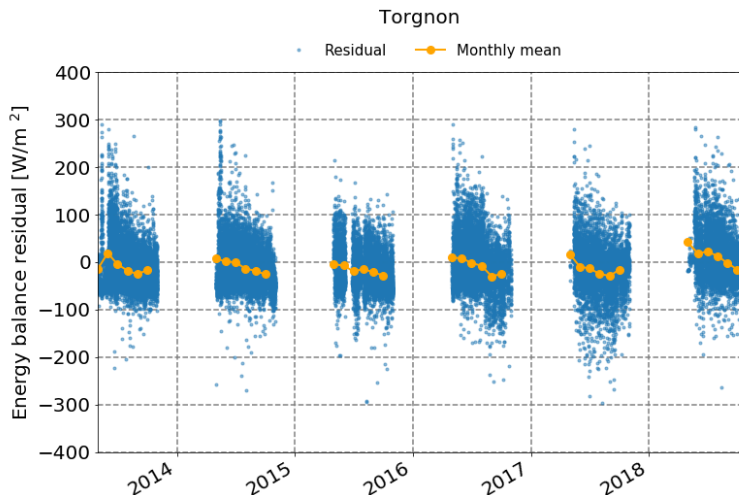


Figure 5.5: Energy balance residual on Torgnon.

in orographically complex terrain than flat and homogeneous ones, the lack of closure of the energy balance in this study falls well within the range observed in a wide range of FLUXNET sites (Stoy et al., 2013) and that the closure of the energy balance is generally not worse for mountain grasslands in complex topography (e.g. Hammerle et al., 2007; Hiller et al., 2008).

The same criteria used successfully by Castelli et al. (2018) are used in another alpine pasture, the Val di Mazia site (LTSER, long-term socio-ecological research), also present in the Trentino Alto-Adige region, not far from the Viote site.

It was decided to discard the data when the error on the closure of the energy balance is too high and therefore the usefulness of  $E_l$  and  $H_l$  for the validation of the model is significantly reduced. We therefore excluded the measurements from our analyzes when the absolute balance sheet closure exceeds  $300 \text{ W m}^{-2}$ :

$$R_s^{obs} - \delta R_{ll}^{obs} - G^{obs} - E_l^{obs} - H_l^{obs} \geq 300 \text{ W m}^{-2} \quad (5.2)$$

and when the relative closure exceeds 0.4, i.e. when there is a

strong imbalance between the fluxes, the radiative ones and heat ones:

$$\frac{R_s^{obs} - \delta R_{ll}^{obs} - G^{obs} - E_l^{obs} - H_l^{obs}}{R_s^{obs} - \delta R_{ll}^{obs}} \geq 0.4 \quad (5.3)$$

Furthermore, only the dates on which the energy balance can be closed are considered valid, that is when all the measures of the energy fluxes are available. Added to this are the dates on which all the measurements for the model components are available. In addition, due to the snow cover during the winter, the analysis is limited to the period from early May to late October. This involves a large reduction in the initial data set.

Once the residual has been calculated, it is used to force the closure of the energy balance. This is done using two commonly adopted approaches (Twine et al., 2000; Wohlfahrt et al., 2009; Wohlfahrt and Widmoser, 2013).

In the first case, which represents the 'worst case scenario', the residue is used to correct only the latent heat, therefore we assume that all the error is committed on it.

$$\Delta = R_s^{obs} - \delta R_{ll}^{obs} - G^{obs} - E_l^{obs} - H_l^{obs} \quad (5.4)$$

$$E_{l,cor}^{obs} = E_l^{obs} + \Delta \quad (5.5)$$

$$H_{l,cor}^{obs} = H_l^{obs} \quad (5.6)$$

In the second case is based on the Bowen ratio and it uses the residue to correct both the latent heat and the sensitive one:

$$B_{ratio} = \frac{E_l^{obs}}{H_l^{obs}} \quad (5.7)$$

$$\Delta H_l = \Delta \cdot \frac{1}{1 + B_{ratio}} = \Delta \cdot \frac{H_l^{obs}}{|H_l^{obs}| + |E_l^{obs}|} \quad (5.8)$$

$$\Delta E_l = \Delta - \Delta H_l \quad (5.9)$$

$$E_{l,cor}^{obs} = E_l^{obs} + \Delta E_l \quad (5.10)$$

$$H_{l,cor}^{obs} = H_l^{obs} + \Delta H_l \quad (5.11)$$

Since it is generally calculated on daytime, i.e. when both  $E_l$  and  $H_l$  are positive, there are no problems at the denominator. To avoid these problems, we consider the absolute value of the heat fluxes.

After this correction, the residual is recalculated to verify that the energy balance is correctly closed.

LAI data for Torgnon are provided as mean monthly values over the entire period. For Viole, the leaf area index values are not available and so they are derived from satellite Terra MODIS. Terra MODIS data ([MOD15A2H](#)) have a 8-days frequency and a resolution of 500m. Massive data download was done using the [Pymodis](#) package.

The values of water field capacity( $\theta_{fc}$ ) and wilting point ( $\theta_{wp}$ )

<b>Soil composition</b>	Viole	Torgnon	$\theta_{fc}$	$\theta_{wp}$
Sand	17%	45%	0.07-0.17	0.02-0.07
Silt	74%	55%	0.28-0.36	0.12-0.22
Clay	9%	5%	0.32-0.40	0.20-0.24

Table 5.1: Soil composition in Viole and Torgnon site.

	Viole	Torgnon
$\theta_{fc}$	0.289	0.248
$\theta_{wp}$	0.153	0.124

Table 5.2: Values of field capacity and wilting point obtained for the two sites based on the soil composition

for the two sites are calculated by means of weighted averages on the soil composition (Tab. 5.1 and 5.2).

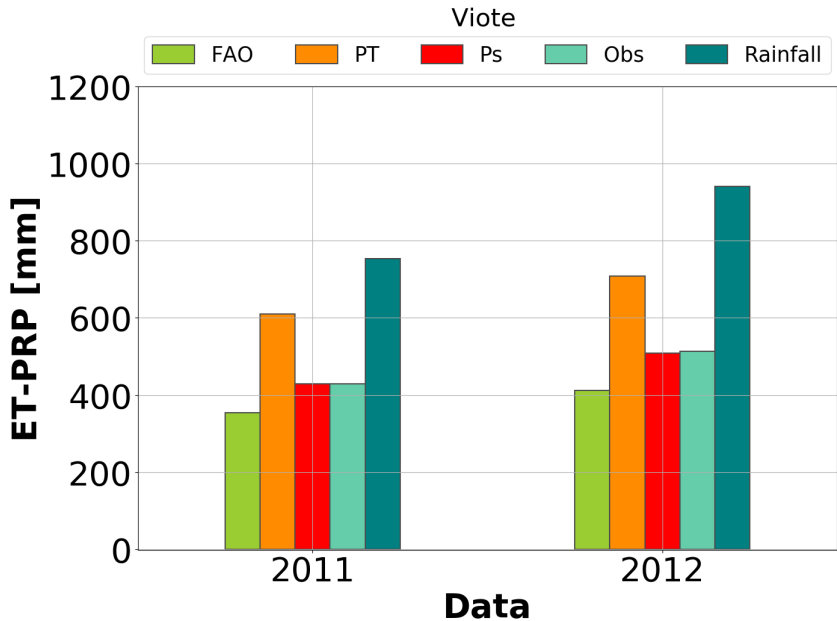


Figure 5.6: Total annual evapotranspiration simulated and observed on Viote.

## 5.4 Model parametrization and results

**Priestley-Taylor** In this component the only parameter present is  $\alpha$ , which links potential to real evapotranspiration. We set  $\alpha$  equal to the average value reported in literature (1.26, Priestley and Taylor, 1972).

**Penman-Monteith FAO** in the Penman-Monteith FAO component there are two sets of parameters: those related to vegetation and those related to soil.

We know that both Viote and Torgnon are pastures, so we can use the parameters for grazing pasture reported by (Allen et al., 1998) and reported in the table 5.3.

Currently there is no possibility of set the crop coefficient ( $K_c$ )

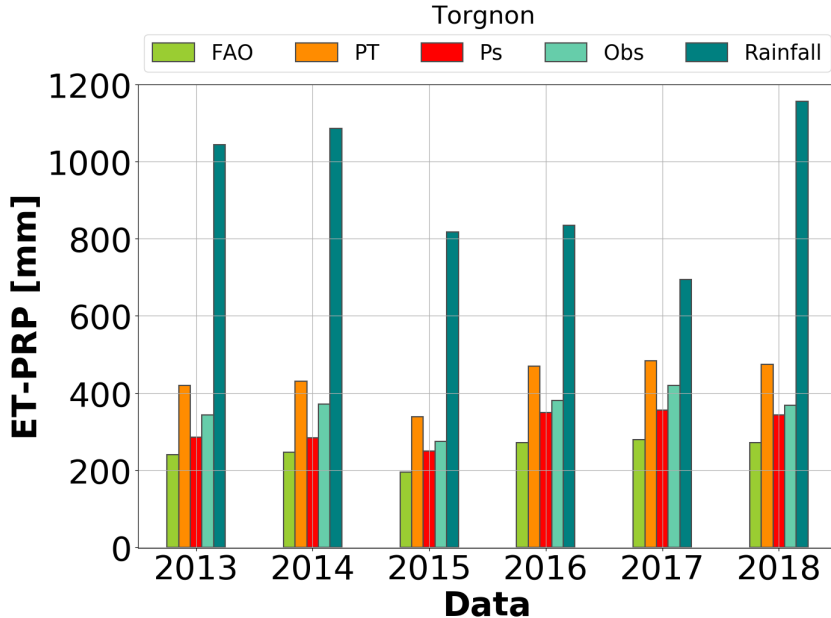


Figure 5.7: Total annual evapotranspiration simulated and observed on Torgnon.

with multiple values, i.e. for the initial stage ( $K_{c,ini}$ ), for the mid-season stage ( $K_{c,mid}$ ) and for the end of the late season stage ( $K_{c,end}$ ), so we decide to use  $K_{c,mid}$  (Allen et al., 1998).

The soil parameters are set by knowing the composition of the soils in the two sites. The values of  $\theta_{fc}$  and  $\theta_{wp}$  are calculated with a weighted average on the composition.

**Prospero** In this component the parameters for stress and soil are set. For the parameters relating to soil and water stress, the same parameterization used for the FAO component is used (Allen et al., 1998).

The parameters of the other stresses are set equal to the values found in the literature, there is no reference range (Jarvis and Mcnaughton, 1986; White et al., 1999; Noe and Giersch, 2004).

The simulations are carried out on all complete periods, (2011-

	Pasture	Viote	Torgnon
Vegetation			
<i>crop coefficient (<math>K_{c,mid}</math>)</i>	0.75	0.75	
<i>roots depth</i>	0.75	0.75	
<i>depletion fraction</i>	0.55	0.55	
<i>canopy height</i>	0.2	0.2	
Soil			
<i>water wilting point</i>	0.153	0.124	
<i>water field capacity</i>	0.289	0.248	

Table 5.3: Values for PM-FAO component for the two sites.

2012 Viote, 2013-2018 Torgnon). Simulations' parameters are not calibrated.

The results of the simulated evapotranspiration are compared with the observed values and the performances of the three models are evaluated. The performances of the three components are evaluated by calculating the *mean absolute error* and *root mean square error* calculated on the whole periods are reported in table 5.5. RMSE and MAE calculated on the results of Prospero are almost equal on both sites. On the contrary, FAO's performances show a variation of more than 50%, at the same time being the model that provides the best results on Viote and the worst on Torgnon.

The results are represented by scatter plots in 5.13 and 5.14. We can see that there is an underestimation of the FAO method compared to the observed, more marked for the Torgnon site, while for the Viote site this underestimation is more linked to the maximum values of  $E_l$ , not returning values of  $E_l$  greater than  $400 \text{ W m}^{-2}$ .

In fact, almost all the simulated values are below the secant (black line). This underestimation can be easily noticed by observing the regression of the calculated-observed data, represented by

Parameters	Viote	Tognon
<b>Vegetation</b>		
<i>canopy height</i>	0.2	0.2
<i>roots depth</i>	0.75	0.75
<i>depletion fraction</i>	0.55	0.55
<b>Stress</b>		
$\alpha$	0.005	0.005
$\theta$	0.85	0.85
$VPD_0$	5.0	5.0
$T_l$	0.0	0.0
$T_o$	18.0	18.0
$T_u$	35.0	35.0
<b>Soil</b>		
<i>water wilting point</i>	0.153	0.124
<i>water field capacity</i>	0.289	0.248

Table 5.4: Parameters used for Prospero simulations in Viote and Torgnon.

	Viote	MAE	RMSE
<i>Prospero</i>	44.8	58.2	
<i>FAO</i>	38.7	49.1	
<i>PT</i>	67.4	88.9	
Torgnon	MAE	RMSE	
<i>Prospero</i>	42.9	53.6	
<i>FAO</i>	62.6	75.7	
<i>PT</i>	52.3	70.2	

Table 5.5: *Root mean square error* and *mean absolute error* obtained on Viote and Torgnon simulations

the orange line, which shows a lower trend compared to the ideal one, represented by the black line.

The results obtained through the Prospero component show a trend more coherent with the theoretical one but with a greater

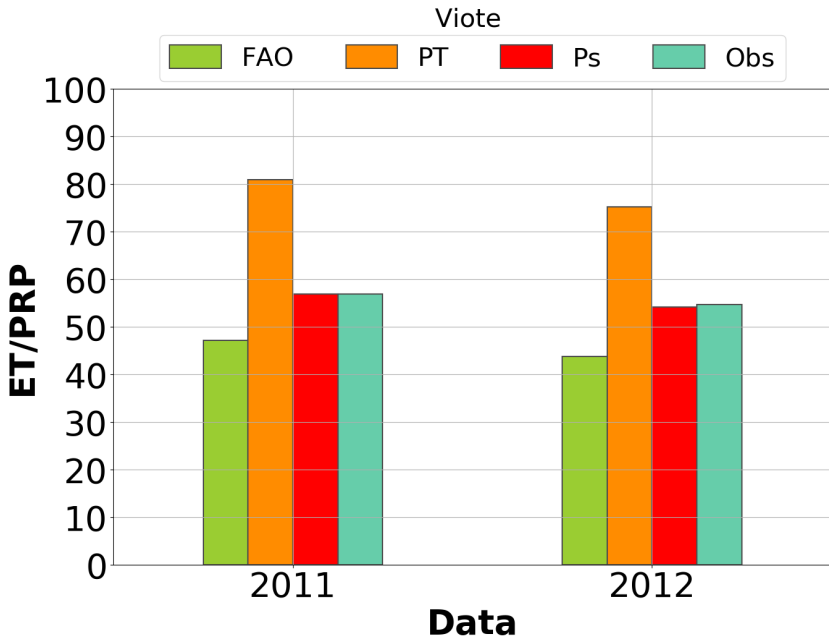


Figure 5.8: Ratio between the total annual evapotranspiration, both simulated and observed, and precipitation on Viote.

dispersion. This dispersion is further accentuated for the minimum values of Viote. This is reflected in a higher RMSE (Tab. 5.5) on Viote than the one obtained with the FAO method. These errors are however comparable with those typically obtained in estimating latent heat (Blyth et al., 2010; Ershadi et al., 2014; Zhu et al., 2014).

Observing also the hourly scale MAE (Fig. 5.4) it can be seen how Prospero gives a more constant trend during the 24 hours, unlike FAO and PT, which show a bias due to the daily cycle, thus demonstrate that they are not able to represent well the daily evolution of evapotranspiration. This type of bias is not present even in the monthly MAE and it can be seen that Prospero's performance is substantially better (Fig. 5.4 and 5.4). Probably Prospero performances at hourly scale are better because it assess the closure

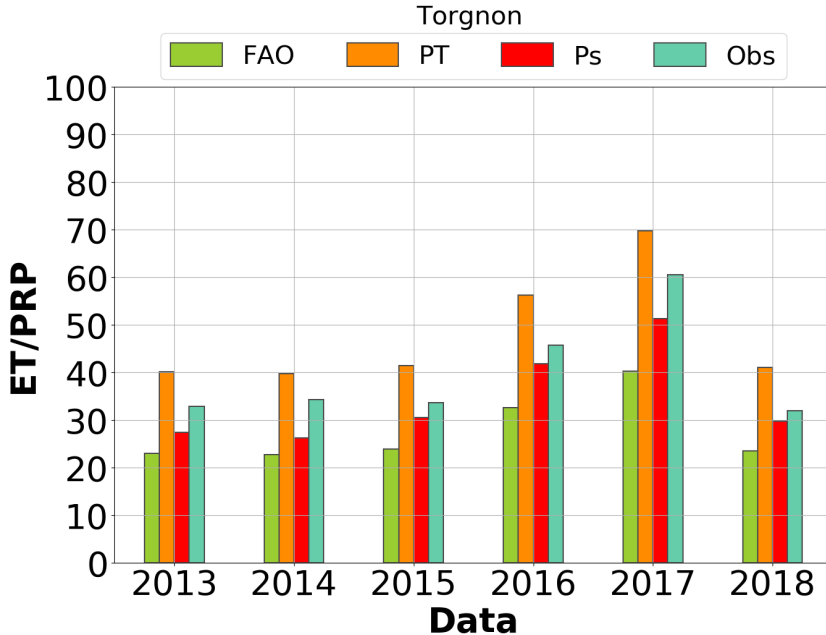


Figure 5.9: Ratio between the total annual evapotranspiration, both simulated and observed, and precipitation on Torgnon.

of the energy balance and it also includes a canopy model that depends on the sun angle. By comparing the estimated values on an annual scale with the observed values we can see that PT has a strong overestimation compared to the observed evapotranspiration, representing about 75-80% of the observed rainfall, while the real evapotranspiration turns out to be approximately 55% annual rainfall. This value is certainly well represented by the Prospero, while FAO underestimates it.

Evapotranspiration in the Torgnon site is slightly lower than in the Viote, probably because it is higher and colder.

In Torgnon evapotranspiration accounts from 30 to 60% of precipitation. This variation is due to the strong variation of annual precipitation, which can reach 400 mm/year. FAO's performances are discrete on the Viote case study, while on the contrary

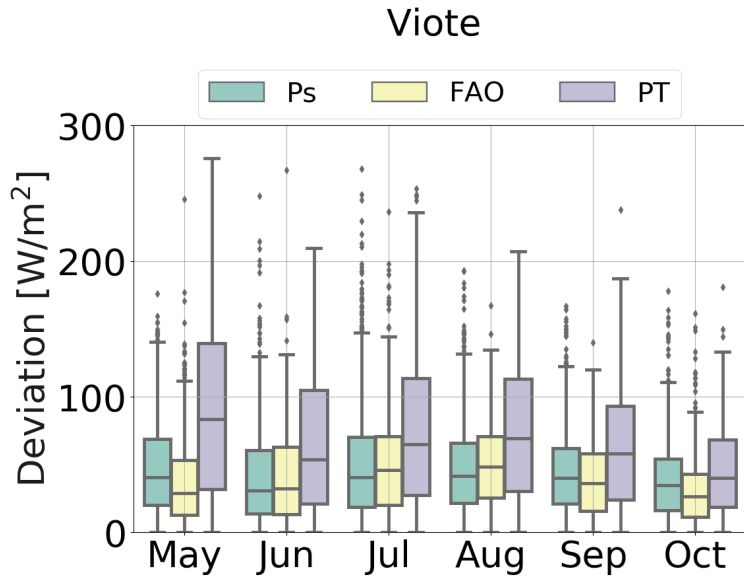


Figure 5.10: Boxplot of the difference between simulated and observed grouped at monthly timescale for Viote site.

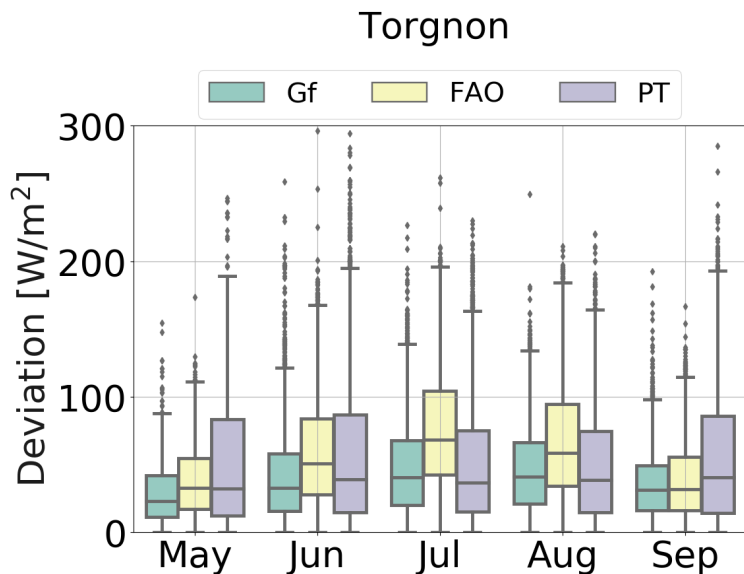


Figure 5.11: Boxplot of the difference between simulated and observed grouped at monthly timescale for Torgnon site.

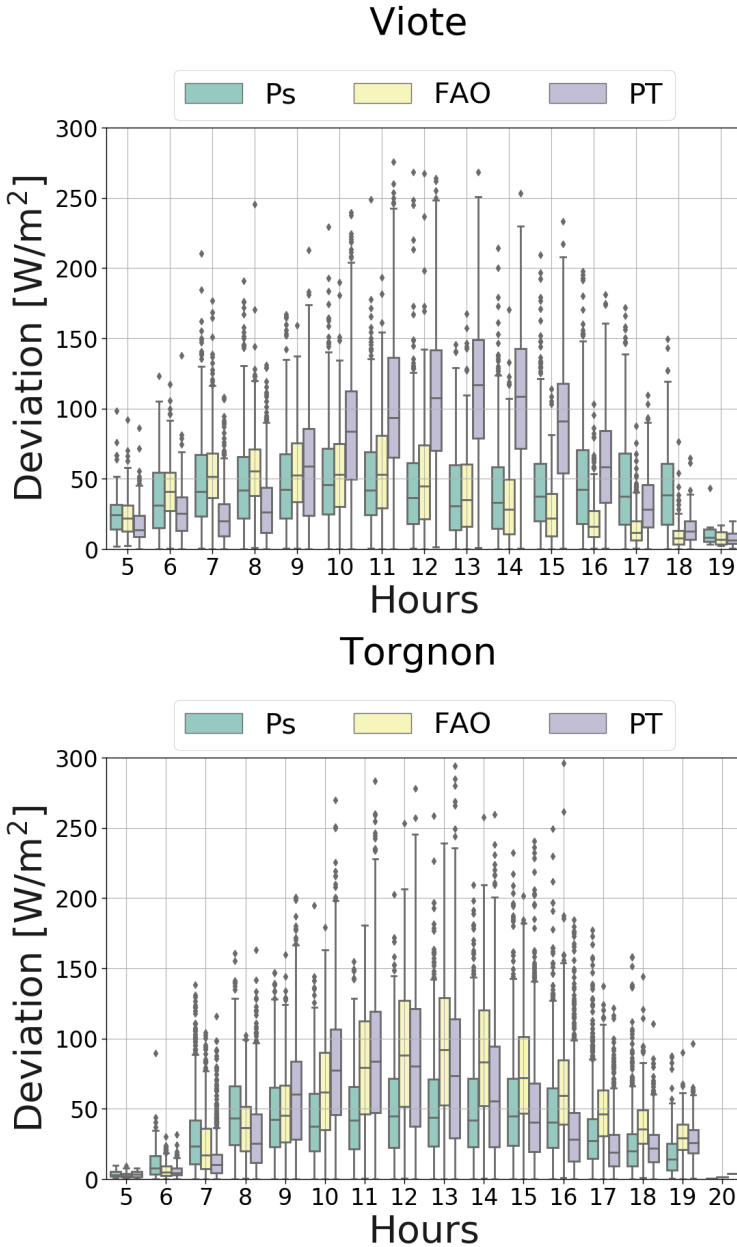


Figure 5.12: Boxplot of the difference between simulated and observed grouped at daily timescale.

they show a big difference on the Torgnon site, especially at an hourly rate (Fig. 5.4 and 5.4).

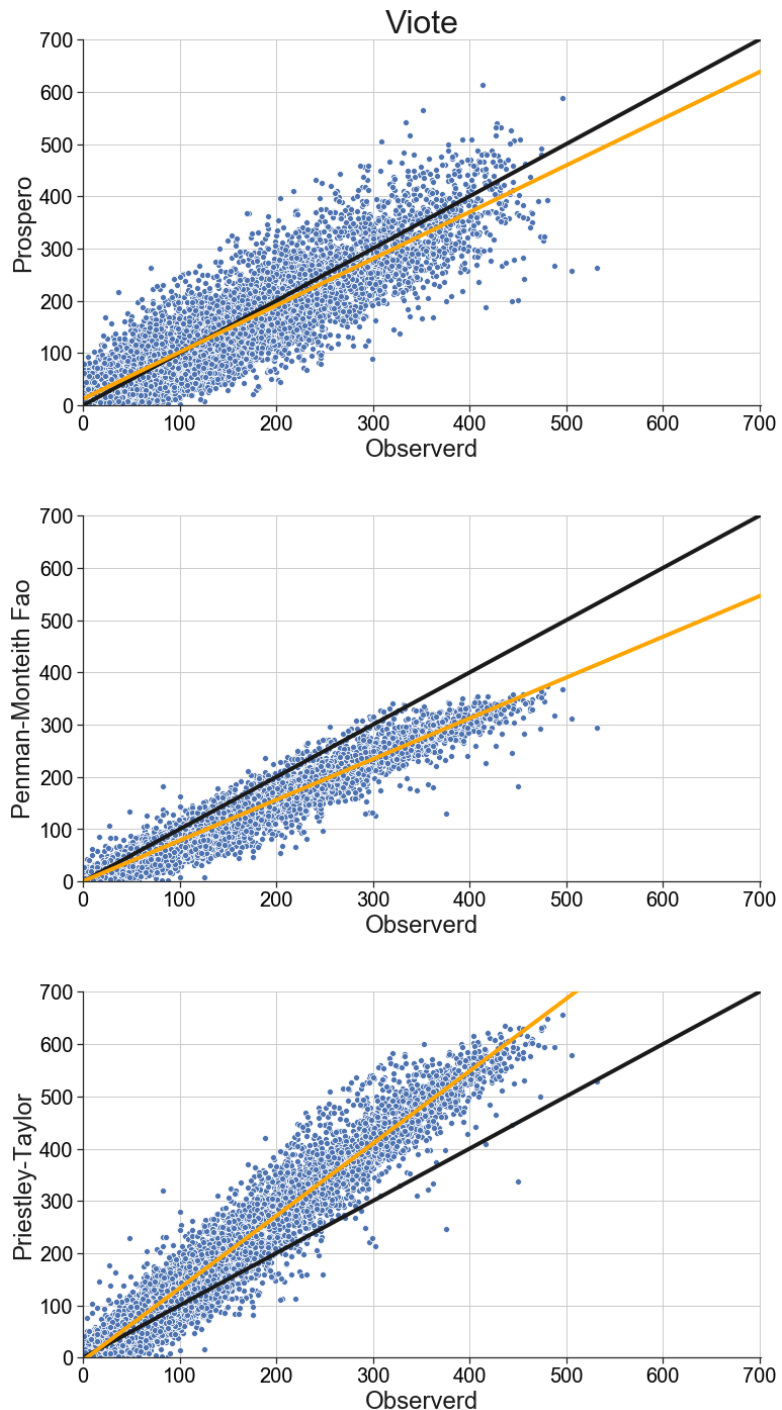


Figure 5.13: Scatter plot simulated vs observed.

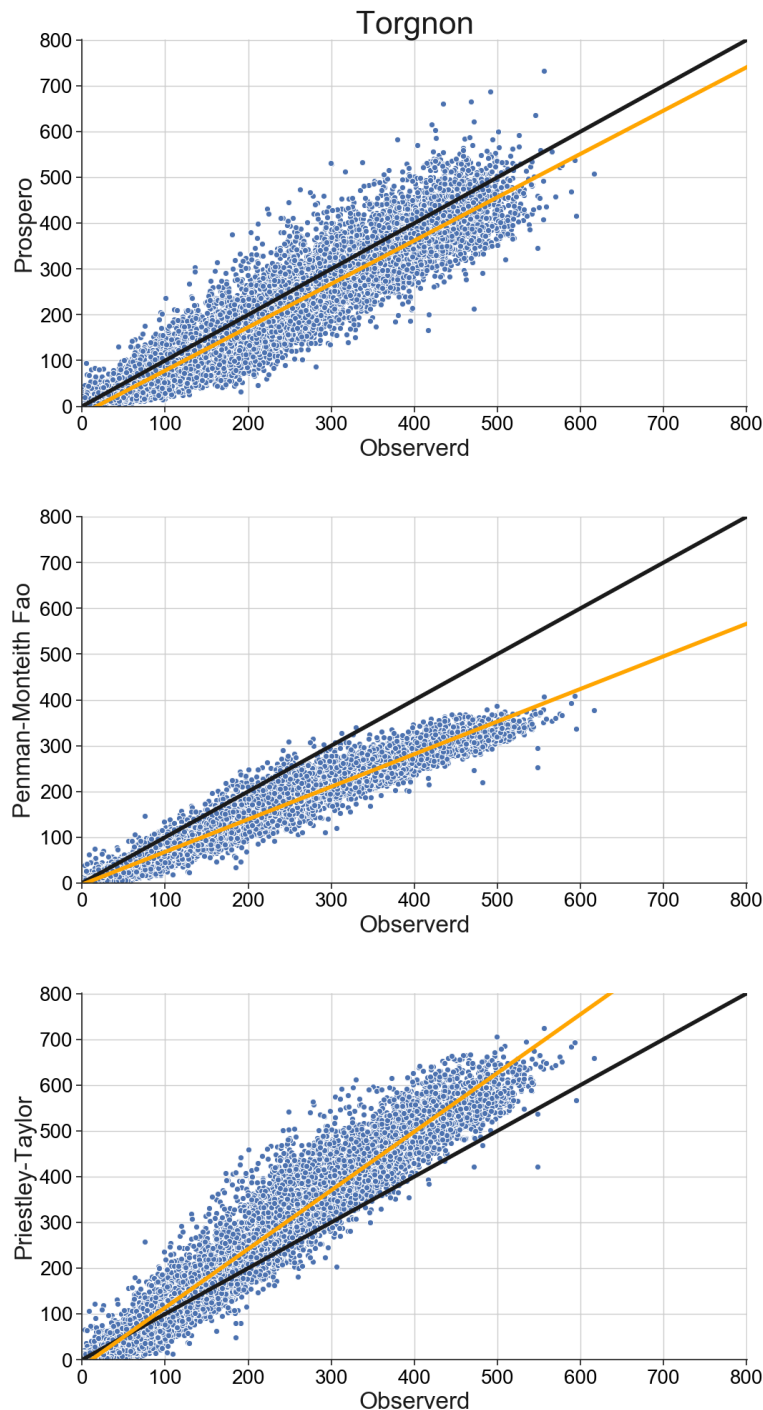


Figure 5.14: Scatter plot simulated vs observed.

In general it can be said that the performances provided by Prospero at plot scale are better than the other methodologies and that even without calibration they capture the measured evapotranspiration pattern well, causing an error comparable with that obtained from other studies carried out on alpine grasslands.



C H A P T E R



## CATCHMENT-BASED ESTIMATES

This case study is part of the SILVA research project, aimed at improving the understanding of the hydrological response in forest basins characterized by different climatic conditions, identifying the fundamental hydrological mechanisms that regulate the seasonal-event-scale inflow-runoff on forest basins and the impact of evapotranspiration on the generation of outflow, analyzing the hydrological response also in different scenarios of land use and modification of evapotranspiration flows.

### 6.1 Rio Ressi

The Rio Ressi is an experimental basin located in the southern part of the Posina river basin ( $116 \text{ km}^2$ ) at the foot of the central-eastern Alps ( $45^\circ 47' 11.79'' \text{ N}$ ;  $11^\circ 15' 54.12'' \text{ E}$ ), with an area of  $0.02 \text{ km}^2$ . The Posina river is a tributary of the Astico river that flows into the Adriatic sea. About 74% of the Posina basin is densely vegetated (Norbiato et al., 2009), partly due to the marked expansion

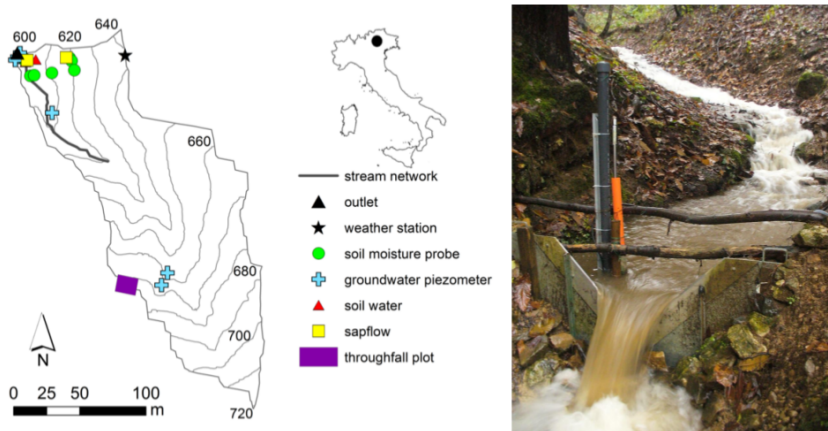


Figure 6.1: Experimental basin of Rio Ressi.

of deciduous forests in the last fifty years following the abandonment of agricultural practices. The climate is humid temperate and the average annual precipitation (1992-2007) recorded by a meteorological station in the central part of the Posina basin (at 597 m s.l.m., about 4.5 km in a straight line from Ressi) is 1695 mm. The average annual temperature is 9.7° C; average monthly temperatures fluctuate between 1.2° C in January and 18.7° C in July. Precipitation is concentrated in spring (150 mm and 159 mm on average, respectively in April and May) and in autumn (236 mm and 246 mm on average in October and November, respectively). The altitudes in the study basin range from 609 to 725 m s.l.m. The average slope is 26°; the appearance is mainly north-west. The canal is about 150 m long. The frequently saturated channel and near-flat near-flow zone comprise about 1.5% of the basin area. The flow stage was measured at an interval of 5 minutes by a pressure transducer behind a V-shaped dam. Flow was measured under different flow conditions using the volumetric method to verify the dam equation. Groundwater levels were monitored with 5 minute resolution in two riparian wells (GW1 and GW2) and in a well at the bottom of the slope (GW3). The

depth of the wells was 2.04, 1.04 and 0.68 m respectively for GW1, GW2 and GW3. The soil moisture near the surface (0-30 cm) was measured at 10 minute intervals using four reflectometers. The probes were installed in different positions along a transect: SM1 was positioned in the riparian zone, about 1 m from the torrent, SM2 when passing between the riparian zone and the slope (foot-slope), SM3 in the central part of the slope and SM4 in the part upper part of the slope.

## 6.2 Data

A meteorological station is located in the Rio Ressi basin which provides temperature, wind speed, radiation, relative humidity and precipitation measurements.

The soil moisture measurements are provided by four piezometric probes that detect the soil moisture in the four different areas of the basin.

In addition, there are flow measurements detected by the hydrometer located in the closing section.

The meteorological variables are available at a frequency of 5 or 10 minutes, they are subsequently resampled on an hourly scale to be consistent with the flow measurements, LAI is derived from throughfall measurements (Zuecco, 2016).

In addition to collecting the necessary hydrometeorological data, a geomorphological analysis of the basin was carried out. This analysis was carried out starting from a model of digital elevation of the ground (resolution of 1 m) and served to delineate the network and the drainage directions, the sky-view factor and the hydrological response units (HRU). Due to the small size of the Rio Ressi basin (about 2.4 ha), the homogeneity of the lithology and soils and the unbranched hydrographic network it was decided to use a single hydrological response unit for the

pre-Alpine basin. Starting from the digital elevation model, the geomorphological analysis is carried out using the Jgrasstools (now, HortonMachine) integrated into GEOframe (Formetta et al., 2011a; Formetta et al., 2013b; Rigon et al., 2011).

Given the small size of the sub-basin and having outlined only one HRU, no interpolation of the meteorological data collected is considered necessary since the measurements are collected directly in the basin.

Forest trees	Value
crop coefficient ( $K_{c,mid}$ )	1.00
roots depth	1.25
depletion fraction	0.7
canopy height	10
water wilting point	0.15
water field capacity	0.27

Table 6.1: FAO's vegetation parameters used for the Rio Ressi simulation

## 6.3 Model calibration

Model calibration is performed by calibrating the ERM parameters (Tab. ) for the year 2015, validation is done on the remaining years.

The model is calibrated in order to maximize the KGE of the simulated runoff compared with the observed one. An accurate description of the parameters and their ranges is provided in Bancheri (2017).

The calibration of the ET components is not carried out even in this case as there is no direct measurement of the evapotranspiration but only an estimate of it derived from the closure of the hydric balance.

The parameters used for FAO are those of the forest trees (Testa et al., 2011) and reported in Tab. 6.1. For PT the value of  $\alpha$  is always kept equal to 1.26. The parameters of Ps, also in this case, are kept equal to those used in the literature and not calibrated.

Reservoir	Parameter	Range
Snow	$\alpha_m$	[0.01 - 1.0]
Snow	$\alpha_f$	[0.0001 - 0.1]
Snow	$\alpha_e$	[ $1.0 \cdot 10^{-5}$ - $1.0 \cdot 10^{-4}$ ]
Snow	$\alpha_l$	[0.3 - 0.9]
Canopy	$k_c$	[0.1 - 0.3]
Root zone	$S_{rz_{max}}$	[100 - 400]
Root zone	a	[0.0001 - 0.01]
Root zone	b	[1.0 - 2.0]
Root zone	B	[0.1 - 0.8]
Direct runoff	$p_{Sat}$	[20.0 - 80.0]
Direct runoff	c	[0.0 - 0.1]
Direct runoff	d	[1.0 - 3.0]
Groundwater	$S_{gw_{max}}$	[500 - 1000]
Groundwater	e	[100 - 600]
Groundwater	f	[1 - 10]

Table 6.2: Parameters range of the Embedded Reservoir Model

## 6.4 Results

Three hydrological simulations were conducted, each using a different GEOframe component for estimating evapotranspiration. At each simulation the hydrological model was calibrated, using the OMS internal calibrator, LUCA (Let Us CALibrate, Hay and Umemoto, 2006), comparing the simulated runoff with the observed one, optimizing the Kling-Gupta efficiency coefficient (KGE).

The analysis for the Rio Ressi basin was conducted for the period

from the beginning of 2014 to the end of 2017. There are also data for the two-year period 2012-2013, however for this period the precipitation was interpolated from nearby stations, so we preferred to exclude this period from the analysis.

The year 2014 was found to be very rainy with almost 3000 mm of annual precipitation.

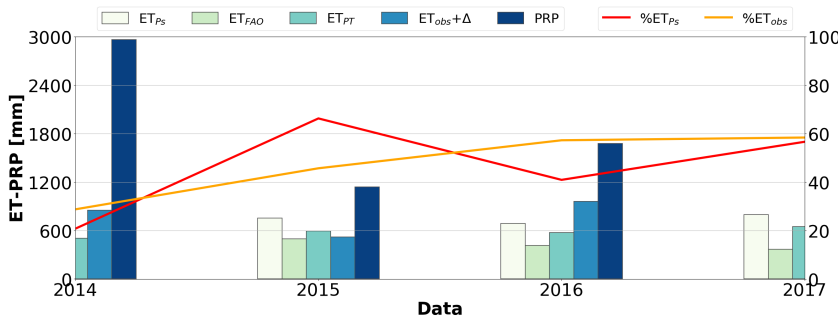


Figure 6.2: Total annual precipitation and evapotranspiration, both simulated with the GEOframe components and derived from the hydrological balance. The ratio ET-P is represented by the lines, red for the simulated ET and orange for the observed.

It was therefore decided to calibrate the model only for the year 2015 and subsequently validate the entire period. As previously mentioned, the simulations were carried out with relative calibration, varying each time the type of evapotranspiration used.

For these simulations the value of Priestley-Taylor  $\alpha$  (parameter that relates the potential evapotranspiration to the real one) was taken equal to the average value (1.26, Priestley and Taylor, 1972), while for the FAO Penman-Monteith method the parameters for forest trees, in order to consider a covering of vegetation similar to that of the Rio Ressi basin (Tab. 6.1). For the simulation conducted with the Prospero component, the same parameters are used for the previous study cases.

In the application of the model to the basin scale, it is assessed how the use of different components to estimate evapotranspiration affect the performance of the hydrological model. This is necessary because in this case there are no direct evapotranspiration measures.

An estimate of the actual evapotranspiration is obtained by closing the hydrological balance:

$$P_{Obs} - \Delta S_{Obs} - R_{Obs} - ET = 0 \quad (6.1)$$

where  $P_{Obs}$  is the measured precipitation,  $\Delta S_{Obs}$  is the observed storage variation, i.e. the change in water content,  $R_{Obs}$  is the runoff measured at hydrometer and ET is the evapotranspiration. The storage variation is calculated starting from the soil moisture [ $m^3/m^3$ ] and ground water depth to water table (expressed in meters) data.

Since there are four piezometric probes for measuring soil moisture, the average value is considered.

Storage is then calculated per unit area such as the average soil moisture of the basin for the depth of the water table:

$$S = \theta \cdot GW_{depth} \quad (6.2)$$

The variation in soil moisture is obtained as the difference between storage at different time steps:

$$\Delta S = S^{t+1} - S^t \quad (6.3)$$

The outflow is generated using the Embedded reservoir (ER, Bancheri, 2017). In addition to evaluating the performance of the hydrological model, the water balance is closed in order to estimate the real evapotranspiration and compare it with that simulated by the model.

$$P_{Obs} - \Delta S_{Sim} - R_{Sim} - ET_{Sim} = Residual_{Sim} \quad (6.4)$$

	<i>Prospero</i>	<i>PM-FAO</i>	<i>PT</i>
<b>KGE (calibrated)</b>	0.76	0.75	0.76
<b>KGE</b>	0.67	0.63	0.54
<b>NS (calibrated)</b>	0.67	0.60	0.60
<b>NS</b>	0.43	0.39	0.45
<b>Pbias</b>	-16.0	-26.5	-34.6
<b>R<sup>2</sup></b>	0.74	0.45	0.65

Table 6.3: Performance of the ERM using different components for the evapotranspiration

$$P_{Obs} - \Delta S_{Obs} - R_{Obs} = ET_{Obs} \quad (6.5)$$

$$\%ET_{Ps} = ET_{Ps}/P_{Obs} \quad (6.6)$$

$$\%ET_{Obs} = ET_{Obs}/P_{Obs} \quad (6.7)$$

This measure is therefore affected by errors deriving from the other measures and therefore by the error on the closure of the water balance.

We can compare the estimated evapotranspiration with that obtained from the water balance.

Despite the spread between estimated and observed evapotranspiration is evident, especially in the winter months, also in this case it is noted that the total annual evapotranspiration obtained with Ps represents better than obtained through the water balance. Furthermore, on an annual scale the ET estimated with Ps represents between 40-65% of the annual rainfall, while the observed evapotranspiration range from 50 to 60% of the annual precipitation.

This result represents a discontinuity with the evapotranspiration estimated on the whole Posina, in which the ET represents 25-30 % of the annual precipitation (Abera et al. 2017, Bancheri 2017).

Furthermore we found that the evapotranspiration computed with PT and FAO is between the 25 and 30% of the annual precipitation, while the one obtained with Prospero and the one derived by the closure of the hydrological water budget range from 40 to 60% of the total annual precipitation, accordingly with Oki and Kanae (2006) and Schlesinger and Jasechko (2014) results.

This apparently contradicts the results obtained by Bancheri (2017) and Abera et al. (2017), in which the evapotranspiration calculated on the whole Posina (of which Ressi is a sub-basin) through the use of Priestley-Taylor in GEOframe, appears to be on average 30% of the annual precipitation.

Further simulations should be conducted over the same period (1995-2013) on the entire Posina using Prospero as a component for evapotranspiration in GEOframe to make a comparison and evaluate the results previously obtained.

Finally we can say that Prospero gives a better representation of the ET, giving the possibility to obtain better performance during the model calibration.

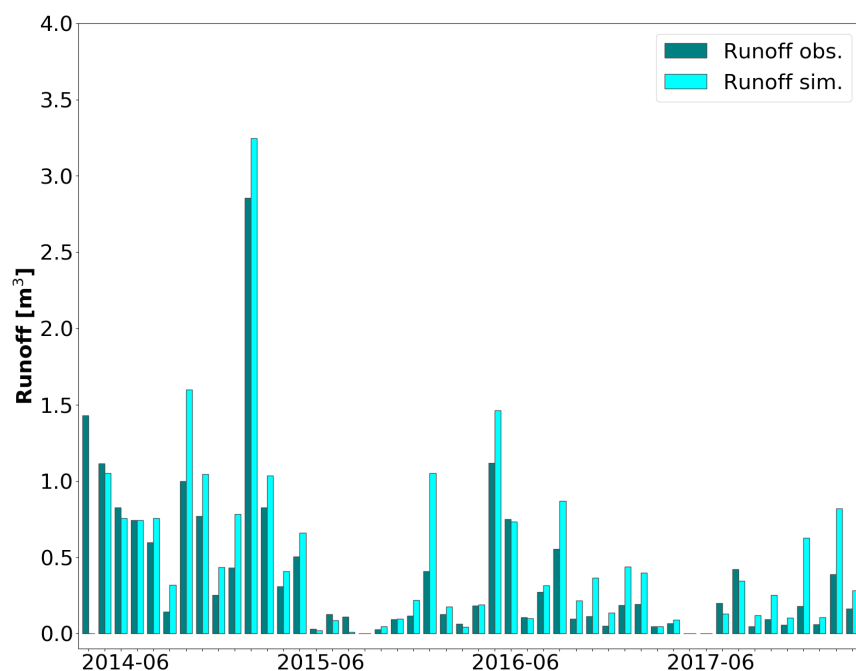
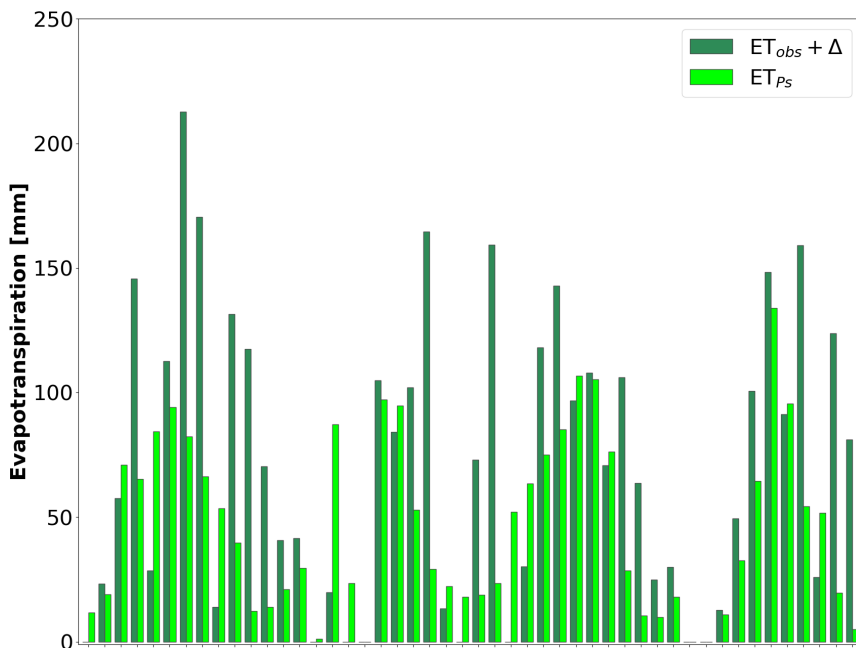


Figure 6.3: Total monthly evapotranspiration and runoff, simulated and observed.

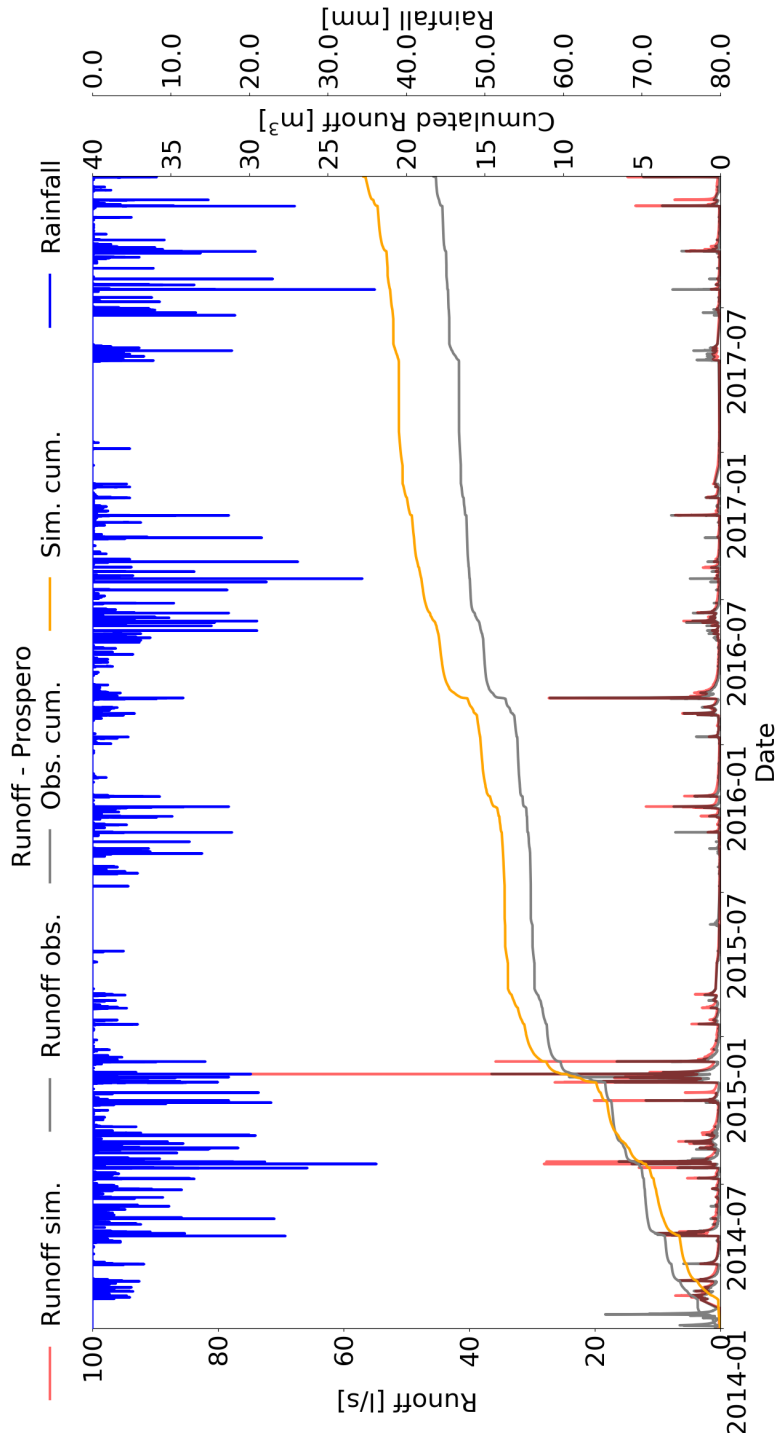


Figure 6.4: Observed and simulated hydrogramm and cumulated runoff, compared with precipitation, obtained with the ERM model and the Prospero component.



C H A P T E R



## CONCLUSION

In this thesis work we discussed about the evaporation and transpiration theory and presented a new model, Prospero, to estimate the latter.

In the chapter 2 we present the transpiration theory starting from the milestones until to the newest works. In particular the physics of transpiration is analyzed, defining the energy balance and its components. Some omissions made evident from recent studies (Schymanski and Or, 2017) are highlighted. We emphasize that the derivation promoted by Penman is not only providing a formula for evapotranspiration but is a resolution of the coupled simplified energy budget with the Dalton law and the sensible heat transfer in turbulent atmosphere that also results in giving the temperature of the evaporating surface, the air humidity and the sensible heat exchange. This results is absolutely clear but possibly not highlighted enough in many Schymanski papers. Based on the work by Lehmann et al. (2008) we also provide a theoretical framework that clearly distinguishes soil evaporation from plant transpiration, even if we could not deploy it in soft-

ware because of time constraints. In the third chapter we face the problem to constrain transpiration to water availability by defining the leaf conductances and how they vary with atmospheric or physiological plants conditions.

During the thesis we applied a Jarvis type of strategy for the stress factor but the implementation was left open to easy extensions with other strategies (like the Ball-Berry-Leuning one) through an appropriate work on the informatics.

In chapter 3 we analyze some strategy commonly used to adapt the transpiration's equations at the canopy scale and include a multi-layer canopy model based on a variation of Lambert-Beer's radiation extinction law. The role of leaves in shadow was discussed.

In chapter 4 is presented the Prospero GEOframe component. The other GEOframe components used to estimate the evapotranspiration, and the GEOframe hydrological model and its informatics structure are reported in Appendix A.

Finally in chapter 5 and 6 Prospero is applied to two different type of case studies, both at point-wise scale and catchment scale as a stand-alone tool. Prospero's Performances are compared with previous GEOframe's tools for evapotranspiration and with observed measurements.

To be specific, Prospero results were compared with data of latent heat collected by eddy covariance stations and in presence of simple canopy structures. On both sites Prospero gave good performances, either when compared with the observed data than with the results obtained by the other evapotranspiration estimator included in GEOframe. If we compute the errors (i.e. RMSE and MAE) respect to the observed measurements obtained on Torgnon and Viole case studies, we obtain that they are in line with the results found by Blyth et al. (2010) Ershadi et al. (2014) Zhu et al. (2014), and the total annual evapotranspiration

---

observed is well fitted by Prospero.

The Prospero model was also successfully coupled with a whole hydrological solution within the GEOframe system, called Embedded Reservoirs Model (ERM) (Bancheri, 2017). The modeling solution was implemented for the Rio Ressi subcatchment where various hydrological data are going to be collected by Prof. Marco Borga (University of Padova) group. Performances of the hydrological model to generate the runoff were evaluated using the different evapotranspiration components. The parameters of the evapotranspiration components are not directly calibrated on evapotranspiration measurements, since the only ones which are the ERM's, parameters.

We observed that using Prospero component plug into ERM gave good performances on a so small catchment, especially for the values of Nash-Sutcliffe and Kling-Gupta efficiency. Performances obtained using Prospero on the calibration period were similar or a little better than the ones obtained with existing evapotranspiration components but a clear improvement on the uncalibrated period in GEOframe performances was obtained when Prospero component was used.

Furthermore we found that the evapotranspiration computed with PT and FAO is between the 25 and 30% of the annual precipitation, while the one obtained with Prospero and the one derived by the closure of the hydrological water budget range from 40 to 60% of the total annual precipitation, accordingly with Oki and Kanae (2006) and Schlesinger and Jasechko (2014) results.

This result must be further investigated because it would state that evaporation in Ressi is much higher than in the rest of Posina catchment as it resulted from previous studies Abera et al., 2017 and Bancheri, 2017. This confirmation is part of the ongoing research that could not be completed for the time restrictions connected to the Ph.D. studies and the fact that data collection

in Ressi is still ongoing.

In conclusion we can say that Prospero represents a valid tool for the evapotranspiration estimation, being a physically based model and guaranteeing the conservation of mass and energy. In accordance with the Priestley-Taylor models at FAO, it makes its simplicity of use one of its strengths, not requiring particularly stringent and accurate parameterization. This also allows easy integration with the GEOframe-NewAGE hydrological system.



## APPENDIX A: GEOFRAME

EOframe-NewAGE (previously known as JGrass - NewAge, Formetta et al., 2011b) is an open-source system for designing modeling solutions for semi distributed hydrological modeling. GEOframe is not a model in the classic sense of the term but it is more a system of components that can be joined together at run-time for obtaining "modeling solutions" customized for the application in exam. In a modeling system like GEOframe each component represents a physical process and it is constructed as a standalone component that can be connected with the others via the input/output (Fig. A.2). In this way each user can easily build-up and modify its own set of components and connect it with the rest of the system provided by the work of other PhD students and researchers. GEOframe components are connected on the Object Modelling System v3.0 (OMS3, David et al., 2013). OMS3 is a Java-based framework for the environmental modeling, able to support multiple programming languages (Fortran, C/C++, Python and R). Very often the models are represented by a monolithic code, built in a specific

environment (for example Linux or Windows) and using a certain language (Fortran, Python, C, etc.). This generally creates compatibility problems when the model is run or must be compiled under different operating systems. In addition, the models are often made for specific case studies, which makes them difficult to apply to other case studies. This is further complicated by the fact that the models are written by few researchers and if the code is not well documented, it is difficult to read for new users. A modeling solution in GEOframe is made by selecting the components that best describe the physics of the problem, after which the components are combined together in a `.sim` file using the OMS3 framework. The connection of the components takes place through the management of the inputs / outputs of the components themselves.

The main components of interest for this work are briefly summarized below. An exhaustive list can be found in table A.1 and an accurate description can be found in the relative works (Bancheri, 2017, Formetta et al., 2014b).

## A.1 Replicability

Probably the phrase that best represents the thinking of our research team was provided by Leek (2013): "I have been frustrated often with statisticians and computer scientists who write papers where they develop new methods and seem to demonstrate that those methods blow away all their competitors. But then no software is available to actually test and see if that is true. Even worse, sometimes I just want to use their method to solve a problem in our pipeline, but I have to code it from scratch![...]In my mind, new methods/analyses without software are just vapor ware." Vaporware and software well express the fundamental idea that science must be reproducible and possibly replicable (Bancheri,

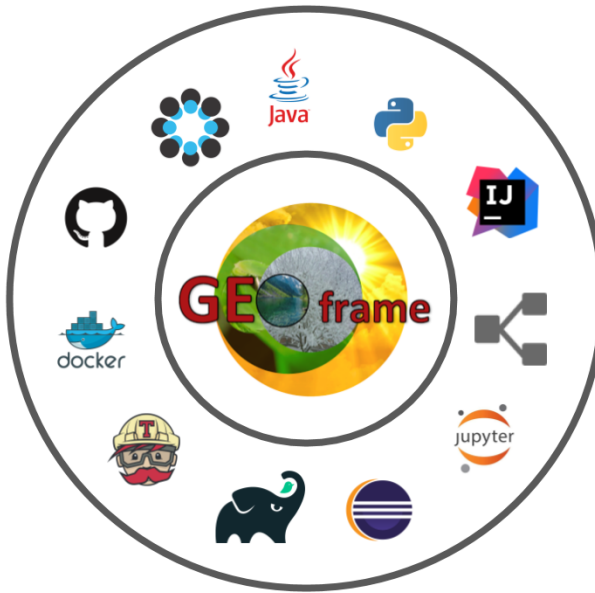


Figure A.1: The GEOframe universe and its component.

2017).

Replicable science means that reproducing the original results

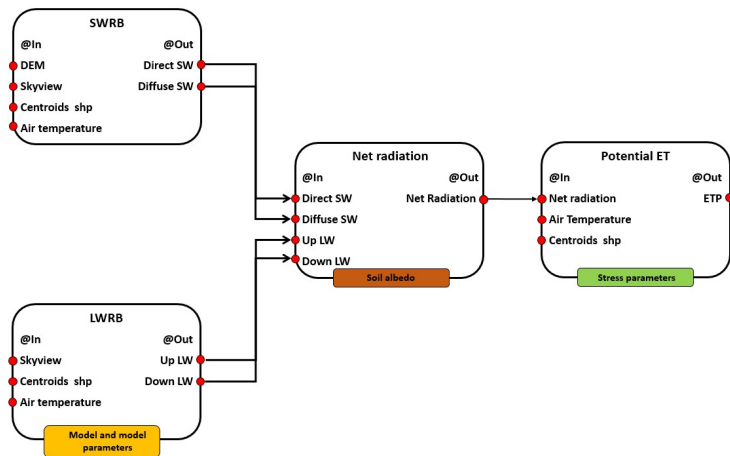


Figure A.2: Example of modelling solution for ET in GEOframe

using the same tools should be possible for any user. Repro-

ducibility offers the possibility of obtaining results from scratch, starting only from the description of the text and using different tools in different contexts.

However, a theoretically reproducible model may not be reproducible in practice, since non-trivial programming and computer skills are often required and this takes time to be acquired. We have therefore outlined some practices to improve the reproducibility and replicability of our results, creating a reproducible research system (RRS), (e.g. Formetta et al. (2014b)).

First, the methods should be shared and any source code made public, under a copyleft license (e.g. GPL v 3.0), allowing everyone to have free access to the code. This allows other users to use our tools and possibly improve them. Building something "quick and dirty", assuming indefinitely delayed cleaning, is something that could easily be avoided by adopting an open source code approach. However, working with open source tools does not only mean sharing codes, but also doing it in the right way, in order to create interest among users, who can also become active collaborators.

It is of fundamental importance to provide documentation of the code according to a standard format, since it helps to spread the developed tools.

This is further encouraged by creating a community of sharing ideas, questions, doubts and support. Trying to follow all the previous steps, the GEOframe organization was founded.

The organization is conceived as a system for computer hydrology, a sharing community for researchers and users. The idea of this community dates back to 2008 but, from an operational point of view, the organization was born in 2016 and received the logo in Figure A.1, with this research project. The need to share our efforts in the scientific community has led us to think about how to do it efficiently, easily and with some basic standards for

collaborators and users.

To support the idea of reproducibility and replicability of the research, certain tools are used to track the evolution of the code, documentation and construction system.

GitHub has been chosen as a public repository both for the source codes and for the GEOframe projects. [GitHub](#) is a web-based git, a version control repository and an Internet hosting service. GitHub takes care of the development history of changes to the registration and version of the source code (git), storing these changes in a public repository (GitHub). In particular, the [GEOframerepository](#) is created for the development of the source code. In addition to sharing the code, GitHub provides test and data cases (possibly open source).

However, during the development of a code it is normal that changes are made that can affect the test case or worse, that no test is performed. For this reason it was decided to use a tool that guarantees continuous integration, that is, that guarantees the test of the source code at each commit.

Using GitHub as a web-based git repository hosting service, [Travis CI](#), is the best choice for a continuous integration service. The continuous integration service, automatically creates executable codes, checks if the tests are performed correctly and returns a positive response if everything is performed correctly. To facilitate the assembly of the Java project, with all dependencies on external classes and / or libraries resolved automatically and updated to the latest versions, Gradle, (Berglund and McCullough, 2011) was chosen as the construction system but valid alternatives are represented by [Maven](#) or [IVY](#).

Gradle allows for a more concise representation of tasks and uses a Groovy-based Domain Specific Language (DSL), (Groovy). Gradle allows you to create a short, clean script that is relatively easy to write and maintain. It is also compatible with the Ivy

and Maven repositories. Collecting a source code in a project managed by a construction system is the key to making it independent of the IDE, allowing developers not to modify their favorite development tool. [Zenodo](#) was previously used as a filing system. Zenodo is a research data repository. It was created by OpenAIRE and CERN to provide a place for researchers to deposit data sets. "Then, once a new version of the software is produced, it is uploaded to Zenodo, a DOI (Digital Identification Object) number is assigned to the version and the code is stored, recoverable and permanently quoted. Recently, for the storage space, it was decided to use [OpenScienceFramework](#) (OSF).

## A.2 GEOframe structure

Even if GEOframe is mainly oriented to the hydrological modeling, it includes also components for data processing, like spatial interpolation or geomorphological analysis. The complete list of components is specified in table A.1 but they can grouped in six categories:

- geomorphic and DEM analyses;
- spatial extrapolation/interpolation of the meteorological tools;
- estimation of the radiation budget;
- estimation of evapotranspiration;
- estimation of runoff production;
- channel routing;

The DEM analysis is performed using the Horton Machine (aka JGrasstools), (Rigon et al. 2006b; Abera et al. 2014; Formetta

et al. 2014a), that allows, starting from a DEM, to extract several hydrological information like the drainage directions, the total contributing areas, the slopes, the river network, the sub-basin partitioning and the topographic characteristics required by computation. Different tools are available to interpolate data collected to the meteorological stations to the centroids subbasin interpolation. Both geostatistic, (Kriging techniques Bancheri et al., 2018) and deterministic, (Inverse Distance Weighting, IDW, Cressman, 1959) and Just Another Model Interpolator (JAMI) methodologies are available. The radiation budget model has been presented and validated in Formetta et al. (2013b) and Formetta et al. (2016) and includes both shortwave and long-wave radiation.

Before this thesis work, evapotranspiration was estimated using two different formulations: the FAO model (Allen et al., 1998), and the Priestly-Taylor model (Priestley and Taylor, 1972).

Snow melting and snow water equivalent is treated in a component which includes three models, as described in Formetta et al. (2013a).

Two different runoff generation models are implemented, the Duffy's model (Duffy, 1996) and the Hymod model (Moore, 1985), even if Duffy model was never really tested.

The discharge, generated at each hillslope, is routed to each associated stream link according to Mantilla et al. (2006).

Typical input/output data files are represented by csv file but GEOframe is also able to manage different data structures like rasters (ASCII and geotiff) or shapefile (.shp), commonly used within the GIS and managed with the Geotools library, Turton (2008). Starting from 2015 a refactoring of the code was performed by Bancheri (2017), even if it was more at design level than to the algorithmic one, with the introduction of the design patterns (DP) (Gamma et al., 1994; Freeman et al., 2008).

Process	Component	Reference
Geomorphological model setup	Horton Machine	Formetta et al. (2014a) Rigon et al. (2006b)
Meteorological interpolation tools	Kriging IDW, JAMI	Bancheri (2017) Formetta et al. (2014a)
Energy balance	Shortwave radiation Clearness index Longwave radiation	Formetta et al. (2013b) Formetta et al. (2016) Formetta et al. (2016)
Evapotranspiration	Penman-Monteith FAO Priestley-Taylor	Formetta et al. (2014a) Formetta et al. (2014a)
Snow melting	Rain-snow separation Snowmelt and SWE	Formetta et al. (2013b) Formetta et al. (2013b)
Runoff production	Adige Embedded reservoirs	Formetta et al. (2014a) Bancheri (2017)
Travel times description	Backward travel times Forward travel times	Bancheri (2017) Bancheri (2017)
Routing	Cuencas Muskingam-Cunge	Formetta et al. (2014a) Bancheri (2017)
Calibration	LUCA Particle-swarm Dream	Formetta et al. (2014a) Formetta et al. (2014a) Formetta et al. (2014a)

Table A.1: List of the current components of GEOframe (Bancheri, 2017)

I contributed to the maintenance of the components of GEOfame. Furthermore, in addition to having worked on the development of Prospero and updating the other evapotranspiration components, I have contributed directly to the development and testing of the Kriging component (Bancheri et al., 2018, see Appendix B).

### A.3 Embedded reservoir model

A detailed description of ERM is presented in Bancheri (2017). The ERM is a semi distributed model for runoff, which describes each HRU with five coupled storages:

- Snow pack;
- Canopy;
- Root zone;
- Surface flow;
- Groundwater.

The detection of the rainfall and the snowfall from the total precipitation, using the Hock model, (Hock, 1999), is integrated in the snow component of GEOframe-NewAge (Formetta et al., 2013a), and used to simulate snow melting and snow water equivalent. The snow melting and the rainfall are the inputs of the canopy layer.

If there is a canopy, precipitation is intercepted, otherwise it reaches directly the soil and so the root zone. The variation of the water storage capacity between different points is described using a parabolic curve for the water storage capacity of the soil, according to Zhao (1980). The precipitation exceeding the root zone capacity is commuted in to surface runoff, modeled using a non-linear reservoir model. Water from the root zone can be extracted through evapotranspiration or as a recharge of the groundwater. Evapotranspiration in the root zone describes both the evaporation from the soils and the transpiration from the canopy. Baseflow from the groundwater is modeled using a non-linear reservoir. Total runoff is the sum of the direct runoff and of the baseflow.

## A.4 Evapotranspiration

The evapotranspiration module includes three components:

- Priestley-Taylor model

- Penman-Monteith FAO
- Prospero

All these components can compute the process both at daily or at (sub)hourly time-step.

#### A.4.1 Priestley-Taylor

The Priestley-Taylor model is one of the most diffused equations for the evapotranspiration. It is based on the relation between evapotranspiration-net radiation, since at middle latitude the evapotranspiration is mainly energy limited. The equation is governed by the  $\alpha$  parameter.

$$ET_{PT} = \alpha \frac{(R_n - G) \cdot \Delta}{(\Delta + \gamma)} \quad (\text{A.1})$$

- $\alpha$  is an empirical coefficient relating actual evaporation to equilibrium evaporation,
- $\Delta$  is the slope of the saturation vapor pressure and air temperature curve ( $\text{kPa } ^\circ\text{C}^{-1}$ ),
- $\gamma$  is the psychrometric constant ( $\text{kPa } ^\circ\text{C}^{-1}$ ),
- $R_n$  is net radiation ( $\text{Wm}^{-2}$ ),
- and  $G$  is ground heat flux ( $\text{Wm}^{-2}$ )

Based upon a number of experiments at mid-latitude environments and in different climates over both land and water surfaces, Priestley and Taylor (1972) established the mean value of  $\alpha = 1.26$  (e.g., McNaughton and Black, 1973; Mukammal and Neumann, 1977; Parlange and Katul, 1992).

The extensive use of this formula is given by the simplicity of the

method and the small amount of input needed. Although the physical representation is relatively simplified, it provides good performance (Abera et al., 2017, Bancheri, 2017).

It is also easy to calibrate, making it suitable for use in hydrological models.

### A.4.2 Penman-Monteith FAO

The PM FAO is the approximation for the PM, defined for a reference crop as a hypothetical crop with an assumed height of 0.12 m, having a surface resistance of  $70 \text{ s m}^{-1}$  and an albedo of 0.23. It is widely used especially in agricultural field.

**The FAO approximation for a grass reference surface** For a wide range of crops the zero plane displacement height  $d$ , and the roughness length governing momentum transfer,  $z_{om}$ , can be estimated from the crop height  $h$  by the following equations:

Variable	Value	Unit
$h$	0.12	[m]
$z_{om}$	$0.123 \cdot h$	[m]
$z_{oh}$	$0.1 \cdot z_{om}$	[m]
LAI	24 h	[-]
$\text{LAI}_{active}$	$0.5 \cdot \text{LAI}$	[-]
$r_l$	$\approx 100$	$[\text{s m}^{-1}]$

Assuming these values, the aerodynamic and surface resistance are:

$$r_a = \frac{208}{u_2} \quad (\text{A.2})$$

$$r_s \approx 70 \quad (\text{A.3})$$

The equation for the reference evapotranspiration becomes:

$$ET_0 = \frac{1}{\lambda} \frac{0.408\Delta_{eTa}(R_n - G) + \gamma \frac{900}{T + 273} u_2(P_{was} - P_{wa})}{\Delta + \gamma(1 + 0.34u_2)} \quad (\text{A.4})$$

The reference evapotranspiration can be converted in the reference latent heat multiply it for the latent heat constant  $\lambda$ :

$$E_0 = ET_0 \cdot \lambda \quad (\text{A.5})$$

Actual evapotranspiration can be obtained using the water stress coefficient  $K_s$  and the single crop coefficient  $K_c$ :

$$ET_{FAO} = E_0 \cdot K_s \cdot K_c \quad (\text{A.6})$$

Values for  $K_c$  are given by FAO.  $K_s$  can be derived as:

$$K_s = \frac{TAW - D_r}{TAW - RAW} = \frac{TAW - D_r}{(1 - p)TAW} \quad (\text{A.7})$$

$$RAW = p \cdot TAW \quad (\text{A.8})$$

$$TAW = 1000(\theta_{FC} - \theta_{WP}) \cdot Z_r \quad (\text{A.9})$$

- $K_s$  is a dimensionless transpiration reduction factor dependent on available soil water [0 - 1],
- $D_r$  root zone depletion [mm],
- TAW total available soil water in the root zone [mm],
- p fraction of TAW that a crop can extract from the root zone without suffering water stress [-].
- $\theta_{FC}$  the water content at field capacity [ $\text{m}^3\text{m}^{-3}$ ],
- $\theta_{WP}$  the water content at wilting point [ $\text{m}^3\text{m}^{-3}$ ],
- $Z_r$  the rooting depth [m].



## APPENDIX B: THE DESIGN, DEPLOYMENT, AND TESTING OF KRIGING MODELS IN GEOFRA ME WITH SIK-0.9.8

The purpose of this study was to create and present a geostatistical software for the spatial interpolation kriging (SIK) of climatological variables, such as temperature and precipitation.

This package was built in order to easily couple with the GEOfra me hydrological model. Additionally our aim was to provide a practical example of an accurately designed software from the perspective of reproducible research, to demonstrate the goodness of the results of the software and have a reliable alternative to more traditional tools.

More than 10 types of theoretical semivariograms and four types of kriging (ordinary, detrended, local ordinary and local detrended kriging) were implemented and gathered into Object Modeling System-compliant components. This, the package provides a real-time optimization for semivariogram and kriging parame-

ters.

Some practices were delineated in this paper and implement in the SIK building in order to make it a reproducible research system(RRS) (e.g. Formetta et al., 2014a).

First of all the kriging's code is available from a control version system under a [GPL v3.0 license](#), using a collective GEOframe organization repository created under [GitHub](#), using [Git](#), and can be found at the following [link](#).

Building tools can be considered a modern evolution of the UNIX [make](#) and take care of gathering the various concurring libraries and linking them to form the final executable file.

There are possible choices for Java projects: [Apache Ant](#), [Maven](#), and [Gradle](#).

All of these provide ways to solve the software dependencies. Both Maven and Gradle can download and update the remote resources needed. We choose Gradle since it uses a more concise syntax, thanks to the use of the [Groovy](#) language, compared to the [XML](#) used by Maven. Using building tools also allows abstraction from the use of integrated development environments (IDEs). Main IDEs for Java are [NetBeans](#), [Eclipse](#), and [IntelliJ](#) and all of them support both Gradle and Maven, and Ant and can import a Gradle or Maven (or Ant) project seamlessly.

These tools can help researchers to use and improve others' codes, especially if they are open source. For this reason, we adopted a proper building tool in order to promote collaborative work and open science.

Another important step in the management of the code was the implementation of a continuous integration system [Jenkins](#).It ensures the building and testing of the source code a teach commit, forcing the good practice of preparing tests for each software module developed. Continuous integration (Meyer, 2014) is the practice of merging all developer working copies to a shared

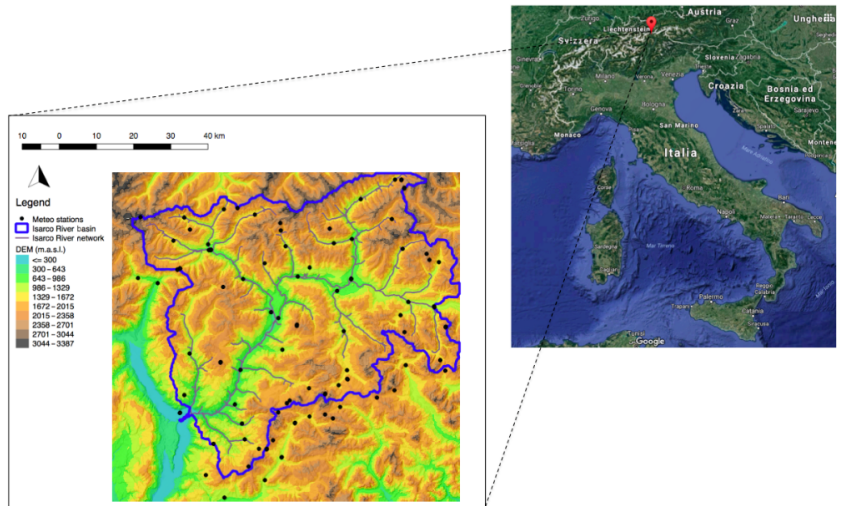


Figure B.1: Geo-location of study area and position of meteorological stations.

mainline several times a day. Unit tests (Beck, 2003) are built with the code and run each time the merging is performed. The continuous integration service automatically builds the executable codes, checks if the tests are performed correctly, and returns a positive answer if all is carried out properly. For this purposes, we chose to use [TravisCI](#), which uses GitHub as a web-based Git repository hosting service, which is a good choice for a continuous integration service. Since GitHub is a repository and not an archival system, we decided to use [Zenodo](#) to provide our products with a Digital Object Identifier (DOI) and then we put the entire project, as used to obtain the results presented in this work, on [Open Science Framework](#). The assignment of the DOI allows researcher peers to retrieve exactly that code in the foreseeable future

The component was tested on the interpolation of a year of hourly temperature measurement rainfall and a rain storm event (11 hours) recorded in 2008, measurements collected from 97 stations located in the Isarco River Valley (Fig. B.1). The Isarco River

is a left tributary of the Adige River, in the Trentino-Alto Adige region, northern Italy. The catchment area is about  $4200\text{ km}^2$  and the altitude ranges from 210 to 3400 m a.s.l.

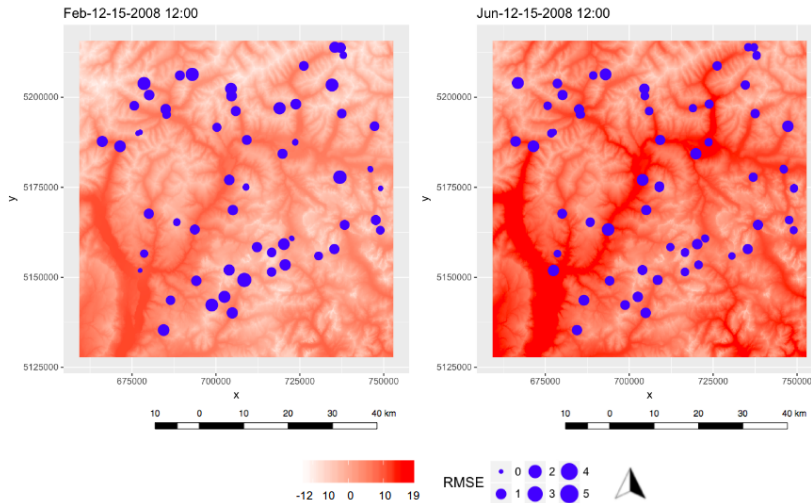


Figure B.2: Maps of spatialized temperature for 15 February 2008 and 15 June 2008. Two bubble plots are overlapped, which represent the RMSE between the measured and interpolated values.

Semivariance analysis was performed and the experimental semivariograms were fitted using all 11 theoretical models in order to use the one that gives the best result. Both local and detrended simulations were performed.

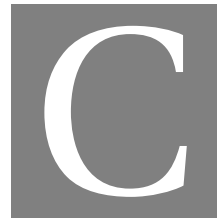
Results obtained from the interpolation of the temperature dataset were compared to the results obtained with R gstat, in order to assess the differences between the two packages, their easiness of use, and their performances. Kriging performances were also assessed using the leave one out cross validation.

The interpolations of both the temperature and the rain-fall gave very good results, with a high agreement between the measured and the interpolated variables. The tests also showed how it is possible to choose between 11 variograms and four kriging alternatives and to compare the outcomes easily. Conversely, the

---

single rainfall event did not show trend with elevation. In comparison with gstat, the SIK package proved to be a good alternative, regarding both the easiness of use and the accuracy of the interpolation.





## APPENDIX C: MORE GREEN AND LESS BLUE WATER IN THE ALPS DURING WARMER SUMMERS

Below a short summary of our work published on Nature Climate Change. In this study it was evaluated how the partition of water between the hydrosphere (streams and runoffs, the blue water) to biosphere (evapotranspiration, the green water) can change in different climatic conditions in the alps (Falkenmark and Rockström, 2006; Orth and Destouni, 2018).

Although relatively small, the European Alps contribute a disproportionately large amount of water, especially during summer, to four major European rivers (Weingartner et al., 2007), and in these rivers' basin reside more than 170 million people. Even if they are referred to as 'the water towers of Europe' (Viviroli et al., 2007), water scarcity and droughts in central Europe are becoming more frequent (Briffa et al., 2009).

In fact due to climate change relative humidity is generally de-

creasing, temperature and evapotranspiration are increasing, snow distribution is shifting to higher elevation with a relative shrink of glaciers and climatic extremes are becoming more frequent (Brunetti et al., 2009; Fatichi et al., 2015; Duethmann and Blöschl, 2018; Beniston et al., 2018; Samaniego et al., 2018).

Additionally climate change can reduce surface-water supply by enhancing evapotranspiration in forested mountains, especially during heatwaves.

We investigated this phenomenon ("drought paradox") for the European Alps using a database with more than one thousand stations and a hyper-resolution ecohydrological simulations to quantify blue (runoff) and green (evapotranspiration) water fluxes. The study was carried out throughout three years (2001-2003) where two of those were extremely wet and dry (2001 and 2003). During the 2003 heatwave, evapotranspiration in large areas over the Alps was above average despite low precipitation, amplifying the runoff deficit by 32% in the area between 1300 and 3000 masl, which is the most important for the runoff production. We also simulated an increase of 3°C air temperature that could enhance annual evapotranspiration up to 100 mm (45 mm on average), which would reduce annual runoff at a rate similar to a 3% precipitation decrease. This suggests that green-water feedbacks (which are often poorly represented in large-scale model simulations) pose an additional threat to water resources, especially in dry summers. Despite uncertainty in the validation of the hyper-resolution ecohydrological modelling with observations, this approach allows more realistic predictions of mountain region water availability.

Simulations were carried out using a physical based ecohydrological model (Tethys-Chloris (T&C) Mastrotheodoros et al., 2019) that resolves water, carbon and energy budgets at the hourly timescale. To account for the high spatial heterogeneity of the re-

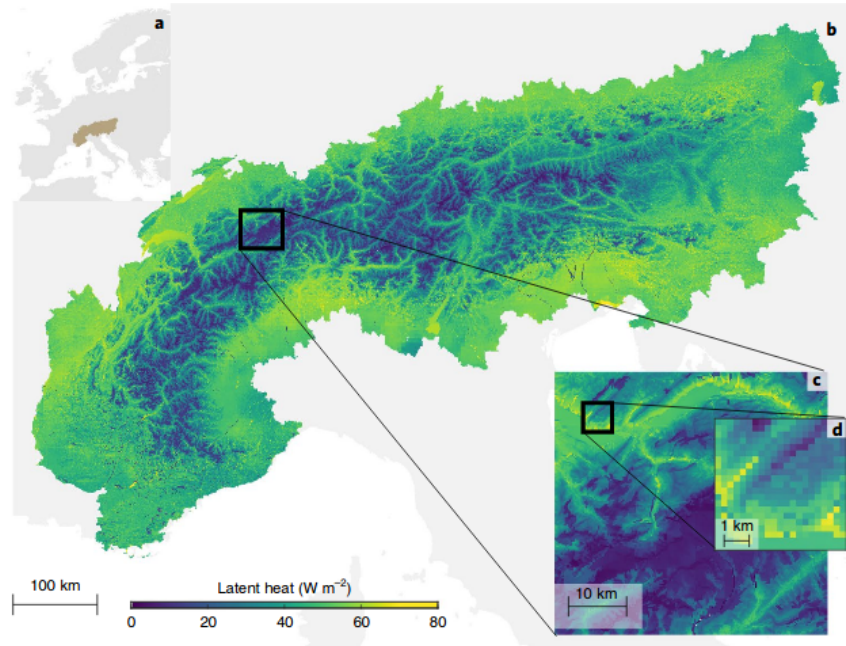


**Figure C.1: Simulation results highlight the spatial heterogeneity in latent heat (ET in energy units).** a, The spatial extent of the European Alps. b, November 2000–October 2003 average latent heat flux for the entire  $257045 \text{ km}^2$  domain simulated with Tethys-Chloris. c,d, Zoom on the Bernese highlands, Switzerland, and illustration of the small-scale spatial heterogeneity captured with the hyper-resolution simulation ( $250 \text{ m} \times 250 \text{ m}$  pixels).

gion, analysis was performed with massively parallel simulations ( $6.1 \cdot 10^5$  CPU hours) at an unprecedented high resolution (250 m grid) for the entire Alpine arch ( $\approx 260 \cdot 10^3 \text{ km}^2$ ).

Results confirms that energy is the dominant driver of ET in the alpine area, obtaining the maximum latent heat in the wetter areas while in the drier regions, such as in the upper Rhone valley, latent heat is overall lower because precipitation ( $\approx 500 \text{ mm yr}^{-1}$ ) becomes the critical constraint for annual ET.

Average precipitation - ET ( $P - ET$ ) was used as a proxy for runoff (Goulden and Bales, 2014) since changes in soil and snow water storage over three hydrological years could be considered

small, and ice melt only marginally contributed to the total water budget (less than 3%) at the annual scale at a rate of roughly  $4\text{ km}^3 \text{ yr}^{-1}$ . The Alpine water budget also displays high temporal variability; P - ET in 2001 was 53% higher than in 2003, which can be explained by both higher precipitation and lower ET. More specifically, the Alps received 225 mm more precipitation in 2001 compared with 2003 (1363 and 1138 mm, respectively, averaged over the entire domain) while ET was 30 mm lower on average. We focused on analyzing runoff deficits, computing how much ET contributed to amplifying the effect of precipitation deficit on runoff during the 2003 May-September period (the growing season). This is the period with active vegetation and when green-water feed-back can be pronounced. We found that in 75% of the catchments, ET amplified the drought impact on runoff. The remaining 25% of the catchments-mostly located in the southwest and northeast of the pan-Alpine domain-experienced dry conditions with water-stressed vegetation and reduced ET.

On the whole alpine domain, ET increased during the drought in an area covering more than  $144000 \text{ km}^2$ .

The increase in green-water flux amplified the precipitation-driven deficit by roughly 22%. In the areas between 1300 and 3000 m a.s.l., enhanced ET created an additional water loss of almost  $4\text{ km}^3$  during the 2003 growing season compared with the 2001-2003 growing season average, amplifying the runoff decrease due to precipitation by 32%.

Our results, which derived from a single mechanistic model, indicate that ET considerably contributed to reduce water yield during the 2003 growing season because vegetation benefited from the unusually warm and sunny conditions in a large part of the Alpine region at higher elevations.

Another important result is that at the annual timescale the temperature-driven ET feedbacks on runoff are less important

---

than the direct effect of changes in precipitation; a 3% reduction in annual precipitation would affect runoff production over the entire pan-Alpine domain similarly to a hypothetical increase in mean annual air temperature of 3°C, even if the scenario of a +3°C change in air temperature is simply based on a space-for-time analysis.

Combined with the expected decrease in ice melt and earlier snow melt (Beniston et al., 2018), our results demonstrated that blue water could be considerably reduced in the European Alps during warmer summers, but green water will continue to increase (Duethmann and Blöschl, 2018), leading to the oxymoron 'lush vegetation-drier rivers'.

Alternatively, the expected increase in plant water use efficiency with higher levels of  $CO_2$  concentration (Mastrotheodoros et al., 2017) as well as large-scale disturbances (for example, forest mortality Dupire et al. 2017), species changes and plant acclimation, which are not considered in this study, may partially offset this ET feedback during warmer summers in the long term, but they will probably not have a major role in the near future.

Furthermore, in certain regions of the Alps, vegetation management is intense, and past disturbances such as wildfires or forest logging may have influenced vegetation composition and function in ways that are not accounted for in the model initialization. While the presented concepts are general, the extension of the results to other mountain regions strongly depends on the relative magnitude of precipitation and ET at the annual scale and during summer. Important factors are also the elevation at which P - ET shifts from positive to negative during warm and dry summers and the areal extent covered by different elevation bands and vegetation types. Nevertheless, results from the Sierra Nevada (Gilbert and Maxwell 2018, Bales et al. 2018) largely agree with our findings. Understanding the partitioning of green- and

## APPENDIX C. APPENDIX C: MORE GREEN AND LESS BLUE WATER IN THE ALPS DURING WARMER SUMMERS

---

blue-water fluxes and their spatial distribution from a few square kilometers to the entire Alps is essential to manage the European water resources under current and future climatic conditions (Orth and Destouni, 2018) . This partition has implications for ecosystem functioning, energy production and water supply. We showed that ecohydrological simulations driven by high - resolution hydrometeorological forcing improve the quantification and understanding of the water budget in mountainous areas and its vulnerability to climate, providing insights into processes that coarser-scale approaches fail to reproduce (Fan et al. 2019, Wood et al. 2011, Maxwell and Condon 2016). This highlights the urgent need of more realistic, high-resolution quantifications of water availability (Barnett et al., 2005) . Our study demonstrates that recent advances in ecohydrological modelling, combined with large-scale datasets and new computational capabilities, offer the possibility to address this urgent need, thus helping to define strategies to counteract or adapt to climate change impacts on water resources.

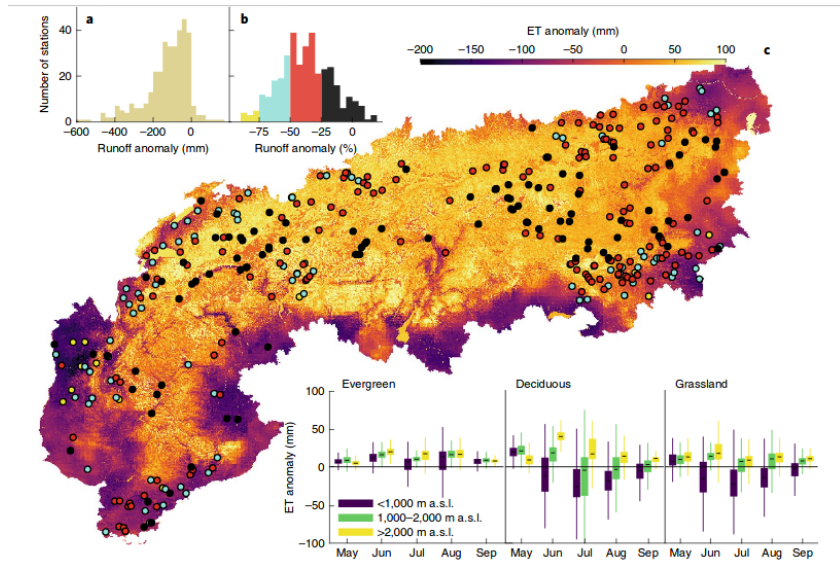
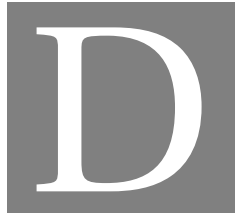


Figure C.2: Analysis of anomalies in blue-and green-water fluxes during the 2003 drought. a, Histogram of observed May-September 2003 total runoff anomalies (mm) for 381 locations. b, Histogram of observed May-September 2003 runoff anomalies (%) for the same locations coloured according to the magnitude of the anomaly (<-75%: yellow, -50 to -75%: cyan, -25 to -50%: red and >-25%: black); growing season 2003 is compared with the mean of each station for the period 2001-2003. c, Spatial distribution of the simulated ET anomaly (mm) during the 2003 growing season (May-September; the reference period for ET is also 2001-2003). The dots represent the 381 locations with hydrological measurements and are coloured as described in b. The three insets in the lower right panel show the box plots of simulated ET anomaly in May-September 2003 for three vegetation types in three elevation classes. The box length provides the interquartile range (IQR), the bottom of the box is the 25<sup>th</sup> percentile (first quartile,  $q_1$ ), the top of the box is the 75<sup>th</sup> percentile (third quartile,  $q_3$ ) and the horizontal line within the box is the median. The lower whisker corresponds to  $q_1 - 1.5I_{QR}$ , and the upper whisker corresponds to  $q_3 + 1.5I_{QR}$ .





## ACKNOWLEDGEMENTS

We thank ARPA Valle d'Aosta ARPA Aosta and in particular Paolo Pogliotti for Torgnon data.

We thank Edmund Mach Foundation of San Michele all'Adige and in particular Damiano Gianelle for Viole data.

A special thanks to the Italian Hydrological Society and to the family of Florisa Melone for establishing the Florisa Melone award and to Giulia Zuecco (university of padova) and alessandro errico (university of Florence) for the collaboration in the SILVA project born within this award.

We thank the projects EcoHydro and LTER financed by Eurac Research, and the PRIN WATZON



## BIBLIOGRAPHY

- W. Abera, A. Antonello, S. Franceschi, G. Formetta, and R. Rigon.  
The udig spatial toolbox for hydro-geomorphic analysis.  
*Geomorphological Techniques*, 2(4.1):1–19, 2014.
- W. Abera, G. Formetta, M. Borga, and R. Rigon.  
Estimating the water budget components and their variability  
in a pre-alpine basin with JGrass-NewAGE.  
*Advances in Water Resources*, 104:37–54, 2017.  
ISSN 03091708.  
doi: 10.1016/j.advwatres.2017.03.010.
- R. G. Allen.  
A penman for all seasons.  
*Journal of Irrigation and Drainage Engineering*, 112(4):348–  
368, nov 1986.  
ISSN 07339437.  
doi: 10.1061/(ASCE)0733-9437(1986)112:4(348).  
URL <http://ascelibrary.org/doi/10.1061/{%}28ASCE{%}290733-9437{%}281986{%}29112{%}3A4{%>
- R. G. Allen, L. S. Pereira, D. Raes, M. Smith, et al.  
Crop evapotranspiration-guidelines for computing crop water  
requirements-fao irrigation and drainage paper 56.  
*Fao, Rome*, 300(9):D05109, 1998.
- P. B. Alton, P. R. North, and S. O. Los.

## BIBLIOGRAPHY

---

The impact of diffuse sunlight on canopy light-use efficiency, gross photosynthetic product and net ecosystem exchange in three forest biomes.

*Global Change Biology*, 13(4):776–787, jan 2007.

ISSN 13541013.

doi: 10.1111/j.1365-2486.2007.01316.x.

URL <http://doi.wiley.com/10.1111/j.1365-2486.2007.01316.x>.

P. Aphalo and P. Jarvis.

Do stomata respond to relative humidity?

*Plant, Cell & Environment*, 14(1):127–132, 1991.

P. Aphalo and P. Jarvis.

An analysis of ball's empirical model of stomatal conductance.

*Annals of Botany*, 72(4):321–327, 1993.

M. Aubinet, A. Grelle, A. Ibrom, Ü. Rannik, J. Moncrieff, T. Foken,

A. S. Kowalski, P. H. Martin, P. Berbigier, C. Bernhofer, et al.

Estimates of the annual net carbon and water exchange of forests: the euroflux methodology.

In *Advances in ecological research*, volume 30, pages 113–175.

Elsevier, 1999.

D. Baldocchi and P. Harley.

Scaling carbon dioxide and water vapour exchange from leaf to canopy in a deciduous forest. ii. model testing and application.

*Plant, Cell & Environment*, 18(10):1157–1173, 1995.

R. C. Bales, M. L. Goulden, C. T. Hunsaker, M. H. Conklin, P. C.

Hartsough, A. T. O'Geen, J. W. Hopmans, and M. Safeeq.

Mechanisms controlling the impact of multi-year drought on mountain hydrology.

*Scientific reports*, 8(1):690, 2018.

- J. T. Ball, I. E. Woodrow, and J. A. Berry.  
A Model Predicting Stomatal Conductance and its Contribution to the Control of Photosynthesis under Different Environmental Conditions.  
*In Progress in Photosynthesis Research*, pages 221–224. Springer, 1987.  
doi: 10.1007/978-94-017-0519-6\_48.
- M. Bancheri.  
*A flexible approach to the estimation of water budgets and its connection to the travel time theory.*  
PhD thesis, University of Trento, 2017.
- M. Bancheri, F. Serafin, M. Bottazzi, W. Abera, G. Formetta, and R. Rigon.  
The design, deployment, and testing of kriging models in geoframe with sik-0.9. 8.  
*Geoscientific Model Development*, 11(6):2189–2207, 2018.
- T. Banerjee, F. De Roo, and M. Mauder.  
Explaining the convector effect in canopy turbulence by means of large-eddy simulation.  
*Hydrology and Earth System Sciences (Online)*, 21(LA-UR-17-22651), 2017.
- G. G. J. Bange.  
On the quantitative explanation of stomatal transpiration.  
*Acta Botanica Neerlandica*, 2(3):255–297, 1953.
- T. P. Barnett, J. C. Adam, and D. P. Lettenmaier.  
Potential impacts of a warming climate on water availability in snow-dominated regions.  
*Nature*, 438(7066):303–309, 2005.
- G. K. Batchelor.

## BIBLIOGRAPHY

---

- An introduction to fluid dynamics. 1967.  
*Cambridge,: UP xviii,* 615, 1967.
- M. Beniston.  
Impacts of climatic change on water and associated economic activities in the swiss alps.  
*Journal of Hydrology*, 412:291–296, 2012.
- M. Beniston, D. Farinotti, M. Stoffel, L. M. Andreassen, E. Copola, N. Eckert, A. Fantini, F. Giaccona, C. Hauck, M. Huss, et al.  
The european mountain cryosphere: a review of its current state, trends, and future challenges.  
*Cryosphere*, 12(2):759–794, 2018.
- M. Berger, J. Moreno, J. A. Johannessen, P. F. Levelt, and R. F. Hanssen.  
Esa's sentinel missions in support of earth system science.  
*Remote Sensing of Environment*, 120:84–90, 2012.
- T. Berglund and M. McCullough.  
*Building and Testing with Gradle*.  
O'Reilly Media, Inc., 1st edition, 2011.  
ISBN 144930463X.
- G. Bertoldi, J. Albertson, W. Kustas, F. Li, and M. Anderson.  
On the opposing roles of air temperature and wind speed variability in flux estimation from remotely sensed land surface states.  
*Water resources research*, 43(10), 2007.
- E. Blyth, J. Gash, A. Lloyd, M. Pryor, G. P. Weedon, and J. Shuttleworth.  
Evaluating the jules land surface model energy fluxes using fluxnet data.  
*Journal of Hydrometeorology*, 11(2):509–519, 2010.

G. Bonan, M. Williams, R. Fisher, and K. Oleson.

Modeling stomatal conductance in the earth system: linking leaf water-use efficiency and water transport along the soil-plant-atmosphere continuum.

*Geoscientific Model Development*, 7(5):2193–2222, 2014a.

G. B. Bonan, M. Williams, R. A. Fisher, and K. W. Oleson.

Modeling stomatal conductance in the earth system: Linking leaf water-use efficiency and water transport along the soil-plant-atmosphere continuum.

*Geoscientific Model Development*, 7(5):2193–2222, 2014b.

ISSN 19919603.

doi: 10.5194/gmd-7-2193-2014.

I. S. Bowen.

The ratio of heat losses by conduction and by evaporation from any water surface.

*Physical Review*, 27(6):779–787, jun 1926.

ISSN 0031899X.

doi: 10.1103/PhysRev.27.779.

URL <https://link.aps.org/doi/10.1103/PhysRev.27.779>.

K. Briffa, G. Van Der Schrier, and P. Jones.

Wet and dry summers in europe since 1750: evidence of increasing drought.

*International Journal of Climatology: A Journal of the Royal Meteorological Society*, 29(13):1894–1905, 2009.

T. J. Brodribb, N. M. Holbrook, M. A. Zwieniecki, and B. Palma.

Leaf hydraulic capacity in ferns, conifers and angiosperms: impacts on photosynthetic maxima.

*New phytologist*, 165(3):839–846, 2005.

## BIBLIOGRAPHY

---

M. Brunetti, G. Lentini, M. Maugeri, T. Nanni, I. Auer, R. Boehm, and W. Schoener.

Climate variability and change in the greater alpine region over the last two centuries based on multi-variable analysis.

*International Journal of Climatology: A Journal of the Royal Meteorological Society*, 29(15):2197–2225, 2009.

W. Brutsaert.

Catchment-scale evaporation and the atmospheric boundary layer.

*Water Resources Research*, 22(9S):39S–45S, 1986.

W. Brutsaert.

*History of the Theories of Evaporation.*

Kluver Academic Publisher, 2013.

ISBN 978-90-481-83651-4.

doi: 10.1007/978-94-017-1497-6.

URL <http://link.springer.com/10.1007/978-94-017-1497-6>.

T. Buckley, K. Mott, and G. Farquhar.

A hydromechanical and biochemical model of stomatal conductance.

*Plant, Cell & Environment*, 26(10):1767–1785, 2003.

T. N. Buckley.

Stomatal responses to humidity: has the ‘black box’ finally been opened?

*Plant, cell & environment*, 39(3):482–484, 2016.

F. Carswell, P. Meir, E. Wandelli, L. Bonates, B. Kruijt, E. Barbosa, A. Nobre, J. Grace, and P. Jarvis.

Photosynthetic capacity in a central amazonian rain forest.

*Tree Physiology*, 20(3):179–186, 2000.

- M. Castelli, M. C. Anderson, Y. Yang, G. Wohlfahrt, G. Bertoldi, G. Niedrist, A. Hammerle, P. Zhao, M. Zebisch, and C. Notarnicola.  
Two-source energy balance modeling of evapotranspiration in Alpine grasslands.  
*Remote Sensing of Environment*, 209(2):327–342, 2018.  
ISSN 00344257.  
doi: 10.1016/j.rse.2018.02.062.
- J. Chen, J. Liu, J. Cihlar, and M. Goulden.  
Daily canopy photosynthesis model through temporal and spatial scaling for remote sensing applications.  
*Ecological modelling*, 124(2-3):99–119, 1999.
- J. M. Chen and J. Cihlar.  
Retrieving leaf area index of boreal conifer forests using landsat tm images.  
*Remote sensing of Environment*, 55(2):153–162, 1996.
- J. M. Chen and S. G. Leblanc.  
A four-scale bidirectional reflectance model based on canopy architecture.  
*IEEE Transactions on geoscience and remote sensing*, 35(5):1316–1337, 1997.
- J. M. Chen, P. M. Rich, S. T. Gower, J. M. Norman, and S. Plummer.  
Leaf area index of boreal forests: Theory, techniques, and measurements.  
*Journal of Geophysical Research: Atmospheres*, 102(D24):29429–29443, 1997.
- J. M. Chen, J. Liu, S. G. Leblanc, R. Lacaze, and J.-L. Roujean.  
Multi-angular optical remote sensing for assessing vegetation structure and carbon absorption.  
*Remote Sensing of Environment*, 84(4):516–525, 2003.

## BIBLIOGRAPHY

---

J. M. Chen, G. Mo, J. Pisek, J. Liu, F. Deng, M. Ishizawa, and D. Chan.

Effects of foliage clumping on the estimation of global terrestrial gross primary productivity.

*Global Biogeochemical Cycles*, 26(1), 2012.

B. Choat, E. C. Lahr, P. J. Melcher, M. A. Zwieniecki, and N. M. Holbrook.

The spatial pattern of air seeding thresholds in mature sugar maple trees.

*Plant, Cell & Environment*, 28(9):1082–1089, 2005.

J. Chorover, R. Kretzschmar, F. Garcia-Pichel, and D. L. Sparks.

Soil biogeochemical processes within the critical zone.

*Elements*, 3(5):321–326, 2007.

G. J. Collatz, M. Ribas-Carbo, and J. Berry.

Coupled photosynthesis-stomatal conductance model for leaves of c<sub>4</sub> plants.

*Functional Plant Biology*, 19(5):519–538, 1992.

E. Cremonese, M. Migliavacca, M. Galvagno, M. Rossini, R. Colombo, E. Pari, L. Busetto, S. Cogliati, M. Lonati, G. Manca, et al.

Alpine grassland phenology: a multi-source data perspective.

In *Phenology 2010: Climate change impacts & adaptations*, pages 20–20. Citeseer, 2010.

G. P. Cressman.

An operational objective analysis system.

*Mon. Wea. Rev*, 87(10):367–374, 1959.

Y. Dai, R. E. Dickinson, and Y.-P. Wang.

A two-big-leaf model for canopy temperature, photosynthesis, and stomatal conductance.

- Journal of Climate*, 17(12):2281–2299, 2004.
- G. Damour, T. Simonneau, H. Cochard, and L. Urban.  
An overview of models of stomatal conductance at the leaf level.  
*Plant, Cell and Environment*, 33(9):1419–1438, 2010.  
ISSN 01407791.  
doi: 10.1111/j.1365-3040.2010.02181.x.
- O. David, J. C. Ascough, W. Lloyd, T. R. Green, K. W. Rojas, G. H. Leavesley, and L. R. Ahuja.  
A software engineering perspective on environmental modeling framework design: The Object Modeling System.  
*Environmental Modelling and Software*, 39:201–213, 2013.  
ISSN 13648152.  
doi: 10.1016/j.envsoft.2012.03.006.  
URL <https://fardapaper.ir/mohavaha/uploads/2017/11/A-software-engineering-perspective-on-environment.pdf>.
- D. G. De Pury and G. D. Farquhar.  
Simple scaling of photosynthesis from leaves to canopies without the errors of big-leaf models.  
*Plant, Cell and Environment*, 20(5):537–557, may 1997.  
ISSN 01407791.  
doi: 10.1111/j.1365-3040.1997.00094.x.  
URL <http://doi.wiley.com/10.1111/j.1365-3040.1997.00094.x>.
- S. Della Chiesa, G. Bertoldi, G. Niedrist, N. Obojes, S. Endrizzi, J. Albertson, G. Wohlfahrt, L. Hörtnagl, and U. Tappeiner.  
Modelling changes in grassland hydrological cycling along an elevational gradient in the alps.

## BIBLIOGRAPHY

---

*Ecohydrology*, 7(6):1453–1473, 2014.

M. C. Demirel, J. Mai, G. M. Gonzalez, J. Koch, L. Samaniego, and S. Stisen.

Combining satellite data and appropriate objective functions for improved spatial pattern performance of a distributed hydrologic model.

*Hydrology and Earth System Sciences*, 22:1299–1315, 2018.

R. C. Dewar.

The ball–berry–leuning and tardieu–davies stomatal models: synthesis and extension within a spatially aggregated picture of guard cell function.

*Plant, Cell & Environment*, 25(11):1383–1398, 2002.

D. Duethmann and G. Blöschl.

Why has catchment evaporation increased in the past 40 years? a data-based study in austria.

*Hydrology & Earth System Sciences*, 22(10), 2018.

C. J. Duffy.

A Two-State Integral-Balance Model for Soil Moisture and Groundwater Dynamics in Complex Terrain.

*Water Resources Research*, 32(8):2421–2434, aug 1996.

ISSN 00431397.

doi: 10.1029/96WR01049.

URL <http://doi.wiley.com/10.1029/96WR01049>.

S. Dupire, T. Curt, and S. Bigot.

Spatio-temporal trends in fire weather in the french alps.

*Science of the total environment*, 595:801–817, 2017.

S. Endrizzi, S. Gruber, M. Dall’Amico, and R. Rigon.

- Geotop 2.0: simulating the combined energy and water balance at and below the land surface accounting for soil freezing, snow cover and terrain effects.  
*Geoscientific Model Development*, 7(6):2831–2857, 2014.
- A. Ershadi, M. F. McCabe, J. P. Evans, N. W. Chaney, and E. F. Wood.  
Multi-site evaluation of terrestrial evaporation models using FLUXNET data.  
*Agricultural and Forest Meteorology*, 187:46–61, 2014.  
ISSN 01681923.  
doi: 10.1016/j.agrformet.2013.11.008.  
URL <http://dx.doi.org/10.1016/j.agrformet.2013.11.008>.
- M. Falkenmark and J. Rockström.  
The new blue and green water paradigm: Breaking new ground for water resources planning and management, 2006.
- J. Famiglietti and E. F. Wood.  
Multiscale modeling of spatially variable water and energy balance processes.  
*Water Resources Research*, 30(11):3061–3078, 1994.
- Y. Fan, M. Clark, D. M. Lawrence, S. Swenson, L. Band, S. L. Brantley, P. Brooks, W. E. Dietrich, A. Flores, G. Grant, et al.  
Hillslope hydrology in global change research and earth system modeling.  
*Water Resources Research*, 55(2):1737–1772, 2019.
- G. D. Farquhar.  
Models of integrated photosynthesis of cells and leaves.  
*Philosophical Transactions of the Royal Society of London. B, Biological Sciences*, 323(1216):357–367, 1989.
- G. D. Farquhar and S. Von Caemmerer.

## BIBLIOGRAPHY

---

- Modelling of photosynthetic response to environmental conditions.  
In *Physiological plant ecology II*, pages 549–587. Springer, 1982.
- G. D. Farquhar, S. v. von Caemmerer, and J. A. Berry.  
A biochemical model of photosynthetic  $\text{CO}_2$  assimilation in leaves of C3 species.  
*Planta*, 149(1):78–90, 1980.
- S. Fatichi, V. Ivanov, and E. Caporali.  
A mechanistic ecohydrological model to investigate complex interactions in cold and warm water-controlled environments:  
1. theoretical framework and plot-scale analysis.  
*Journal of Advances in Modeling Earth Systems*, 4(2), 2012.
- S. Fatichi, P. Molnar, T. Mastrotheodoros, and P. Burlando.  
Diurnal and seasonal changes in near-surface humidity in a complex orography.  
*Journal of Geophysical Research: Atmospheres*, 120(6):2358–2374, 2015.
- S. Fatichi, C. Pappas, and V. Ivanov.  
Modeling plant–water interactions: an ecohydrological overview from the cell to the global scale, *wires water*, 3, 327–368, 2016.
- T. Foken.  
50 years of the Monin–Obukhov similarity theory.  
*Boundary-Layer Meteorology*, 119(3):431–447, 2006.
- T. Foken.  
The energy balance closure problem: an overview.  
*Ecological Applications*, 18(6):1351–1367, 2008.
- J. Foley.

A , r defries, g p asner, c barford, g bonan, s r carpenter, f s chapin, m t coe, g c daily, h k gibbs, j h helkowski, t holloway, e a howard, c j kucharik, c monfreda, j a patz, i c prentice, n ramankutty, and p k snyder (2005) global consequences of land use.

*Science*, 309:570–574.

G. Formetta, R. Mantilla, S. Franceschi, A. Antonello, and R. Rigon.

The JGrass-NewAge system for forecasting and managing the hydrological budgets at the basin scale: Models of flow generation and propagation/routing.

*Geoscientific Model Development*, 4(4):943–955, 2011a.

ISSN 1991959X.

doi: 10.5194/gmd-4-943-2011.

URL [www.geosci-model-dev.net/4/943/2011/](http://www.geosci-model-dev.net/4/943/2011/).

G. Formetta, R. Mantilla, S. Franceschi, A. Antonello, and R. Rigon.

The jgrass-newage system for forecasting and managing the hydrological budgets at the basin scale: models of flow generation and propagation/routing.

*Geoscientific Model Development*, 4(4):943, 2011b.

G. Formetta, R. Rigon, J. Chávez, and O. David.

Modeling shortwave solar radiation using the jgrass-newage system.

*Geoscientific Model Development*, 6(4):915–928, 2013a.

G. Formetta, R. Rigon, J. L. Chávez, and O. David.

Modeling shortwave solar radiation using the JGrass-NewAge system.

*Geoscientific Model Development*, 6(4):915–928, jul 2013b.

ISSN 1991959X.

## BIBLIOGRAPHY

---

doi: 10.5194/gmd-6-915-2013.

URL <https://www.geosci-model-dev.net/6/915/2013/>.

G. Formetta, A. Antonello, S. Franceschi, O. David, and R. Rigon.  
Hydrological modelling with components: A GIS-based open-source framework.

*Environmental Modelling and Software*, 55:190–200, may 2014a.

ISSN 13648152.

doi: 10.1016/j.envsoft.2014.01.019.

URL <https://www.sciencedirect.com/science/article/pii/S1364815214000292>.

G. Formetta, A. Antonello, S. Franceschi, O. David, and R. Rigon.  
Hydrological modelling with components: A gis-based open-source framework.

*Environmental Modelling & Software*, 55:190–200, 2014b.

G. Formetta, M. Bancheri, O. David, and R. Rigon.

Performance of site-specific parameterizations of longwave radiation.

*Hydrology and Earth System Sciences*, 20(11):4641–4654, nov 2016.

ISSN 16077938.

doi: 10.5194/hess-20-4641-2016.

URL <https://www.hydrol-earth-syst-sci.net/20/4641/2016/>.

A. S. L. Frank P. Incropera, David P. DeWitt, Theodore L. Bergman.  
*Fundamentals of Heat and Mass Transfer.pdf*, volume 13.  
2002.

URL [http://cds.cern.ch/record/1339915/files/9780471457282{\\_}TOC.pdf](http://cds.cern.ch/record/1339915/files/9780471457282{_}TOC.pdf).

E. Freeman, E. Robson, B. Bates, and K. Sierra.

*Head first design patterns.*

" O'Reilly Media, Inc.", 2008.

A. Friend.

Modelling canopy co<sub>2</sub> fluxes: are 'big-leaf' simplifications justified?

*Global Ecology and Biogeography*, 10(6):603–619, 2001.

M. Galvagno, G. Wohlfahrt, E. Cremonese, M. Rossini, R. Colombo, G. Filippa, T. Julitta, G. Manca, C. Siniscalco, U. Morra di Cellà, and M. Migliavacca.

Phenology and carbon dioxide source/sink strength of a sub-alpine grassland in response to an exceptionally short snow season.

*Environmental Research Letters*, 8(2):25008, 2013.

URL <http://stacks.iop.org/1748-9326/8/i=2/a=025008>.

E. Gamma, R. Helm, R. Johnson, and J. Vlissides.

Design patterns: Micro-architectures for reusable object-oriented design.

*Reading: Addison-Wesley*, 1994.

J. M. Gilbert and R. M. Maxwell.

Contrasting warming and drought in snowmelt-dominated agricultural basins: revealing the role of elevation gradients in regional response to temperature change.

*Environmental Research Letters*, 13(7):074023, 2018.

M. L. Goulden and R. C. Bales.

Mountain runoff vulnerability to increased evapotranspiration with vegetation expansion.

*Proceedings of the National Academy of Sciences*, 111(39):14071–14075, 2014.

## BIBLIOGRAPHY

---

A. Hammerle, A. Haslwanter, M. Schmitt, M. Bahn, U. Tappeiner, A. Cernusca, and G. Wohlfahrt.

Eddy covariance measurements of carbon dioxide, latent and sensible energy fluxes above a meadow on a mountain slope.

*Boundary-layer meteorology*, 122(2):397–416, 2007.

L. E. Hay and M. Umemoto.

*Multiple-objective stepwise calibration using Luca.*

Number 2006-1323. US Geological Survey, 2006.

ISBN OFR - 2006-1323.

R. Hiller, M. J. Zeeman, and W. Eugster.

Eddy-covariance flux measurements in the complex terrain of an alpine valley in switzerland.

*Boundary-Layer Meteorology*, 127(3):449–467, 2008.

R. Hock.

A distributed temperature-index ice-and snowmelt model including potential direct solar radiation.

*Journal of Glaciology*, 45(149):101–111, 1999.

N. M. Holbrook, M. J. Burns, and C. B. Field.

Negative xylem pressures in plants: a test of the balancing pressure technique.

*Science*, 270(5239):1193–1194, 1995.

T. Hölttä, H. Cochard, E. Nikinmaa, and M. Mencuccini.

Capacitive effect of cavitation in xylem conduits: results from a dynamic model.

*Plant, Cell & Environment*, 32(1):10–21, 2009.

V. Y. Ivanov, R. L. Bras, and E. R. Vivoni.

Vegetation-hydrology dynamics in complex terrain of semi-arid areas: 1. a mechanistic approach to modeling dynamic feedbacks.

*Water Resources Research*, 44(3), 2008.

P. G. Jarvis.

The Interpretation of the Variations in Leaf Water Potential and Stomatal Conductance Found in Canopies in the Field.

*Philosophical Transactions of the Royal Society B: Biological Sciences*, 273(927):593–610, 1976.

ISSN 0962-8436.

doi: 10.1098/rstb.1976.0035.

URL <http://rstb.royalsocietypublishing.org/cgi/doi/10.1098/rstb.1976.0035>.

P. G. Jarvis and K. G. Mcnaughton.

Stomatal Control of Transpiration: Scaling Up from Leaf to Region.

*Advances in Ecological Research*, 15(C):1–49, jan 1986.

ISSN 00652504.

doi: 10.1016/S0065-2504(08)60119-1.

URL <https://www.sciencedirect.com/science/article/pii/S0065250408601191>.

M. Jung, M. Reichstein, P. Ciais, S. I. Seneviratne, J. Sheffield, M. L. Goulden, G. Bonan, A. Cescatti, J. Chen, R. De Jeu, A. J. Dolman, W. Eugster, D. Gerten, D. Gianelle, N. Gobron, J. Heinke, J. Kimball, B. E. Law, L. Montagnani, Q. Mu, B. Mueller, K. Oleson, D. Papale, A. D. Richardson, O. Roupsard, S. Running, E. Tomelleri, N. Viovy, U. Weber, C. Williams, E. Wood, S. Zaehle, and K. Zhang.

Recent decline in the global land evapotranspiration trend due to limited moisture supply.

*Nature*, 467(7318):951–954, 2010.

ISSN 00280836.

doi: 10.1038/nature09396.

## BIBLIOGRAPHY

---

URL <http://www.ncbi.nlm.nih.gov/pubmed/20935626>  
<http://www.nature.com.ezproxy.library.wisc.edu/nature/journal/v467/n7318/full/nature09396.html>{%}5Cn<http://www.nature.com.ezproxy.library.wisc.edu/nature/journal/v467/n7318/pdf/nature09396.pdf>.

G. G. Katul, R. Oren, S. Manzoni, C. Higgins, and M. B. Parlange.  
Evapotranspiration: A process driving mass transport and energy exchange in the soil-plant-atmosphere-climate system,  
sep 2012.

ISSN 87551209.

URL <http://doi.wiley.com/10.1029/2011RG000366>.

G. G. Katul, D. Cava, M. Siqueira, and D. Poggi.  
Scalar turbulence within the canopy sublayer.  
*Coherent flow structures at Earth's Surface*, pages 73–95, 2013.

S. Y. Kotchenova, X. Song, N. V. Shabanov, C. S. Potter,  
Y. Knyazikhin, and R. B. Myneni.  
Lidar remote sensing for modeling gross primary production  
of deciduous forests.  
*Remote Sensing of Environment*, 92(2):158–172, 2004.

C.-T. Lai, G. Katul, R. Oren, D. Ellsworth, and K. Schäfer.  
Modeling co<sub>2</sub> and water vapor turbulent flux distributions  
within a forest canopy.  
*Journal of Geophysical Research: Atmospheres*, 105(D21):26333–  
26351, 2000.

P. Lehmann and D. Or.  
Effects of stomata clustering on leaf gas exchange.  
*New Phytologist*, 207(4):1015–1025, sep 2015.

- ISSN 14698137.  
doi: 10.1111/nph.13442.  
URL <http://doi.wiley.com/10.1111/nph.13442>.
- P. Lehmann, S. Assouline, and D. Or.  
Characteristic lengths affecting evaporative drying of porous media.  
*Physical Review E*, 77(5):056309, 2008.
- R. Leuning.  
Modelling Stomatal Behaviour and Photosynthesis of Eucalyptus grandis.  
*Functional Plant Biology*, 17(2):159, 1990.  
ISSN 1445-4408.  
doi: 10.1071/PP9900159.  
URL <http://www.publish.csiro.au/?paper=PP9900159>.
- R. Leuning.  
A critical appraisal of a combined stomatal-photosynthesis model for C3 plants.  
*Plant, Cell & Environment*, 18(4):339–355, apr 1995.  
ISSN 13653040.  
doi: 10.1111/j.1365-3040.1995.tb00370.x.  
URL <http://doi.wiley.com/10.1111/j.1365-3040.1995.tb00370.x>.
- S. Liu, L. Lu, D. Mao, and L. Jia.  
Evaluating parameterizations of aerodynamic resistance to heat transfer using field measurements.  
2007.
- C. Macfarlane, D. White, and M. Adams.

## BIBLIOGRAPHY

---

The apparent feed-forward response to vapour pressure deficit of stomata in droughted, field-grown *eucalyptus globulus* labill.

*Plant, Cell & Environment*, 27(10):1268–1280, 2004.

D. S. Mackay, D. E. Roberts, B. E. Ewers, J. S. Sperry, N. G. McDowell, and W. T. Pockman.

Interdependence of chronic hydraulic dysfunction and canopy processes can improve integrated models of tree response to drought.

*Water Resources Research*, 51(8):6156–6176, 2015.

G. Manoli, S. Bonetti, J.-C. Domec, M. Putti, G. Katul, and M. Marani.

Tree root systems competing for soil moisture in a 3d soil–plant model.

*Advances in water resources*, 66:32–42, 2014.

R. Mantilla, V. K. Gupta, and O. J. Mesa.

Role of coupled flow dynamics and real network structures on Hortonian scaling of peak flows.

*Journal of Hydrology*, 322(1-4):155–167, may 2006.

ISSN 00221694.

doi: 10.1016/j.jhydrol.2005.03.022.

URL <https://linkinghub.elsevier.com/retrieve/pii/S0022169405001113>.

S. Manzoni, G. Vico, G. Katul, S. Palmroth, R. B. Jackson, and A. Porporato.

Hydraulic limits on maximum plant transpiration and the emergence of the safety–efficiency trade-off.

*New Phytologist*, 198(1):169–178, 2013.

J. Martínez-Vilalta and N. Garcia-Forner.

Water potential regulation, stomatal behaviour and hydraulic transport under drought: deconstructing the iso/anisohydric concept.

*Plant, Cell & Environment*, 40(6):962–976, 2017.

T. Mastrotheodoros, C. Pappas, P. Molnar, P. Burlando, T. F. Keenan, P. Gentile, C. M. Gough, and S. Fatichi.

Linking plant functional trait plasticity and the large increase in forest water use efficiency.

*Journal of Geophysical Research: Biogeosciences*, 122(9):2393–2408, 2017.

T. Mastrotheodoros, C. Pappas, P. Molnar, P. Burlando, P. Hadjidoukas, and S. Fatichi.

Ecohydrological dynamics in the alps: Insights from a modelling analysis of the spatial variability.

*Ecohydrology*, 12(1):e2054, 2019.

T. Mastrotheodoros, C. Pappas, P. Molnar, P. Burlando, G. Manoli, J. Parajka, R. Rigon, B. Szeles, M. Bottazzi, P. Hadjidoukas, et al.

More green and less blue water in the alps during warmer summers.

*Nature Climate Change*, pages 1–7, 2020.

R. M. Maxwell and L. E. Condon.

Connections between groundwater flow and transpiration partitioning.

*Science*, 353(6297):377–380, 2016.

J. McDonough.

A'synthetic scalar'subgrid-scale model for large-eddy simulation of turbulent combustion.

In *Proc. 2002 Spring Tech. Mtg. Central States Sec., Combust. Inst.* Citeseer, 2002.

## BIBLIOGRAPHY

---

J. M. McDonough.

Introductory lectures on turbulence: physics, mathematics and modeling.

2007.

K. McNaughton and T. A. Black.

A study of evapotranspiration from a douglas fir forest using the energy balance approach.

*Water Resources Research*, 9(6):1579–1590, 1973.

P. Meir, B. Kruijt, M. Broadmeadow, E. Barbosa, O. Kull, F. Carswell, A. Nobre, and P. Jarvis.

Acclimation of photosynthetic capacity to irradiance in tree canopies in relation to leaf nitrogen concentration and leaf mass per unit area.

*Plant, Cell & Environment*, 25(3):343–357, 2002.

P. Melcher, F. Meinzer, D. Yount, G. Goldstein, and U. Zimmermann.

Comparative measurements of xylem pressure in transpiring and non-transpiring leaves by means of the pressure chamber and the xylem pressure probe.

*Journal of Experimental Botany*, 49(327):1757–1760, 1998.

L. Mercado, J. Lloyd, F. Carswell, Y. Malhi, P. Meir, and A. D. Nobre. Modelling amazonian forest eddy covariance data: a comparison of big leaf versus sun/shade models for the c-14 tower at manaus i. canopy photosynthesis.

*Acta Amazonica*, 36(1):69–82, 2006.

L. M. Mercado, C. Huntingford, J. H. Gash, P. M. Cox, and V. Jo-gireddy.

Improving the representation of radiation interception and photosynthesis for climate model applications.

- Tellus B: Chemical and Physical Meteorology*, 59(3):553–565, 2007.
- L. Misson, D. P. Rasse, C. Vincke, M. Aubinet, and L. François.  
Predicting transpiration from forest stands in Belgium for the 21st century.  
*Agricultural and Forest Meteorology*, 111(4):265–282, jun 2002.  
ISSN 01681923.  
doi: 10.1016/S0168-1923(02)00039-4.  
URL <https://www.sciencedirect.com/science/article/pii/S0168192302000394>.
- P. J. Mitchell, E. J. Veneklaas, H. Lambers, and S. S. Burgess.  
Using multiple trait associations to define hydraulic functional types in plant communities of south-western australia.  
*Oecologia*, 158(3):385–397, 2008.
- J. Monteith.  
Solar radiation and productivity in tropical ecosystems.  
*Journal of applied ecology*, 9(3):747–766, 1972.
- J. Monteith.  
Principles of environmental physics edward arnold.  
*London*, 214p, 1973.
- J. Monteith.  
Evaporation from land surfaces: progress in analysis and prediction since 1948.  
In *National conference on advances in evapotranspiration, Hyatt Regency Chicago, Ill.(USA), 16-17 Dec 1985*. American Society of Agricultural Engineers, 1985.
- J. L. Monteith.  
Evaporation and environment.

## BIBLIOGRAPHY

---

In *Symposia of the society for experimental biology*, volume 19, pages 205–234. Cambridge University Press (CUP) Cambridge, 1965.

R. Moore.

The probability-distributed principle and runoff production at point and basin scales.

*Hydrological Sciences Journal*, 30(2):273–297, 1985.

M. Moran, A. Rahman, J. Washburne, D. Goodrich, M. Weltz, and W. Kustas.

Combining the penman-monteith equation with measurements of surface temperature and reflectance to estimate evaporation rates of semiarid grassland.

*Agricultural and forest Meteorology*, 80(2-4):87–109, 1996.

F. I. Morton.

Operational estimates of areal evapotranspiration and their significance to the science and practice of hydrology.

*Journal of Hydrology*, 66(1-4):1–76, 1983.

K. A. Mott.

Do stomata respond to co<sub>2</sub> concentrations other than intercellular?

*Plant physiology*, 86(1):200–203, 1988.

E. Mukammal and H. Neumann.

Application of the priestley-taylor evaporation model to assess the influence of soil moisture on the evaporation from a large weighing lysimeter and class a pan.

*Boundary-Layer Meteorology*, 12(2):243–256, 1977.

G. Niedrist, E. Tasser, G. Bertoldi, S. Della Chiesa, N. Obojes, L. Egarter-Vigl, and U. Tappeiner.

- Down to future: Transplanted mountain meadows react with increasing phytomass or shifting species composition.  
*Flora*, 224:172–182, 2016.
- E. Nikinmaa, R. Sievänen, and T. Hölttä.  
Dynamics of leaf gas exchange, xylem and phloem transport, water potential and carbohydrate concentration in a realistic 3-d model tree crown.  
*Annals of botany*, 114(4):653–666, 2014.
- P. S. Nobel et al.  
*Physicochemical & environmental plant physiology*.  
Academic press, 1999.
- S. M. Noe and C. Giersch.  
A simple dynamic model of photosynthesis in oak leaves: Coupling leaf conductance and photosynthetic carbon fixation by a variable intracellular CO<sub>2</sub> pool.  
*Functional Plant Biology*, 31(12):1195–1204, dec 2004.  
ISSN 14454408.  
doi: 10.1071/FP03251.  
URL <http://www.publish.csiro.au/?paper=FP03251>.
- D. Norbiato, M. Borga, R. Merz, G. Blöschl, and A. Carton.  
Controls on event runoff coefficients in the eastern italian alps.  
*Journal of Hydrology*, 375(3-4):312–325, 2009.
- NORMAN and J. M.  
"Modelling the complete crop canopy", 'Modification of the Aerial Environment of Plants'.  
*Am. Soc. Agr. Eng. Monograph*, 2:249–277, 1979.  
URL <https://ci.nii.ac.jp/naid/10012299681/>.
- T. Oki and S. Kanae.

## BIBLIOGRAPHY

---

- Global hydrological cycles and world water resources.  
*Science*, 313(5790):1068–1072, aug 2006.  
ISSN 00368075.  
doi: 10.1126/science.1128845.  
URL <http://www.ncbi.nlm.nih.gov/pubmed/16931749> <http://www.sciencemag.org/content/313/5790/1068>.
- D. Or, P. Lehmann, E. Shahraeeni, and N. Shokri.  
Advances in Soil Evaporation Physics—A Review.  
*Vadose Zone Journal*, 12(4):0, nov 2013.  
ISSN 00222313.  
doi: 10.1016/0022-2313(76)90010-7.  
URL <https://www.soils.org/publications/vzj/abstracts/12/4/vzj2012.0163>.
- R. Orth and G. Destouni.  
Drought reduces blue-water fluxes more strongly than green-water fluxes in europe.  
*Nature communications*, 9(1):1–8, 2018.
- D. Papale, M. Migliavacca, E. Cremonese, A. Cescatti, G. Alberti, M. Balzarolo, L. B. Marchesini, E. Canfora, R. Casa, P. Duce, et al.  
Carbon, water and energy fluxes of terrestrial ecosystems in italy.  
In *The Greenhouse Gas Balance of Italy*, pages 11–45. Springer, 2015.
- C. Pappas, S. Faticchi, and P. Burlando.  
Modeling terrestrial carbon and water dynamics across climatic gradients: does plant trait diversity matter?  
*New Phytologist*, 209(1):137–151, 2016.
- M. B. Parlange and G. G. Katul.

An advection-aridity evaporation model.

*Water Resources Research*, 28(1):127–132, 1992.

C. A. Paulson.

The mathematical representation of wind speed and temperature profiles in the unstable atmospheric surface layer.

*Journal of Applied Meteorology*, 9(6):857–861, 1970.

H. L. Penman.

Natural evaporation from open water, bare soil and grass.

*Proceedings of the Royal Society of London. Series A, Mathematical and physical sciences*, 193(1032):120–145, 1948.

ISSN 09501207.

doi: 10.1098/rspa.1948.0037.

N. Pepin, R. S. Bradley, H. Diaz, M. Bara  r, E. Caceres, N. Forsythe, H. Fowler, G. Greenwood, M. Hashmi, X. Liu, et al.

Elevation-dependent warming in mountain regions of the world.

*Nature climate change*, 5(5):424–430, 2015.

L. Prandtl.

7. bericht  ber untersuchungen zur ausgebildeten turbulenz.

*ZAMM-Journal of Applied Mathematics and Mechanics/Zeitschrift f r Angewandte Mathematik und Mechanik*, 5 (2):136–139, 1925.

L. Prandtl.

*Application of the "magnus effect" to the wind propulsion of ships.*

National Advisory Committee for Aeronautics, 1926.

I. C. Prentice, X. Liang, B. E. Medlyn, Y. Wang, et al.

Reliable, robust and realistic: the three r's of next-generation land-surface modelling.

2015.

C. H. B. Priestley and R. Taylor.

On the assessment of surface heat flux and evaporation using large-scale parameters.

*Monthly weather review*, 100(2):81–92, 1972.

T. Pützc, M. Hannesd, and U. Wollschlägere.

Estimating precipitation and actual evapotranspiration from precision lysimeter measurements.

*Procedia Environmental Sciences*, 19:543–552, 2013.

M. R. Raupach and J. J. Finnigan.

"Single-layer models of evaporation from plant canopies are incorrect but useful, whereas multilayer models are correct but useless": discuss.

*Australian Journal of Plant Physiology*, 15(6):705–716, 1988.

ISSN 03107841.

doi: 10.1071/PP9880705.

URL <http://www.publish.csiro.au/?paper=PP9880705> <http://www.publish.csiro.au/fp/pdf/PP9880705.pdf>.

R. Rigon, G. Bertoldi, and T. M. Over.

Geotop: A distributed hydrological model with coupled water and energy budgets.

*Journal of Hydrometeorology*, 7(3):371–388, 2006a.

R. Rigon, E. Ghesla, C. Tiso, and A. Cozzini.

The HORTON machine: a system for DEM analysis The reference manual.

*Università degli Studi di Trento*, 2006b.

R. Rigon, P. D'Odorico, and G. Bertoldi.

The geomorphic structure of the runoff peak.

- Hydrology and Earth System Sciences*, 15(6):1853–1863, jun 2011.  
ISSN 1607-7938.  
doi: 10.5194/hess-15-1853-2011.  
URL <https://www.hydrol-earth-syst-sci.net/15/1853/2011/>.
- A. E. Rizzoli, M. Donatelli, R. Muettzel, T. Otjens, M. Sevensson, F. Evert, F. Villa, and J. Bolte.  
Seamframe, a proposal for an integrated modelling framework for agricultural systems.  
In *Proceedings of the 8th ESA Congress*, pages 331–332, 2004.
- C. R. Rollinson and M. W. Kaye.  
Modeling monthly temperature in mountainous ecoregions: importance of spatial scale for ecological research.  
*Climate Research*, 64(2):99–110, 2015.
- Y. Ryu, D. D. Baldocchi, H. Kobayashi, C. Van Ingen, J. Li, T. A. Black, J. Beringer, E. Van Gorsel, A. Knohl, B. E. Law, and O. Roupsard.  
Integration of MODIS land and atmosphere products with a coupled-process model to estimate gross primary productivity and evapotranspiration from 1 km to global scales.  
*Global Biogeochemical Cycles*, 25(4), 2011.  
ISSN 08866236.  
doi: 10.1029/2011GB004053.
- L. Samaniego, S. Thober, R. Kumar, N. Wanders, O. Rakovec, M. Pan, M. Zink, J. Sheffield, E. F. Wood, and A. Marx.  
Anthropogenic warming exacerbates european soil moisture droughts.  
*Nature Climate Change*, 8(5):421, 2018.
- R. Samson and R. Lemeur.

## BIBLIOGRAPHY

---

Energy balance storage terms and big-leaf evapotranspiration in a mixed deciduous forest.

*Annals of Forest Science*, 58(5):529–541, jul 2001.

ISSN 12864560.

doi: 10.1051/forest:2001143.

URL <http://www.edpsciences.org/10.1051/forest:2001143>.

B. Sapoval, M. Rosso, and J.-F. Gouyet.

The fractal nature of a diffusion front and the relation to percolation.

*Journal de Physique Lettres*, 46(4):149–156, 1985.

W. H. Schlesinger and S. Jasechko.

Transpiration in the global water cycle.

*Agricultural and Forest Meteorology*, 189-190:115–117, jun 2014.

ISSN 01681923.

doi: 10.1016/j.agrformet.2014.01.011.

URL <https://www.sciencedirect.com/science/article/pii/S0168192314000203https://www.sciencedirect.com/science/article/pii/S0168192314000203>.

P. F. Scholander, E. D. Bradstreet, E. Hemmingsen, and H. Hammel.

Sap pressure in vascular plants: negative hydrostatic pressure can be measured in plants.

*Science*, 148(3668):339–346, 1965.

S. J. Schymanski and D. Or.

- Leaf-scale experiments reveal an important omission in the Penman-Monteith equation.  
*Hydrology and Earth System Sciences*, 21(2):685–706, feb 2017.  
ISSN 16077938.  
doi: 10.5194/hess-21-685-2017.  
URL <https://www.hydrol-earth-syst-sci.net/21/685/2017/>.
- P. J. Sellers, M. D. Heiser, and F. G. Hall.  
Relations between surface conductance and spectral vegetation indices at intermediate (100 m<sup>2</sup> to 15 km<sup>2</sup>) length scales.  
*Journal of Geophysical Research: Atmospheres*, 97(D17):19033–19059, 1992.
- E. Shahraeeni, P. Lehmann, and D. Or.  
Coupling of evaporative fluxes from drying porous surfaces with air boundary layer: Characteristics of evaporation from discrete pores.  
*Water Resources Research*, 48(9), 2012.
- Z.-S. She, X. Chen, and F. Hussain.  
Quantifying wall turbulence via a symmetry approach: a lie group theory.  
*Journal of Fluid Mechanics*, 827:322–356, 2017.
- C. Shen, J. Niu, and M. S. Phanikumar.  
Evaluating controls on coupled hydrologic and vegetation dynamics in a humid continental climate watershed using a subsurface-land surface processes model.  
*Water Resources Research*, 49(5):2552–2572, 2013.
- N. Shokri and D. Or.  
What determines drying rates at the onset of diffusion controlled stage-2 evaporation from porous media?  
*Water Resources Research*, 47(9), 2011.

## BIBLIOGRAPHY

---

- T. Sinclair, C. Murphy, and K. Knoerr.  
Development and evaluation of simplified models for simulating canopy photosynthesis and transpiration.  
*Journal of Applied Ecology*, pages 813–829, 1976.
- M. Siqueira, G. Katul, and A. Porporato.  
Soil moisture feedbacks on convection triggers: The role of soil–plant hydrodynamics.  
*Journal of Hydrometeorology*, 10(1):96–112, 2009.
- M. Sprintsin, J. M. Chen, A. Desai, and C. M. Gough.  
Evaluation of leaf-to-canopy upscaling methodologies against carbon flux data in north america.  
*Journal of Geophysical Research: Biogeosciences*, 117(G1), 2012.
- P. C. Stoy, M. Mauder, T. Foken, B. Marcolla, E. Boegh, A. Ibrom, M. A. Arain, A. Arneth, M. Aurela, C. Bernhofer, et al.  
A data-driven analysis of energy balance closure across fluxnet research sites: The role of landscape scale heterogeneity.  
*Agricultural and forest meteorology*, 171:137–152, 2013.
- A. D. Stroock, V. V. Pagay, M. A. Zwieniecki, and N. Michele Holbrook.  
The physicochemical hydrodynamics of vascular plants.  
*Annual Review of Fluid Mechanics*, 46:615–642, 2014.
- Z. Su and C. Jacobs.  
*ENVISAT: actual evaporation*.  
Beleidscommissie Remote Sensing (BCRS), 2001.
- Z. Su, H. Pelgrum, and M. Menenti.  
Aggregation effects of surface heterogeneity in land surface processes.  
1999.

C. L. Tague, N. G. McDowell, and C. D. Allen.

An integrated model of environmental effects on growth, carbohydrate balance, and mortality of *pinus ponderosa* forests in the southern rocky mountains.

*PLoS One*, 8(11), 2013.

F. Tardieu, T. Lafarge, and T. Simonneau.

Stomatal control by fed or endogenous xylem aba in sunflower: interpretation of correlations between leaf water potential and stomatal conductance in anisohydric species.

*Plant, Cell & Environment*, 19(1):75–84, 1996.

G. Testa, F. Gresta, and S. L. Cosentino.

*Dry matter and qualitative characteristics of alfalfa as affected by harvest times and soil water content*, volume 34 of FAO - Food and Agriculture Organization of the United.

FAO, 2011.

ISBN 0254-5284.

doi: 10.1016/j.eja.2010.12.001.

URL <http://www.fao.org/docrep/X0490E/X0490E00.htm>.

I. Turton.

Geo tools.

In *Open source approaches in spatial data handling*, pages 153–169. Springer, 2008.

T. E. Twine, W. Kustas, J. Norman, D. Cook, P. Houser, T. Meyers, J. Prueger, P. Starks, and M. Wesely.

Correcting eddy-covariance flux underestimates over a grassland.

*Agricultural and Forest Meteorology*, 103(3):279–300, 2000.

A. Verhoef and G. Egea.

Modeling plant transpiration under limited soil water: Comparison of different plant and soil hydraulic parameterizations and preliminary implications for their use in land surface models.

*Agricultural and Forest Meteorology*, 191:22–32, 2014.

D. Viviroli, H. H. Dürr, B. Messerli, M. Meybeck, and R. Weingartner.

Mountains of the world, water towers for humanity: Typology, mapping, and global significance.

*Water resources research*, 43(7), 2007.

Y.-P. Wang and R. Leuning.

A two-leaf model for canopy conductance, photosynthesis and partitioning of available energy i:: Model description and comparison with a multi-layered model.

*Agricultural and Forest Meteorology*, 91(1-2):89–111, 1998.

R. Weingartner, D. Viviroli, and B. Schädler.

Water resources in mountain regions: a methodological approach to assess the water balance in a highland-lowland-system.

*Hydrological Processes: An International Journal*, 21(5):578–585, 2007.

M. Weiß and L. Menzel.

A global comparison of four potential evapotranspiration equations and heir relevance to stream flow modelling in semi-arid environments.

*Advances in Geosciences*, 18:15–23, jun 2008.

ISSN 16807359.

doi: 10.5194/adgeo-18-15-2008.

URL <https://www.adv-geosci.net/18/15/2008/>.

D. A. White, C. L. Beadle, P. J. Sands, D. Worledge, and J. L. Honeysett.

Quantifying the effect of cumulative water stress on stomatal conductance of *Eucalyptus globulus* and *Eucalyptus nitens*: A phenomenological approach.

*Australian Journal of Plant Physiology*, 26(1):17–27, 1999.

ISSN 03107841.

doi: 10.1071/PP98023.

D. Wilkinson.

Percolation effects in immiscible displacement.

*Physical Review A*, 34(2):1380, 1986.

G. Wohlfahrt and P. Widmoser.

Can an energy balance model provide additional constraints on how to close the energy imbalance?

*Agricultural and forest meteorology*, 169:85–91, 2013.

G. Wohlfahrt, A. Haslwanter, L. Hörtnagl, R. L. Jasoni, L. F. Fenstermaker, J. A. Arnone III, and A. Hammerle.

On the consequences of the energy imbalance for calculating surface conductance to water vapour.

*Agricultural and forest meteorology*, 149(9):1556–1559, 2009.

S. Wong, I. Cowan, and G. Farquhar.

Stomatal conductance correlates with photosynthetic capacity.

*Nature*, 282(5737):424, 1979.

E. F. Wood, J. K. Roundy, T. J. Troy, L. Van Beek, M. F. Bierkens, E. Blyth, A. de Roo, P. Döll, M. Ek, J. Famiglietti, et al.

Hyperresolution global land surface modeling: Meeting a grand challenge for monitoring earth's terrestrial water.

*Water Resources Research*, 47(5), 2011.

## BIBLIOGRAPHY

---

K. Yang, N. Tamai, and T. Koike.

Analytical solution of surface layer similarity equations.

*Journal of Applied Meteorology*, 40(9):1647–1653, 2001.

R. Zhao.

The xinanjiang model.

*Proceedings of the Oxford Symposium*, 1980.

X. Zhou, E. Istanbulluoglu, and E. R. Vivoni.

Modeling the ecohydrological role of aspect-controlled radiation on tree-grass-shrub coexistence in a semiarid climate.

*Water Resources Research*, 49(5):2872–2895, 2013.

G. Zhu, Y. Su, X. Li, K. Zhang, C. Li, and N. Ning.

Modelling evapotranspiration in an alpine grassland ecosystem on qinghai-tibetan plateau.

*Hydrological Processes*, 28(3):610–619, 2014.

G. Zuecco.

Processes space-time variability and hydrological response of headwater catchments: role of rainfall, vegetation and antecedent conditions.

2016.